Bouscary, C., et al., 2023, Sustained deformation across the Sub-Himalayas since 200 ka: Geology, https://doi.org/10.1130/G51656.1

Supplemental Material

Supplementary Text

Tables S1–S11

Figures S1–S5

Supplemental Material for:

Sustained deformation across the Sub-Himalayas since 200 ka

Bouscary Chloé[1,*], King E. Georgina[1], Grujic Djordje[2], Lavé Jérôme[3], Almeida Rafael[4], Hetényi György[5], Herman Frédéric[1]

[1]*Institute of Earth Surface Dynamics, University of Lausanne, Lausanne, Switzerland;*
[2]*Department of Earth and Environmental Sciences, Dalhousie University, Halifax, Canada;*
[3]*Centre de Recherches Pétrographiques et Géochimiques (CRPG), UMR 7358 CNRS, University of Lorraine, Nancy, France;*
[4] *Department of Geological Sciences, San Diego State University, San Diego, USA;*
[5]*Institute of Earth Sciences, University of Lausanne, Lausanne, Switzerland*

* *Chloé Bouscary; Email: chloebouscary@gmail.com*

Contents

1. Sample selection

A total of 33 samples were collected across the Sub-Himalayan fold-and-thrust belt (FTB), from western Nepal to eastern Bhutan, and analyzed using luminescence thermochronometry. Sample locations are shown in Fig. 1A and are detailed in Table 1 of the main article, and Table S2 of the Supplementary data file. All samples are fluviatile/molassic sedimentary rocks from the Siwalik Group, collected along rivers situated within the Sub-Himalayan FTB, delimited by the Main Boundary Thrust (MBT) in the North, and the Main Frontal Thrust (MFT) in the South. NG.1 is the only sample that lies south of the MFT.

Samples NG.1, 2, 3, 4, 5, 6, 7, 8, 10, and 11 were sampled North of Nepalgunj, in western Nepal (see Hirschmiller et al., 2014 for a cross-section of the area). Samples BUT.1, 2, 3, 4, 5 were collected more towards the east, in the Butwal area, central Nepal, along the Tinau Khola. Samples SU-9 and BAR-1 are two sandstones from the Bakaya valley (see Lavé and Avouac, 2000 for a cross-section of the area), south of Kathmandu, central Nepal. Samples RA-K01, 02, 03, 04, 05, 06 were collected across the Kamala thrust sheets, along the Kamala river, central Nepal (see Hirschmiller et al., 2014 for a cross-section of the area). Sandstone samples CA14-4 and CA14-7 (see Lavé and Avouac, 2001 for a cross-section of the area), were taken from along the Koshi Khola, eastern Nepal. Samples SJT.01A, 03, 05, 07 (siltstones), and SJT.08, 10, 11, 12 (sandstones) were collected in the Samdrup Jongkhar region, eastern Bhutan (Coutand et al., 2016). Further details on the samples can be found in the main text of the article, in the Supplementary data file, and below.

2. Luminescence thermochronometry

2.1. Sample preparation

All sample preparation and measurements were done under subdued red-light conditions, following the standard approach described in King et al. (2016). After removing any potentially light exposed material of the samples (outer 1-3 cm) using a water-cooled diamond saw, the light safe part

of the samples was crushed and sieved to extract the grain-size fraction of interest (180-212 μm). Carbonates and organic material were then removed using 10 % HCl and 30 % H_2O_2 respectively, before a density separation with sodium polytungstate of $\rho < 2.58$ g.cm^{-3} was used to isolate the K-feldspar enriched fraction of the samples.

2.2. Environmental dose rate

The environmental dose rates $\dot{D}$ were determined using the Dose Rate and Age Calculator DRAC developed by Durcan et al. (2015). A representative part of each sample was sent to ActLabs – Activation Laboratories Ltd, Ancaster, Canada, for inductively coupled plasma mass spectrometry (ICP-MS) to determine the radioisotope concentrations of U, Th, K and Rb. Thin-section images were used to determine the original grain size of the samples (before crushing) with the Digital Grain Size software developed by Buscombe (2013). The grain size 180-212 μm was used when the average grain size of the sample was equivalent to or smaller than the grain size of the feldspar extract analysed (180-212 μm). The dose rate was then determined using DRAC, using the conversion factors of Guérin et al. (2011), the alpha grain-size attenuation factors of Brennan et al. (1991), the beta grain-size attenuation factors of Guérin et al. (2012), an alpha-efficiency (a-value) of 0.15 ± 0.05 (Balescu and Lamothe, 1994), and a water content of 10 ± 10 weight % (sandstone samples). As the samples are thought to have been at the surface for a relatively short period of time (for less than 2 k.y. because of high erosion rates), cosmic dose rates were not incorporated in the final environmental dose rate estimations. Radio-isotopic concentrations, grain size, and final dose rates are listed in Table S3 of the Supplementary data file for more information.

2.3. Luminescence measurements

The samples were measured in the luminescence laboratories at the University of Bern and the University of Lausanne, Switzerland, using a multi-elevated temperature (MET) post-infrared

infrared-stimulated luminescence (pIR IRSL) – MET-pIR-IRSL – single aliquot regenerative dose (SAR) protocol (Li and Li, 2011) on ~2 mm diameter aliquots of K-feldspar grains. Luminescence measurements were conducted on automated TL/OSL-DA-20 Risø luminescence readers. Aliquots were stimulated with infrared LEDs, and signals were detected in the blue part of the visible spectrum using a BG39 and BG3 filter pack.

All measurements were done under the same conditions. After a preheat at 250 °C for 60 s, four IRSL signals (IRSL.50, 100, 150, 225) were measured by infrared stimulation at 50, 100, 150 and 225 °C for a duration of 100 s each (L_x). A test dose of 75-95 Gy (beta radiation) was then given to the aliquots, before another preheat and measurement of the test dose signal (T_x) for each stimulation temperature (IRSL at 50, 100, 150, and 225 °C). Each measurement cycle was followed by an infrared bleaching at 290 °C for 60 s to remove any remaining signal before the measurement cycle. For each sample, three measurements were done to constrain (i) the trapped charge concentration, (ii) the sample specific rate of athermal signal loss (anomalous fading), and (iii) the sample thermal stability (Table S1 and Fig. S3).

(i) Trapped charge concentrations were measured on three aliquots per sample. The natural luminescence signal stored in the feldspar minerals, $\tilde{n}_{nat}$, was first measured, before nine regenerative doses between 0 and 6000 Gy were given to the aliquots to construct sample specific dose response curves. Data were then fitted using equation 5 of King et al. (2016) to derive the trapping kinetic parameter D_0.

(ii) Athermal signal loss was measured using the same three aliquots used in the previous step. After the administration of a fixed regenerative dose of 75-95 Gy, equal to the test dose, aliquots were preheated prior to storage at ambient temperature following Auclair et al. (2003), and measured following different delay periods from 0 to 48,000 s. Data were fitted using equations 3 and 4 of King et al. (2016) and the model of Huntley (2006) for the natural samples, to extract the athermal kinetic

parameter ρ'. Dose response curves were then corrected for anomalous fading, and equivalent doses D_e were calculated for each aliquot.

(iii) Thermal loss was measured with isothermal decay measurements on one representative aliquot of each sample. The isothermal decay of each IRSL signal was measured using four isothermal storage temperatures at 190, 210, 230, and 250 °C, following Bouscary and King (2022), with isothermal delay times of 1 to 10,000 s. Data were fitted using the band-tail states model (BTS; Li and Li, 2013), using equations 6 and 7 of King et al. (2016), to extract the thermal kinetic parameters E_t, E_u, and s.

Table S1: *(i) Dose response curve, (ii) anomalous fading, and (iii) isothermal decay luminescence measurement protocols for K-feldspars aliquots with the MET-pIR-IRSL protocol.*

Steps	(i) Dose response curve	(ii) Anomalous fading	(iii) Isothermal decay
1	Natural / regenerative dose 0-6000 Gy (Lx)	Fixed regenerative dose Gy (Lx)	Fixed regenerative dose Gy (Lx)
2	Heat to 250 °C for 60 s	Heat to 250 °C for 60 s	Heat to 250 °C for 60 s
3	-	Storage $T°_{ambient}$, 0-48000s	Storage $T°_{190\text{-}250}$, 0-10000s
4	IR stimulation at 50 °C for 100 s		
5	IR stimulation at 100 °C for 100 s		
6	IR stimulation at 150 °C for 100 s		
7	IR stimulation at 225 °C for 100 s		
8	Test dose (Tx)		
9	Heat to 250 °C for 60 s		
10	IR stimulation at 50 °C for 100 s		
11	IR stimulation at 100 °C for 100 s		
12	IR stimulation at 150 °C for 100 s		
13	IR stimulation at 225 °C for 100 s		
14	Hot-bleach, IR stimulation at 290 °C for 60 s		
	Repeat		

Dose recovery tests were done to control the quality of the data. Six new aliquots were prepared and bleached with natural sunlight for 4 h or with a solar simulator for 1 h. Three discs were used to measure the unbleached residual signal, and three discs were given a laboratory dose to obtain dose

recovery ratios following residual subtraction. The laboratory dose used was either a dose similar to the D_e of the IRSL.50 signal, or a dose of 150 Gy for samples close to saturation.

All luminescence signals were extracted from the luminescence decay curves by integrating the signal over the 5 first channels (2 s), and subtracting the background calculated over the last 50 channels (20 s). Aliquots were accepted and included in the study when they fulfilled the sample acceptance criteria, i.e. signal greater than 3σ above background, recycling ratio within 10 % of unity, maximum test dose uncertainty < 10 %, and recuperation < 10 % of the natural signal.

2.4. Results and data screening

All aliquots of all samples passed the aliquot acceptance criteria for all IRSL measurements, and the measurements were reproducible within error for each sample (n = 3). Dose recovery ratios (after residual subtraction) yielded a dose recovery ratio within 15 % of unity, which was deemed acceptable in this study. Data were also rejected when luminescence signal showed no clear monotonic decay.

To evaluate aliquot saturation, the approach of Kars et al. (2008) was used to screen whether the samples were in athermal steady-state, or whether they exhibited disequilibrium (i.e. contained a thermal signal). Natural luminescence $\tilde{n}_{nat}$ values were compared with those predicted for athermal steady-state $\tilde{n}_{SS}$. Samples are considered saturated when $\tilde{n}_{nat} \geq 0.86.\tilde{n}_{SS}$. Of the 33 samples measured, 5 are in athermal steady-state for all the measured signals (NG.10, RA-K01, RA-K04, RA-K06, and CA14-4). 15 other samples are within the limit of saturation for at least one IRSL signal. In total, 10 samples have their IRSL.50 signal saturated, 6 their IRSL.100 signal, 10 their IRSL.150 signal, and 15 their IRSL.225 signal. The high number of saturated samples for the IRSL.50 might relate to the high fading rates for this signal. The saturation of the post-IRSL signals, particularly of the IRSL.225, is probably linked to low counting statistics for less bright luminescence emissions or to the higher thermal stability of this signal.

Another screening was done to remove samples that are potentially in thermal equilibrium with surface temperature. A temperature at 20 °C, reflecting the approximate average surface temperature throughout the Holocene (last few meters of exhumation of the rocks) was chosen. Thermal steady-state values for a temperature of 20 °C, $\tilde{n}_{20}$, were calculated for each sample and compared with the natural luminescence values, $\tilde{n}_{nat}$. As above, samples are considered saturated when $\tilde{n}_{nat} \geq 0.86.\tilde{n}_{20}$. All signals that are within the limit of saturation for athermal steady-state, are also all in saturation for surface temperature. Out of the 33 samples measured, 11 are in thermal steady-state for surface temperature for all the measured signals (the 5 that are also in athermal steady-state, as described above, and NG.6, NG.7, NG.8, RA-K02, SJT01A), and 15 other samples are within the limit of saturation for at least one IRSL signal. In total, 18 samples have their IRSL.50 signal saturated, 16 their IRSL.100 signal, 15 their IRSL.150 signal, and 23 their IRSL.225 signal. Only 7 samples (NG.4, NG.5, BUT.2, BUT.3, BUT.4, SU-9, and BAR-1) have no signals in equilibrium with surface temperature.

Non-saturated data were also screened to see if the cooling ages are in decreasing order with increasing MET temperature (Fig. S1). We expect to cooling ages to be older for more thermally stable IRSL signals (higher IRSL measurement temperatures). Including uncertainties, only samples NG.3 and BAR.1 present ages that are out-of-order. The reason for these age inversions most likely reflects that the fading values are overestimated for the saturated samples. As our data passed the dose recovery test and other rejection criteria, it seems somewhat arbitrary to delete ages based on a presumed progression of increasing age with increasing measurement temperature. For this reason we prefer to include all of the ages that are not saturated and that fulfil our acceptance criteria as detailed above.

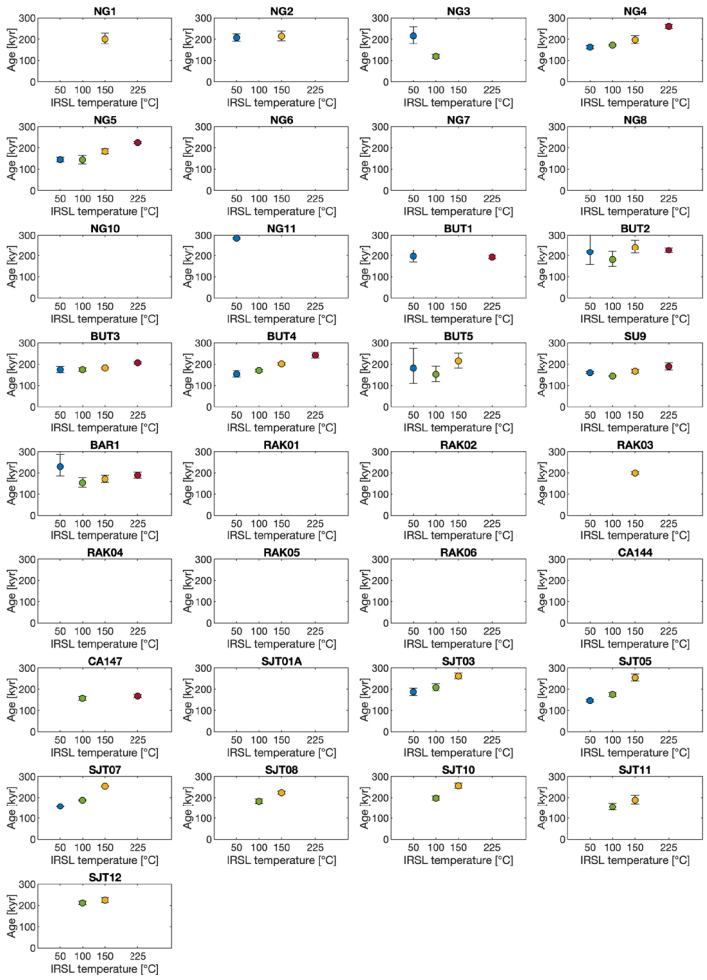

Fig. S1: *Distribution of the luminescence thermochronometry cooling ages with increasing MET-IRSL signal temperature. Only non-saturated signals are represented.*

3. Inversion of thermochronometric data

3.1. Maximum burial temperature

To invert thermochronometric data for exhumation rates, the thermal history of the sample should be considered. In the Ganga plain or the Himalayan foredeep basin, the limited flexure of the rigid lid of the Indian plate (Lyon-Caen and Molnar, 1985) greatly limits the depth of burial of the Himalayan molasses. Consequently, in the Sub-Himalayan FTB, the exhumed rocks of the Siwalik Groups were buried only to depths of up to ~5 km, corresponding to a maximum burial temperature

of 120 °C, assuming a homogeneous geothermal gradient of 20 °C/km (Mugnier et al., 1995; van der Beek et al., 2006).

When maximum burial temperatures are not already constrained by vitrinite reflectance data, as for the SJT transect (Coutand et al., 2016), maximum burial temperatures were estimated from each sample maximum burial depth, derived from the stratigraphic location of the sample and balanced cross-section reconstruction, using a fixed geothermal gradient of 20 °C/km and a surface temperature of 20 °C. These maximum burial temperatures are minimum estimates that do not consider the overthrusting rocks from the hanging walls of near thrusts.

The maximum stratigraphic depths that the sampled rocks reached define the maximum stratigraphic burial temperatures that the rocks experienced. First, the stratigraphic location of the sample is derived from the geographical distance of the sample and the thrust dip angle:

Stratigraphic position = geographical distance to the thrust . sin(thrust dip angle)

The stratigraphic burial depth is then the total thickness of the stratigraphy minus the stratigraphic position.

Stratigraphic burial depth = total thickness of the stratigraphy - stratigraphic position

And the maximum burial temperature is derived from the stratigraphic burial depth, a geothermal gradient of 20 °C/km, and a surface temperature of 20 °C:

*Maximum burial temperature = stratigraphic burial depth * geothermal gradient + surface temperature*

So for example, if the sample is today at 2.6 km of the thrust and that the thrust dip at a 30° angle, the stratigraphic position of the sample is of 1.3 km. Considering a total thickness of the Siwalik Group of 2.5 km, then the sample was buried to a depth of 1.2 km, which is equivalent to a temperature of 44 °C.

Maximum burial depth and burial temperatures for each sample are listed in Table S6.

3.2. Exhumation rates

Average exhumation histories are calculated for each non-saturated IRSL signal. The models are run for 1 M.y., between 1 Ma and 0 Ma (today), with a time step of 1000 yr (nstep = 1001), to ensure that the luminescence signals generated are in steady-state, i.e., are in dynamic equilibrium between rates of electron trapping and detrapping for the maximum burial temperature prior to rock cooling. Time-temperature cooling paths were calculated for fixed exhumation rates between 0 mm/yr (no exhumation) and 20 mm/yr, in increments of 0.1 mm/yr, assuming a fixed homogeneous geothermal gradient at 20 °C/km, and a surface temperature of 20 °C. Maximum temperature was fixed as the maximum possible burial temperature for the specific sample under investigation, derived from the maximum burial depth that the sample experienced (see Table S6).

For each exhumation rate-derived time-temperature path (Fig. S2A), a forward model calculates the modelled trap occupancy values, $\tilde{n}_{mod}$, for each IRSL signal, using the sample specific natural kinetic parameters and equation 5 of King et al. (2016) (Fig. S2B). Final $\tilde{n}_{mod}$ values, $\tilde{n}_{mod}(end)$, were extracted and compared to the natural luminescence signals of the samples, $\tilde{n}_{nat}$. Only exhumation rates that yielded $\tilde{n}_{mod}(end)$ values within uncertainty of $\tilde{n}_{nat}$ ($s\tilde{n}_{nat}$, fixed at a minimum of 5 % of $\tilde{n}_{nat}$) were retained (Fig. S2B). Exhumation rates are then extracted from the minimum difference between $\tilde{n}_{mod}(end)$ and $\tilde{n}_{nat}$ for each IRSL signal. Errors on the exhumation rates values are calculated in the same way, from the minimum and maximum exhumation rates that correspond to the minimum and maximum $\tilde{n}_{nat}$ values including error ($\tilde{n}_{nat}$ - $s\tilde{n}_{nat}$ and $\tilde{n}_{nat}$ + $s\tilde{n}_{nat}$) (Fig. S2C).

Samples specific exhumation rates are then averaged over the different non-saturated luminescence signals of the samples. See Table 1 of the main article for transect specific exhumation rates, and Table S7 for the sample specific thrust slip rates and shortening rates.

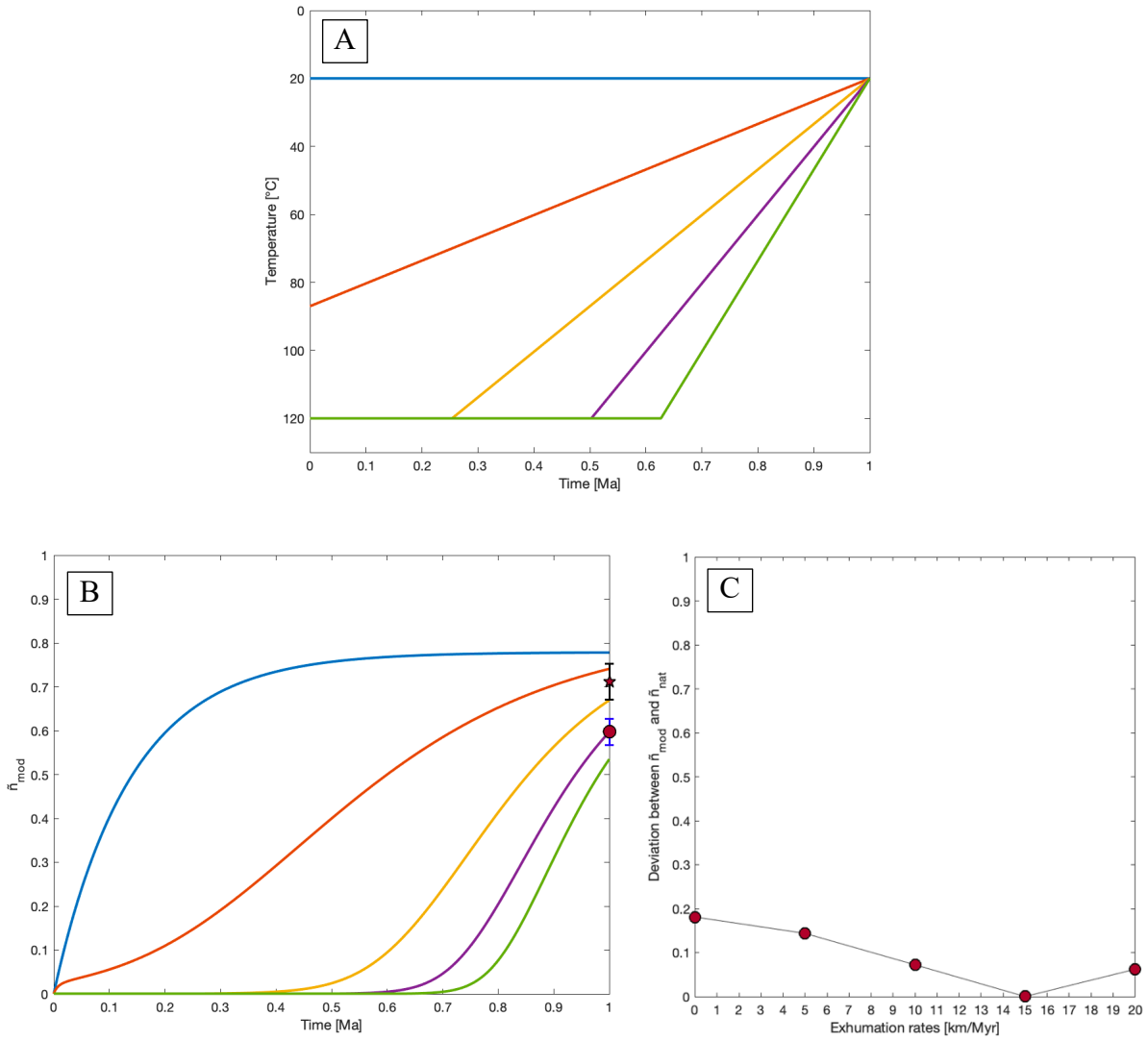

Fig. S2: *Modelled average exhumation rates for an IRSL signal of a sample.* ***A.*** *Example of a few time-temperature paths corresponding to 5 exhumation rates at 0 (blue), 5 (orange), 10 (yellow), 15 (purple), and 20 mm/yr (green). The time 1 Ma corresponds to the present day.* ***B.*** $\tilde{n}_{mod}$ *signals for each exhumation rate. The red circle and star represent the* $\tilde{n}_{nat}$ *and 0.86 ** $\tilde{n}_{SS}$ *values for the IRSL of the sample, and their error range* $s\tilde{n}_{nat}$ *and* $s\tilde{n}_{SS}$ *in blue and black respectively. The time 1 Ma corresponds to the present day.* ***C.*** *Deviation between the final* $\tilde{n}_{mod}$ *value,* $\tilde{n}_{mod}(end)$*, and the natural signal of the sample,* $\tilde{n}_{nat}$*, for each exhumation rate. When the misfit is closest to the x-axis, it corresponds to the exhumation rate that generates an* $\tilde{n}_{mod}(end)$ *value closest to* $\tilde{n}_{nat}$ *for the sample signal, i.e., here to 15 mm/yr.*

Figures and tables in the Supplementary data file

Table S2: *Sample names, thrust sheet, locations, elevations, and transect name and location.*

Table S3*: Radioisotope concentrations, grain size range, and calculated total environmental dose rate ($\dot{D}$). Errors are calculated as 3 % of the values.*

Table S4: *Summary of kinetic and fitted parameters for all four IRSL temperatures, using kinetic parameters derived from four isothermal temperatures between 190 and 250 °C (Bouscary and King, 2022). Uncertainties are listed as 1σ for all values, except for D_e, for which errors are listed as 5 % of D_e. Fading rates are expressed both as ρ' and as g-values normalised to 2 days, g_{2d}, Huntley and Lamothe (2001). Saturated samples are shown in grey.*

Table S5: *Saturation indicator values, and age of the samples for all four IRSL temperatures. Saturated samples are shown in grey.*

Table S6: *Samples with their reference thrust, geographical distance to the Main Frontal Thrust (MFT), and stratigraphic burial depth and associated maximum burial temperature, derived from the stratigraphic location of the sample today, and cross-section reconstruction.*

Table S7: *Samples with their IRSL signal specific exhumation rate, and their sample specific exhumation rate, i.e., the average of the non-saturated IRSL signal specific exhumation rates.*

Table S8: *Samples with their averaged apparent age, exhumation rate, and thrust slip rates with a fixed dip angle of 30°, and with a dip angle range between 25 and 45°.*

Table S9: ***A.*** *Compilation of Global Positioning System (GPS) derived geodetic convergence rates from the literature, and* ***B.*** *their references.*

Table S10: *Compilation of literature data used in Fig. 3B for* ***A.*** *the Holocene and late Quaternary, and* ***B.*** *the Miocene-Pliocene, and* ***C.*** *their references.*

Table S11: *Percentage of convergence taken by the Sub-Himalayan FTB thrusts during the late Quaternary (last 200 k.y.).*

Fig. S3: *Luminescence measurement and model fit results for all samples. (A, D, G, J) Anomalous fading data fitted using equations 3 and 4 of King et al. (2016), for the IRSL at 50, 100, 150, and 225 °C respectively. (B, E, H, K) Luminescence dose response accounting for fading, fitted using equation 5 of King et al. (2016). The black solid line is the unfaded dose response curve, and the yellow dots represent the* $\tilde{n}_{nat}$ *values of each aliquot. (C, F, I, L) Isothermal decay data fitted with the BTS model, using equations 6 and 7 of King et al. (2016).*

Fig. S4: *Steady-state saturation plots (Kars plots) for all samples, contrasting natural luminescence values,* $\tilde{n}_{nat}$*, with steady-state luminescence values,* $\tilde{n}_{SS}$*, predicted for each of the samples. The 1:1 line delimits saturated samples (blue area) to unsaturated samples (white area), with the saturation limit indicated by the blue line.*

Fig. S5: *Surface temperature saturation plots for all samples, contrasting natural luminescence values,* $\tilde{n}_{nat}$*, with the luminescence values for a surface temperature of 20 °C,* $\tilde{n}_{Tmin} = \tilde{n}_{20}$*, predicted for each of the samples. The 1:1 line delimits saturated samples (blue area) to unsaturated samples (white area), with the saturation limit indicated by the blue line.*

References

Auclair, M., Lamothe, M., and Huot, S. (2003). Measurement of anomalous fading for feldspar IRSL using SAR. Radiation Measurement s37, 487–492.

Balescu, S., and Lamothe, M. (1994). Comparison of TL and IRSL age estimates of feldspar coarse grains from waterlain sediments. Quaternary Science Reviews 13, 437–444.

Bouscary, C., and King, G.E. (2022). Luminescence thermochronometry of feldspar minerals: Optimisation of measurement conditions for the derivation of thermal kinetic parameters using isothermal holding experiments. Quaternary Geochronology, 67, 101240, 1–14.

Brennan, B.J., Lyons, R.G., and Phillips, S.W. (1991). Attenuation of alpha particle track dose for spherical grains. International Journal of Radiation Applications and Instrumentation, Part D, Nuclear Tracks and Radiation Measurements 18(1-2), 249–253.

Buscombe, D. (2013). Transferable wavelet method for grain-size distribution from images of sediment surfaces and thin sections, and other natural granular patterns. Sedimentology 60, 1709–1732.

Coutand, I., Barrier, L., Govin, G., Grujic, D., Hoorn, C., Dupont-Nivet, G., and Najman, Y. (2016). Late Miocene-Pleistocene evolution of India-Eurasia convergence partitioning between the Bhutan Himalaya and the Shillong Plateau: New evidences from foreland basin deposits along the Dungsam Chu section, eastern Bhutan. Tectonics, 35(12), 2963–2994.

Durcan, J.A., King, G.E., and Duller, G.A.T. (2015). DRAC: dose rate and age calculator for trapped charge dating. Quaternary Geochronology 28, 54–61.

Guérin, G., Mercier, N., and Adamiec, G. (2011). Dose-rate conversion factors: update. Ancient TL 29(1), 5–8.

Guérin, G., Mercier, N., Nathan, R., Adamiec, G., and Lefrais, Y. (2012). On the use of the infinite matrix assumption and associated concepts: a critical review. Radiation Measurements 47, 778–785.

Hirschmiller, J., Grujic, D., Bookhagen, B., Coutand, I., Huyghe, P., Mugnier, J.L., and Ojha, T. (2014). What controls the growth of the Himalayan foreland fold-and-thrust belt? Geology, 42(3), 247–250.

Huntley, D.J., and Lamothe, M. (2001). Ubiquity of anomalous fading in K-feldspars and the measurement and correction for it in optical dating. Canada Journal of Earth Sciences 38 (7), 1093–1106.

Huntley, D.J. (2006). An explanation of the power-law decay of luminescence. Journal of Physics: Condensed Matter 18, 1359–1365.

Kars, R.H., Wallinga, J., and Cohen, K.M. (2008). A new approach towards anomalous fading correction for feldspar IRSL dating —tests on samples in field saturation. Radiation Measurements 43(2–6), 786–790.

King, G.E., Herman, F., Lambert, R., Valla, P.G., and Guralnik, B. (2016). Multi-OSL thermochronometry of feldspar. Quaternary Geochronology 33, 76–87.

Lavé, J., and Avouac, J.P. (2000). Active folding of fluvial terraces across the Siwaliks Hills, Himalayas of central Nepal. Journal of Geophysical Research: Solid Earth, 105(B3), 5735–5770.

Lavé, J., and Avouac, J.P. (2001). Fluvial incision and tectonic uplift across the Himalayas of central Nepal. Journal of Geophysical Research: Solid Earth, 106(B11), 26561–26591.

Li, B., and Li, S.-H. (2011). Luminescence dating of K-feldspar from sediments: a protocol without anomalous fading correction. Quaternary Geochronology 6 (5), 468–479.

Li, B., and Li, S.-H. (2013). The effect of band-tail states on the thermal stability of the infrared stimulated luminescence from K-feldspar. Journal of Luminescence. 136, 5–10.

Lyon-Caen, H., and Molnar, P. (1985). Gravity anomalies, flexure of the Indian plate, and the structure, support and evolution of the Himalaya and Ganga Basin. Tectonics, 4(6), 513–538.

Mugnier, J.L., Chalaron, E., Mascle, G., Pradier, B., and Herail, G. (1995). Structural and thermal evolution of the Siwaliks of western Nepal. Journal of Nepal Geological Society, 11, 171–178.

van der Beek, P., Robert, X., Mugnier, J.L., Bernet, M., Huyghe, P., and Labrin, E. (2006). Late Miocene–Recent exhumation of the central Himalaya and recycling in the foreland basin assessed by apatite fission-track thermochronology of Siwalik sediments, Nepal. Basin Research, 18(4), 413–434.

Supplementary data for:

Sustained deformation across the Sub-Himalayas since 200 ka

Bouscary Chloé[1,*], King E. Georgina[1], Grujic Djordje[2], Lavé Jérôme[3], Almeida Rafael[4], Hetényi György[5], Herman Frédéric[1]

[1]*Institute of Earth Surface Dynamics, University of Lausanne, Lausanne, Switzerland;*
[2]*Department of Earth and Environmental Sciences, Dalhousie University, Halifax, Canada;*
[3]*Centre de Recherches Pétrographiques et Géochimiques (CRPG), UMR 7358 CNRS, University of Lorraine, Nancy, France;*
[4]*Department of Geological Sciences, San Diego State University, San Diego, USA;*
[5]*Institute of Earth Sciences, University of Lausanne, Lausanne, Switzerland*

* *Chloé Bouscary; Email: chloebouscary@gmail.com*

Contents

Table S2: *Sample names, thrust sheet, locations, elevations, and transect name and location.*

Samples	Thrust sheet	Latitude [°N]	Longitude [°E]	Elevation [m]	Location
NG1	MFT	28.262821	81.670180	183	Nepalgunj, western Nepal
NG2	MFT 2	28.317368	81.674567	322	Nepalgunj, western Nepal
NG3	MFT 2	28.326395	81.688989	538	Nepalgunj, western Nepal
NG4	MFT 2	28.340852	81.676234	642	Nepalgunj, western Nepal
NG5	MFT 2	28.347636	81.689799	535	Nepalgunj, western Nepal
NG6	IST	28.359138	81.713772	326	Nepalgunj, western Nepal
NG7	IST	28.397584	81.695364	1003	Nepalgunj, western Nepal
NG8	IST 2	28.460761	81.715641	584	Nepalgunj, western Nepal
NG10	IST 2	28.514287	81.641148	451	Nepalgunj, western Nepal
NG11	IST 2	28.518265	81.663073	417	Nepalgunj, western Nepal
BUT.1	MFT	27.718947	83.465539	204	Butwal, Tinau Khola, central Nepal
BUT.2	MFT	27.724558	83.469619	300	Butwal, Tinau Khola, central Nepal
BUT.3	MFT	27.732506	83.469019	298	Butwal, Tinau Khola, central Nepal
BUT.4	MFT	27.739872	83.464492	317	Butwal, Tinau Khola, central Nepal
BUT.5	MFT	27.745197	83.468461	322	Butwal, Tinau Khola, central Nepal
SU-9	MFT	27.253400	85.180339	200	Bakaya, South Kathmandu, central Nepal
BAR-1	MFT	27.253575	85.180429	200	Bakaya, South Kathmandu, central Nepal
RA-K01	IST	27.160843	85.906740	392	Kamala, Kamala Khola, central Nepal
RA-K02	IST	27.171164	85.903100	412	Kamala, Kamala Khola, central Nepal
RA-K03	IST	27.178396	85.910660	424	Kamala, Kamala Khola, central Nepal
RA-K04	IST	27.168627	85.923910	416	Kamala, Kamala Khola, central Nepal
RA-K05	IST	27.194206	85.927315	419	Kamala, Kamala Khola, central Nepal
RA-K06	IST	27.199530	85.933945	453	Kamala, Kamala Khola, central Nepal
CA14-4	MFT	26.862100	87.149400	125	Koshi Khola, eastern Nepal
CA14-7	MFT	26.866317	87.150467	120	Koshi Khola, eastern Nepal
SJT01A	MFT	26.797950	91.501160	161	Samdrup Jongkhar, eastern Bhutan
SJT03	MFT	26.810030	91.495700	181	Samdrup Jongkhar, eastern Bhutan
SJT05	MFT	26.816790	91.494850	210	Samdrup Jongkhar, eastern Bhutan
SJT07	MFT	26.819660	91.486420	219	Samdrup Jongkhar, eastern Bhutan
SJT08	MFT	26.820360	91.483500	227	Samdrup Jongkhar, eastern Bhutan
SJT10	MFT	26.825490	91.480980	239	Samdrup Jongkhar, eastern Bhutan
SJT11	MFT	26.829300	91.480540	255	Samdrup Jongkhar, Eastern Bhutan
SJT12	MFT	26.831640	91.481050	270	Samdrup Jongkhar, Eastern Bhutan

Note: Samples NG.1-11 and SJT.01A-12 collected by D. Grujic; samples RA-K01-6 collected by R. Almeida; samples BUT, SU-9, BAR-1, CA14-4 and CA14-7 collected by J. Lavé.

Table S3*: Radioisotope concentrations, grain size range, and calculated total environmental dose rate ($\dot{D}$). Errors are calculated as 3 % of the values.*

Samples	U [ppm]	Th [ppm]	K [%]	Rb [ppm]	Grain size [µm]	$\dot{D}$ (Gy/ka)
NG1	2.1 ± 0.1	10.3 ± 0.3	0.90 ± 0.03	52 ± 2	180-212	2.87 ± 0.17
NG2	2.4 ± 0.1	11.9 ± 0.4	1.44 ± 0.04	69 ± 2	180-212	3.53 ± 0.22
NG3	1.6 ± 0.0	9.4 ± 0.3	1.06 ± 0.03	50 ± 2	180-212	2.82 ± 0.17
NG4	1.7 ± 0.1	10.8 ± 0.3	1.07 ± 0.03	57 ± 2	180-212	2.96 ± 0.18
NG5	1.1 ± 0.0	5.9 ± 0.2	1.09 ± 0.03	55 ± 2	180-212	2.48 ± 0.15
NG6	1.1 ± 0.0	5.4 ± 0.2	1.01 ± 0.03	46 ± 1	180-212	2.37 ± 0.14
NG7	1.3 ± 0.0	7.2 ± 0.2	0.85 ± 0.03	52 ± 2	180-212	2.41 ± 0.14
NG8	2.3 ± 0.1	13.4 ± 0.4	1.94 ± 0.06	108 ± 3	180-212	4.06 ± 0.26
NG10	2.0 ± 0.1	13.1 ± 0.4	1.54 ± 0.05	72 ± 2	180-212	3.61 ± 0.22
NG11	2.0 ± 0.1	10.2 ± 0.3	0.96 ± 0.03	48 ± 1	180-212	2.89 ± 0.17
BUT.1	1.7 ± 0.1	9.2 ± 0.3	0.83 ± 0.02	39 ± 1	180-212	2.63 ± 0.15
BUT.2	1.7 ± 0.1	7.6 ± 0.2	0.95 ± 0.03	47 ± 1	180-212	2.62 ± 0.15
BUT.3	1.9 ± 0.1	8.3 ± 0.2	1.22 ± 0.04	59 ± 2	180-212	2.96 ± 0.18
BUT.4	1.8 ± 0.1	7.3 ± 0.2	1.24 ± 0.04	68 ± 2	180-212	2.88 ± 0.17
BUT.5	1.8 ± 0.1	5.2 ± 0.2	0.75 ± 0.02	39 ± 1	180-212	2.29 ± 0.13
SU-9	1.6 ± 0.0	9.5 ± 0.3	1.22 ± 0.04	59 ± 2	180-212	2.97 ± 0.18
BAR-1	1.7 ± 0.1	10.1 ± 0.3	1.15 ± 0.03	52 ± 2	180-212	2.98 ± 0.18
RA-K01	2.6 ± 0.1	15.3 ± 0.5	1.98 ± 0.06	105 ± 3	180-212	4.30 ± 0.28
RA-K02	4.5 ± 0.1	11.9 ± 0.4	2.13 ± 0.06	124 ± 4	180-212	4.65 ± 0.30
RA-K03	3.9 ± 0.1	11.8 ± 0.4	2.29 ± 0.07	128 ± 4	180-212	4.64 ± 0.30
RA-K04	3.2 ± 0.1	12.9 ± 0.4	2.30 ± 0.07	134 ± 4	180-212	4.56 ± 0.30
RA-K05	2.4 ± 0.1	11.7 ± 0.4	1.98 ± 0.06	106 ± 3	180-212	4.00 ± 0.26
RA-K06	2.2 ± 0.1	1.4 ± 0.0	1.97 ± 0.06	104 ± 3	180-212	3.20 ± 0.21
CA14-4	2.2 ± 0.1	11.9 ± 0.4	0.76 ± 0.02	44 ± 1	180-212	2.88 ± 0.17
CA14-7	2.0 ± 0.1	11.8 ± 0.4	1.11 ± 0.03	57 ± 2	180-212	3.13 ± 0.19
SJT01A	3.0 ± 0.1	10.9 ± 0.3	1.54 ± 0.05	77 ± 2	180-212	3.69 ± 0.23
SJT03	1.7 ± 0.1	8.3 ± 0.2	1.20 ± 0.04	66 ± 2	180-212	2.89 ± 0.17
SJT05	2.6 ± 0.1	12.7 ± 0.4	1.64 ± 0.05	102 ± 3	180-212	3.82 ± 0.24
SJT07	2.3 ± 0.1	10.8 ± 0.3	1.10 ± 0.03	63 ± 2	180-212	3.13 ± 0.19
SJT08	1.8 ± 0.1	9.4 ± 0.3	1.66 ± 0.05	88 ± 3	180-212	3.40 ± 0.21
SJT10	1.7 ± 0.1	10.9 ± 0.3	1.44 ± 0.04	62 ± 2	180-212	3.29 ± 0.20
SJT11	2.9 ± 0.1	15.6 ± 0.5	1.93 ± 0.06	94 ± 3	180-212	4.35 ± 0.28
SJT12	1.6 ± 0.0	8.2 ± 0.2	1.93 ± 0.06	88 ± 3	180-212	3.51 ± 0.22

Table S4: *Summary of kinetic and fitted parameters for all four IRSL temperatures, using kinetic parameters derived from four isothermal temperatures between 190 and 250 °C (Bouscary and King, 2022). Uncertainties are listed as 1σ for all values, except for D_e, for which errors are listed as 5 % of D_e. Fading rates are expressed both as ρ' and as g-values normalised to 2 days, g_{2d}, Huntley and Lamothe (2001). Saturated samples are shown in grey.*

Sample / IRSL		E_t [eV]	E_u [eV]	$\log_{10} s$ [s^{-1}]	$\log_{10}$ ρ' [-]	g_{2d} [%/dec.]	D_e [Gy]	D_0 [Gy]	$\tilde{n}_{nat}$ [-]
NG1	**50**	1.64 ± 0.08	0.09 ± 0.01	12.09 ± 0.77	-5.56 ± 0.04	3.90 ± 0.41	817 ± 41	459 ± 24	0.40 ± 0.03
	100	1.70 ± 0.14	0.11 ± 0.01	12.11 ± 1.34	-5.86 ± 0.19	2.12 ± 0.95	523 ± 26	350 ± 17	0.54 ± 0.04
	150	1.63 ± 0.19	0.10 ± 0.01	11.32 ± 1.85	-5.96 ± 0.23	1.57 ± 0.86	577 ± 29	466 ± 30	0.53 ± 0.03
	225	1.14 ± 0.13	0.12 ± 0.01	6.66 ± 1.23	<-7.00**	-0.44 ± -0.76	433 ± 22	360 ± 20	0.70 ± 0.04
NG2	**50**	1.56 ± 0.08	0.09 ± 0.01	10.91 ± 0.73	-5.56 ± 0.04	3.75 ± 0.33	732 ± 37	701 ± 22	0.31 ± 0.01
	100	1.55 ± 0.10	0.10 ± 0.01	10.59 ± 0.96	-5.58 ± 0.06	3.72 ± 0.48	1035 ± 52	561 ± 19	0.42 ± 0.02
	150	1.53 ± 0.13	0.08 ± 0.01	10.25 ± 1.19	-5.95 ± 0.09	1.64 ± 0.32	756 ± 38	560 ± 17	0.55 ± 0.03
	225	1.42 ± 0.10	0.07 ± 0.01	8.79 ± 0.92	-6.02 ± 0.07	1.43 ± 0.21	898 ± 45	492 ± 18	0.65 ± 0.03
NG3	**50**	1.50 ± 0.08	0.09 ± 0.01	10.58 ± 0.76	-5.70 ± 0.06	2.81 ± 0.38	606 ± 30	622 ± 28	0.37 ± 0.04
	100	1.43 ± 0.15	0.09 ± 0.01	9.70 ± 1.44	<-7.00**	-2.50 ± -2.35	337 ± 17	495 ± 19	0.49 ± 0.03
	150	1.78 ± 0.20	0.08 ± 0.01	12.99 ± 1.89	-5.59 ± 0.29	3.44 ± 2.29	1140 ± 57	683 ± 33	0.40 ± 0.04
	225	1.31 ± 0.13	0.06 ± 0.01	8.14 ± 1.18	-5.99 ± 0.83	1.54 ± 3.04	784 ± 39	512 ± 22	0.60 ± 0.07
NG4	**50**	1.49 ± 0.04	0.07 ± 0.01*	11.16 ± 0.40	-5.74 ± 0.04	2.61 ± 0.23	477 ± 24	514 ± 12	0.37 ± 0.01
	100	1.48 ± 0.05	0.07 ± 0.01	10.73 ± 0.53	-5.98 ± 0.13	1.60 ± 0.48	507 ± 25	507 ± 13	0.48 ± 0.01
	150	1.51 ± 0.07	0.07 ± 0.01	10.58 ± 0.69	-6.19 ± 0.15	0.95 ± 0.33	582 ± 29	605 ± 18	0.52 ± 0.03
	225	1.50 ± 0.07	0.07 ± 0.01*	9.84 ± 0.63	-6.24 ± 0.14	0.91 ± 0.28	769 ± 38	533 ± 18	0.65 ± 0.01
NG5	**50**	1.55 ± 0.05	0.08 ± 0.01	11.59 ± 0.52	-5.72 ± 0.04	2.81 ± 0.23	359 ± 18	476 ± 9	0.32 ± 0.02
	100	1.53 ± 0.06	0.08 ± 0.01*	10.94 ± 0.54	-6.05 ± 0.09	1.38 ± 0.27	357 ± 18	473 ± 9	0.42 ± 0.04
	150	1.53 ± 0.06	0.07 ± 0.01*	10.48 ± 0.57	-6.27 ± 0.14	0.84 ± 0.27	456 ± 23	547 ± 13	0.49 ± 0.02
	225	1.49 ± 0.07	0.08 ± 0.01*	9.56 ± 0.62	-7.00 ± 0.28	0.44 ± 0.26	557 ± 28	481 ± 16	0.64 ± 0.01
NG6	**50**	1.54 ± 0.06	0.07 ± 0.01	11.76 ± 0.57	-5.40 ± 0.03	5.32 ± 0.36	1022 ± 51	689 ± 29	0.26 ± 0.06
	100	1.56 ± 0.07	0.07 ± 0.01	11.48 ± 0.65	-5.58 ± 0.11	3.64 ± 0.88	902 ± 45	569 ± 14	0.39 ± 0.03
	150	1.57 ± 0.09	0.06 ± 0.01	11.11 ± 0.83	-5.73 ± 0.14	2.69 ± 0.82	1219 ± 61	614 ± 15	0.52 ± 0.05
	225	1.50 ± 0.09	0.08 ± 0.01	9.76 ± 0.87	-6.02 ± 0.26	1.37 ± 0.79	1101 ± 55	539 ± 17	0.67 ± 0.04
NG7	**50**	1.52 ± 0.05	0.09 ± 0.00	10.28 ± 0.50	-5.65 ± 0.08	3.10 ± 0.53	926 ± 46	567 ± 19	0.44 ± 0.07
	100	1.55 ± 0.07	0.08 ± 0.01*	10.44 ± 0.69	-5.88 ± 0.11	1.85 ± 0.46	1010 ± 51	413 ± 16	0.64 ± 0.09
	150	1.48 ± 0.07	0.07 ± 0.01*	9.76 ± 0.67	-5.94 ± 0.16	1.62 ± 0.60	973 ± 49	407 ± 15	0.66 ± 0.09
	225	1.64 ± 0.08	0.08 ± 0.01*	10.99 ± 0.75	-5.90 ± 0.14	1.81 ± 0.59	1235 ± 62	379 ± 14	0.68 ± 0.07
NG8	**50**	1.57 ± 0.06	0.08 ± 0.01	11.57 ± 0.60	-5.75 ± 0.07	2.49 ± 0.38	806 ± 40	441 ± 8	0.53 ± 0.01
	100	1.53 ± 0.07	0.08 ± 0.01	10.68 ± 0.71	-6.03 ± 0.14	1.32 ± 0.42	865 ± 43	508 ± 10	0.64 ± 0.02
	150	1.62 ± 0.09	0.07 ± 0.01	11.10 ± 0.85	-5.95 ± 0.13	1.58 ± 0.48	1429 ± 71	552 ± 14	0.68 ± 0.02
	225	1.70 ± 0.10	0.09 ± 0.01	11.31 ± 0.94	-6.08 ± 0.21	1.18 ± 0.54	1491 ± 75	468 ± 15	0.77 ± 0.01
NG10	**50**	1.52 ± 0.03	0.09 ± 0.01*	10.49 ± 0.29	-5.62 ± 0.04	3.28 ± 0.33	1404 ± 70	557 ± 12	0.48 ± 0.03
	100	1.51 ± 0.03	0.09 ± 0.01	10.34 ± 0.31	-5.85 ± 0.09	1.97 ± 0.40	1329 ± 66	478 ± 11	0.64 ± 0.02

	150	1.51 ± 0.03	0.08 ± 0.01*	10.05 ± 0.31	-5.87 ± 0.12	1.90 ± 0.51	2010 ± 101	516 ± 14	0.68 ± 0.03
	225	1.52 ± 0.06	0.09 ± 0.01	9.67 ± 0.49	-5.84 ± 0.13	1.99 ± 0.60	1867 ± 93	462 ± 17	0.73 ± 0.02
NG11	**50**	1.50 ± 0.05	0.08 ± 0.01*	10.19 ± 0.43	-5.73 ± 0.04	2.48 ± 0.24	826 ± 41	673 ± 21	0.43 ± 0.01*
	100	1.40 ± 0.15	0.08 ± 0.01	9.10 ± 1.39	-6.31 ± 0.29	0.70 ± 0.46	720 ± 36	482 ± 14	0.68 ± 0.01
	150	1.12 ± 0.13	0.05 ± 0.01	6.47 ± 1.26	-6.24 ± 0.52	0.82 ± 0.97	764 ± 38	469 ± 14	0.69 ± 0.02
	225	1.36 ± 0.16	0.07 ± 0.01	8.42 ± 1.52	-6.21 ± 0.52	0.83 ± 0.98	963 ± 48	463 ± 21	0.74 ± 0.08
BUT.1	**50**	1.43 ± 0.07	0.09 ± 0.01	9.44 ± 0.64	-5.58 ± 0.04	3.47 ± 0.34	517 ± 26	758 ± 25	0.24 ± 0.03
	100	1.56 ± 0.16	0.08 ± 0.01	10.66 ± 1.54	-5.63 ± 0.14	3.12 ± 1.02	801 ± 40	556 ± 29	0.41 ± 0.06
	150	1.59 ± 0.17	0.09 ± 0.01	10.77 ± 1.61	-5.39 ± 0.12	5.48 ± 1.54	1667 ± 83	492 ± 23	0.38 ± 0.02
	225	1.46 ± 0.11	0.08 ± 0.01	9.29 ± 0.99	-6.37 ± 0.75	0.59 ± 1.02	508 ± 25	389 ± 19	0.65 ± 0.01
BUT.2	**50**	1.54 ± 0.06	0.08 ± 0.01*	10.45 ± 0.54	-5.70 ± 0.05	2.64 ± 0.32	573 ± 29	663 ± 23	0.34 ± 0.07
	100	1.55 ± 0.09	0.08 ± 0.01	10.33 ± 0.82	-6.23 ± 0.28	0.83 ± 0.54	474 ± 24	507 ± 19	0.52 ± 0.06
	150	1.56 ± 0.10	0.07 ± 0.01	10.47 ± 0.97	-5.94 ± 0.13	1.54 ± 0.48	633 ± 32	523 ± 22	0.52 ± 0.03
	225	1.60 ± 0.10	0.08 ± 0.01	10.48 ± 0.93	-6.36 ± 0.21	0.60 ± 0.29	596 ± 30	407 ± 21	0.68 ± 0.02
BUT.3	**50**	1.53 ± 0.06	0.09 ± 0.01	10.90 ± 0.59	-5.68 ± 0.02	2.79 ± 0.11	514 ± 26	586 ± 20	0.33 ± 0.02
	100	1.55 ± 0.06	0.08 ± 0.01*	10.96 ± 0.57	-5.95 ± 0.08	1.51 ± 0.28	514 ± 26	461 ± 14	0.50 ± 0.01
	150	1.47 ± 0.06	0.07 ± 0.01*	9.92 ± 0.57	-6.29 ± 0.19	0.69 ± 0.31	539 ± 27	505 ± 17	0.57 ± 0.01
	225	1.50 ± 0.06	0.08 ± 0.01*	9.59 ± 0.59	-6.42 ± 0.24	0.52 ± 0.29	609 ± 30	445 ± 18	0.67 ± 0.01
BUT.4	**50**	1.54 ± 0.06	0.08 ± 0.01	11.20 ± 0.60	-5.68 ± 0.01	2.78 ± 0.10	442 ± 22	540 ± 11	0.32 ± 0.02
	100	1.52 ± 0.06	0.08 ± 0.01*	10.74 ± 0.53	-5.90 ± 0.06	1.70 ± 0.23	488 ± 24	520 ± 13	0.44 ± 0.01
	150	1.51 ± 0.06	0.08 ± 0.01*	10.24 ± 0.59	-6.06 ± 0.09	1.22 ± 0.26	578 ± 29	597 ± 16	0.49 ± 0.01
	225	1.53 ± 0.06	0.08 ± 0.01*	9.95 ± 0.54	-6.21 ± 0.08	0.85 ± 0.16	696 ± 35	532 ± 18	0.62 ± 0.02
BUT.5	**50**	1.38 ± 0.08	0.10 ± 0.01	9.04 ± 0.80	-5.58 ± 0.11	3.47 ± 0.84	414 ± 21	711 ± 26	0.22 ± 0.07
	100	1.50 ± 0.07	0.09 ± 0.01	9.96 ± 0.69	-6.24 ± 0.73	0.80 ± 1.30	350 ± 17	591 ± 24	0.38 ± 0.06
	150	1.42 ± 0.08	0.08 ± 0.01*	8.69 ± 0.72	-6.13 ± 0.39	1.04 ± 0.91	493 ± 25	599 ± 23	0.46 ± 0.05
	225	1.66 ± 0.08	0.09 ± 0.01*	10.55 ± 0.79	-5.76 ± 0.14	2.39 ± 0.79	970 ± 48	511 ± 22	0.53 ± 0.03
SU-9	**50**	1.57 ± 0.07	0.09 ± 0.01	11.20 ± 0.66	-5.52 ± 0.05	4.17 ± 0.46	476 ± 24	555 ± 14	0.26 ± 0.01
	100	1.51 ± 0.07	0.08 ± 0.01	10.49 ± 0.67	-5.85 ± 0.08	2.06 ± 0.40	429 ± 21	454 ± 13	0.42 ± 0.01*
	150	1.56 ± 0.07	0.07 ± 0.01*	10.58 ± 0.68	-6.01 ± 0.12	1.44 ± 0.39	495 ± 25	504 ± 17	0.48 ± 0.02
	225	1.55 ± 0.09	0.08 ± 0.01	10.00 ± 0.84	-6.16 ± 0.09	1.03 ± 0.21	560 ± 28	443 ± 17	0.60 ± 0.03
BAR-1	**50**	1.61 ± 0.08	0.09 ± 0.01	11.54 ± 0.79	-5.40 ± 0.04	5.42 ± 0.55	681 ± 34	584 ± 16	0.24 ± 0.03
	100	1.58 ± 0.08	0.08 ± 0.01	11.11 ± 0.77	-5.75 ± 0.05	2.51 ± 0.29	456 ± 23	483 ± 15	0.38 ± 0.03
	150	1.67 ± 0.11	0.08 ± 0.01	11.60 ± 1.02	-5.83 ± 0.07	2.11 ± 0.35	509 ± 25	528 ± 18	0.42 ± 0.02
	225	1.56 ± 0.10	0.08 ± 0.01	10.16 ± 0.91	-6.03 ± 0.11	1.43 ± 0.34	563 ± 28	455 ± 18	0.55 ± 0.02
RA-K01	**50**	1.48 ± 0.08	0.09 ± 0.01	10.16 ± 0.77	-5.38 ± 0.06	5.49 ± 0.81	2493 ± 125	708 ± 21	0.37 ± 0.02
	100	1.47 ± 0.09	0.08 ± 0.01	9.87 ± 0.84	-5.78 ± 0.07	2.39 ± 0.42	1301 ± 65	518 ± 14	0.59 ± 0.01
	150	1.41 ± 0.11	0.08 ± 0.01	9.16 ± 1.07	-5.98 ± 0.18	1.46 ± 0.59	1021 ± 51	529 ± 17	0.65 ± 0.02
	225	1.33 ± 0.11	0.07 ± 0.01	8.10 ± 1.07	-6.20 ± 0.19	0.90 ± 0.39	973 ± 49	461 ± 17	0.74 ± 0.01
RA-K02	**50**	1.56 ± 0.04	0.07 ± 0.01*	11.55 ± 0.44	-5.66 ± 0.04	2.95 ± 0.30	898 ± 45	488 ± 7	0.47 ± 0.02

	100	1.61 ± 0.05	0.08 ± 0.01*	11.30 ± 0.49	-5.89 ± 0.10	1.75 ± 0.39	815 ± 41	488 ± 5	0.58 ± 0.02
	150	1.63 ± 0.07	0.07 ± 0.01*	11.08 ± 0.63	-5.91 ± 0.10	1.69 ± 0.41	1129 ± 56	569 ± 11	0.62 ± 0.03
	225	1.52 ± 0.08	0.08 ± 0.01*	9.61 ± 0.72	-6.34 ± 0.25	0.64 ± 0.37	959 ± 48	496 ± 15	0.76 ± 0.02
RA-K03	**50**	1.57 ± 0.07	0.08 ± 0.01	11.36 ± 0.64	-5.60 ± 0.03	3.35 ± 0.27	1359 ± 68	543 ± 12	0.47 ± 0.01
	100	1.61 ± 0.05	0.08 ± 0.01*	11.40 ± 0.47	-5.92 ± 0.11	1.66 ± 0.42	867 ± 43	516 ± 12	0.59 ± 0.01
	150	1.62 ± 0.06	0.07 ± 0.01*	11.08 ± 0.61	-6.18 ± 0.16	0.92 ± 0.34	926 ± 46	582 ± 14	0.67 ± 0.01
	225	1.59 ± 0.07	0.08 ± 0.01*	10.45 ± 0.70	-6.02 ± 0.13	1.35 ± 0.39	1442 ± 72	517 ± 17	0.73 ± 0.01
RA-K04	**50**	1.41 ± 0.07	0.09 ± 0.01	9.43 ± 0.70	-5.64 ± 0.07	3.16 ± 0.54	2303 ± 115	526 ± 8	0.56 ± 0.04
	100	1.45 ± 0.09	0.08 ± 0.01	9.63 ± 0.81	-5.93 ± 0.13	1.61 ± 0.50	1180 ± 59	472 ± 6	0.67 ± 0.03
	150	1.40 ± 0.11	0.08 ± 0.01	9.05 ± 1.05	-6.07 ± 0.16	1.20 ± 0.43	1188 ± 59	538 ± 12	0.71 ± 0.01
	225	1.32 ± 0.11	0.07 ± 0.01	7.99 ± 1.05	-6.34 ± 0.27	0.64 ± 0.40	1145 ± 57	470 ± 14	0.81 ± 0.01
RA-K05	**50**	1.54 ± 0.05	0.07 ± 0.01*	11.39 ± 0.47	-5.75 ± 0.07	2.44 ± 0.40	701 ± 35	461 ± 8	0.49 ± 0.02
	100	1.58 ± 0.05	0.08 ± 0.01*	11.16 ± 0.50	-6.23 ± 0.17	0.82 ± 0.32	697 ± 35	460 ± 6	0.67 ± 0.02
	150	1.58 ± 0.06	0.07 ± 0.01*	10.60 ± 0.59	-6.47 ± 0.32	0.49 ± 0.35	861 ± 43	526 ± 11	0.74 ± 0.03
	225	1.45 ± 0.07	0.08 ± 0.01*	8.96 ± 0.68	-7.00 ± 0.59	0.30 ± 0.39	957 ± 48	477 ± 13	0.82 ± 0.01
RA-K06	**50**	1.44 ± 0.13	0.07 ± 0.01	9.15 ± 1.24	-5.67 ± 0.08	2.90 ± 0.56	1624 ± 81	442 ± 9	0.62 ± 0.08
	100	1.36 ± 0.12	0.07 ± 0.01	8.42 ± 1.12	-5.95 ± 0.16	1.54 ± 0.57	1390 ± 70	472 ± 7	0.70 ± 0.03
	150	1.35 ± 0.12	0.07 ± 0.01	8.31 ± 1.10	-6.02 ± 0.15	1.31 ± 0.45	1642 ± 82	532 ± 12	0.74 ± 0.01
	225	1.32 ± 0.11	0.07 ± 0.01	8.01 ± 1.06	-6.31 ± 0.37	0.70 ± 0.60	1361 ± 68	470 ± 15	0.83 ± 0.01
CA14-4	**50**	1.72 ± 0.07	0.08 ± 0.01	13.22 ± 0.64	-5.40 ± 0.07	5.59 ± 0.85	975 ± 49	397 ± 24	0.31 ± 0.06
	100	1.67 ± 0.19	0.07 ± 0.01	12.18 ± 1.78	-5.38 ± 0.15	5.56 ± 1.86	1101 ± 55	343 ± 22	0.42 ± 0.07
	150	1.87 ± 0.24	0.06 ± 0.01	13.68 ± 2.32	-5.39 ± 0.27	4.93 ± 3.03	1232 ± 62	411 ± 9	0.54 ± 0.01*
	225	2.23 ± 0.47	0.09 ± 0.02	16.47 ± 4.42	-5.37 ± 0.19	5.54 ± 2.42	1219 ± 61	410 ± 16	0.55 ± 0.01*
CA14-7	**50**	1.70 ± 0.07	0.09 ± 0.01	12.35 ± 0.69	-5.44 ± 0.05	5.01 ± 0.60	1090 ± 54	587 ± 55	0.31 ± 0.04
	100	1.45 ± 0.11	0.08 ± 0.01	9.86 ± 1.01	-5.89 ± 0.16	1.82 ± 0.67	491 ± 25	430 ± 16	0.48 ± 0.01
	150	1.99 ± 0.19	0.09 ± 0.01	14.91 ± 1.81	-5.93 ± 0.17	1.66 ± 0.65	509 ± 25	443 ± 14	0.50 ± 0.03
	225	1.48 ± 0.15	0.07 ± 0.01	9.61 ± 1.39	-6.36 ± 0.36	0.62 ± 0.53	524 ± 26	412 ± 17	0.64 ± 0.01
SJT01A	**50**	1.52 ± 0.07	0.08 ± 0.01	11.05 ± 0.70	-5.45 ± 0.02	4.90 ± 0.23	855 ± 43	550 ± 10	0.30 ± 0.01
	100	1.53 ± 0.06	0.08 ± 0.01	10.79 ± 0.60	-5.66 ± 0.02	3.11 ± 0.17	892 ± 45	578 ± 12	0.44 ± 0.01
	150	1.55 ± 0.06	0.08 ± 0.01*	10.54 ± 0.60	-5.83 ± 0.03	2.13 ± 0.16	1036 ± 52	620 ± 16	0.55 ± 0.01*
	225	1.57 ± 0.06	0.08 ± 0.01*	10.14 ± 0.56	-5.97 ± 0.03	1.54 ± 0.10	1206 ± 60	520 ± 17	0.68 ± 0.01
SJT03	**50**	1.53 ± 0.07	0.08 ± 0.01	11.20 ± 0.66	-5.51 ± 0.02	4.33 ± 0.21	540 ± 27	497 ± 12	0.29 ± 0.01
	100	1.56 ± 0.05	0.07 ± 0.01*	11.24 ± 0.52	-5.68 ± 0.01	2.98 ± 0.11	602 ± 30	565 ± 13	0.37 ± 0.02
	150	1.59 ± 0.06	0.08 ± 0.01*	11.08 ± 0.55	-5.81 ± 0.03	2.21 ± 0.15	754 ± 38	595 ± 16	0.47 ± 0.01
	225	1.59 ± 0.06	0.08 ± 0.01*	10.51 ± 0.58	-5.98 ± 0.03	1.51 ± 0.12	881 ± 44	494 ± 16	0.63 ± 0.02
SJT05	**50**	1.52 ± 0.07	0.08 ± 0.01	11.12 ± 0.69	-5.47 ± 0.02	4.68 ± 0.20	557 ± 28	531 ± 10	0.27 ± 0.01
	100	1.53 ± 0.07	0.07 ± 0.01	10.82 ± 0.67	-5.66 ± 0.02	3.09 ± 0.16	664 ± 33	599 ± 15	0.37 ± 0.01
	150	1.58 ± 0.08	0.07 ± 0.01*	10.88 ± 0.74	-5.73 ± 0.02	2.64 ± 0.13	971 ± 49	631 ± 19	0.48 ± 0.01
	225	1.55 ± 0.07	0.08 ± 0.01*	10.00 ± 0.69	-5.89 ± 0.04	1.87 ± 0.18	1157 ± 58	512 ± 18	0.63 ± 0.01*

SJT07	**50**	1.53 ± 0.06	0.08 ± 0.01	11.22 ± 0.61	-5.50 ± 0.02	4.37 ± 0.23	492 ± 25	485 ± 9	0.28 ± 0.01*
	100	1.57 ± 0.05	0.08 ± 0.01*	11.22 ± 0.53	-5.65 ± 0.02	3.16 ± 0.13	588 ± 29	549 ± 12	0.36 ± 0.01*
	150	1.61 ± 0.06	0.08 ± 0.01*	11.18 ± 0.56	-5.75 ± 0.02	2.52 ± 0.11	795 ± 40	588 ± 14	0.46 ± 0.01*
	225	1.63 ± 0.06	0.08 ± 0.01*	10.81 ± 0.58	-5.92 ± 0.03	1.74 ± 0.12	925 ± 46	500 ± 16	0.61 ± 0.01
SJT08	**50**	1.60 ± 0.07	0.08 ± 0.01	11.79 ± 0.65	-5.32 ± 0.03	6.61 ± 0.48	1371 ± 69	501 ± 12	0.26 ± 0.01
	100	1.54 ± 0.07	0.08 ± 0.01	10.89 ± 0.63	-5.66 ± 0.04	3.13 ± 0.26	622 ± 31	550 ± 15	0.38 ± 0.01
	150	1.61 ± 0.08	0.08 ± 0.01	11.15 ± 0.77	-5.81 ± 0.07	2.27 ± 0.33	759 ± 38	591 ± 18	0.48 ± 0.01
	225	1.55 ± 0.08	0.08 ± 0.01*	10.10 ± 0.72	-5.98 ± 0.08	1.53 ± 0.27	834 ± 42	502 ± 18	0.61 ± 0.01*
SJT10	**50**	1.56 ± 0.06	0.08 ± 0.01	11.53 ± 0.61	-5.36 ± 0.05	5.95 ± 0.69	2527 ± 126	521 ± 13	0.30 ± 0.02
	100	1.56 ± 0.06	0.08 ± 0.01*	11.10 ± 0.59	-5.78 ± 0.06	2.39 ± 0.32	649 ± 32	541 ± 14	0.45 ± 0.01
	150	1.59 ± 0.06	0.07 ± 0.01*	10.89 ± 0.57	-5.87 ± 0.10	1.95 ± 0.46	842 ± 42	570 ± 16	0.54 ± 0.01
	225	1.58 ± 0.06	0.08 ± 0.01*	10.24 ± 0.52	-6.04 ± 0.07	1.33 ± 0.21	921 ± 46	484 ± 17	0.67 ± 0.01
SJT11	**50**	1.57 ± 0.06	0.08 ± 0.01	11.58 ± 0.61	-5.31 ± 0.06	6.71 ± 0.85	1189 ± 59	585 ± 16	0.24 ± 0.01
	100	1.53 ± 0.06	0.08 ± 0.01*	10.70 ± 0.59	-5.68 ± 0.04	3.00 ± 0.30	677 ± 34	594 ± 16	0.39 ± 0.02
	150	1.56 ± 0.06	0.08 ± 0.01*	10.53 ± 0.61	-5.85 ± 0.05	2.09 ± 0.21	823 ± 41	610 ± 20	0.51 ± 0.03
	225	1.51 ± 0.06	0.08 ± 0.01*	9.52 ± 0.59	-6.00 ± 0.05	1.50 ± 0.17	989 ± 49	501 ± 19	0.66 ± 0.01
SJT12	**50**	1.57 ± 0.07	0.09 ± 0.01	11.29 ± 0.68	-5.42 ± 0.04	5.29 ± 0.55	934 ± 47	558 ± 14	0.29 ± 0.02
	100	1.57 ± 0.07	0.08 ± 0.01	11.00 ± 0.69	-5.68 ± 0.03	2.99 ± 0.21	741 ± 37	544 ± 14	0.43 ± 0.01
	150	1.59 ± 0.08	0.08 ± 0.01*	10.79 ± 0.73	-5.86 ± 0.05	2.04 ± 0.25	787 ± 39	572 ± 17	0.51 ± 0.01
	225	1.47 ± 0.07	0.07 ± 0.01*	9.28 ± 0.61	-6.01 ± 0.04	1.45 ± 0.14	887 ± 44	488 ± 17	0.64 ± 0.01

* Uncertainties < 0.005.

** Values of $\log_{10} \rho$' below -7.00, arbitrarily fixes at -7.00.

Table S5: *Saturation indicator values, and age of the samples for all four IRSL temperatures. Saturated samples are shown in grey.*

Sample / IRSL		$\tilde{n}_{nat}$ [-]	$0.86 * \tilde{n}_{SS}$ [-]	$0.86 * \tilde{n}_{20}$ [-]	D_e [Gy]	$2.D_0$ [Gy]	Age [ka]
NG1	50	0.40 ± 0.03	0.40 ± 0.04	0.36 ± 0.02	817 ± 41	918 ± 48	285 (- 58 / + 93)
	100	0.54 ± 0.04	0.59 ± 0.13	0.54 ± 0.03	523 ± 26	700 ± 33	183 (- 26 / + 33)
	150	0.53 ± 0.03	0.64 ± 0.14	0.57 ± 0.03	577 ± 29	931 ± 60	201 (- 23 / + 27)
	225	0.70 ± 0.04	0.86 ± 0.01*	0.20 ± 0.01	433 ± 22	720 ± 41	151 (- 17 / + 20)
NG2	50	0.31 ± 0.01	0.40 ± 0.03	0.35 ± 0.02	732 ± 37	1403 ± 45	207 (- 16 / + 18)
	100	0.42 ± 0.02	0.42 ± 0.05	0.36 ± 0.02	1035 ± 52	1122 ± 38	293 (- 45 / + 63)
	150	0.55 ± 0.03	0.63 ± 0.05	0.57 ± 0.03	756 ± 38	1120 ± 34	214 (- 22 / + 25)
	225	0.65 ± 0.03	0.66 ± 0.03	0.59 ± 0.03	898 ± 45	983 ± 35	254 (- 29 / + 37)
NG3	50	0.37 ± 0.04	0.49 ± 0.04	0.38 ± 0.02	606 ± 30	1245 ± 57	215 (- 36 / + 43)
	100	0.49 ± 0.03	0.86 ± 0.01*	0.61 ± 0.04	337 ± 17	989 ± 37	119 (- 9 / + 10)
	150	0.40 ± 0.04	0.42 ± 0.24	0.40 ± 0.02	1140 ± 57	1367 ± 67	404 (- 87 / + 140)
	225	0.60 ± 0.07	0.65 ± 0.60	0.48 ± 0.03	784 ± 39	1025 ± 44	278 (- 62 / + 95)
NG4	50	0.37 ± 0.01	0.52 ± 0.03	0.39 ± 0.02	477 ± 24	1028 ± 24	162 (- 7 / + 8)
	100	0.48 ± 0.01	0.64 ± 0.07	0.50 ± 0.03	507 ± 25	1013 ± 26	172 (- 4 / + 4)
	150	0.52 ± 0.03	0.72 ± 0.06	0.61 ± 0.04	582 ± 29	1210 ± 36	197 (- 18 / + 20)
	225	0.65 ± 0.01	0.73 ± 0.05	0.66 ± 0.04	769 ± 38	1066 ± 37	260 (- 10 / + 10)
NG5	50	0.32 ± 0.02	0.50 ± 0.03	0.41 ± 0.02	359 ± 18	953 ± 19	145 (- 11 / + 12)
	100	0.42 ± 0.04	0.67 ± 0.04	0.57 ± 0.03	357 ± 18	946 ± 19	144 (- 19 / + 21)
	150	0.49 ± 0.02	0.74 ± 0.05	0.66 ± 0.04	456 ± 23	1093 ± 27	184 (- 12 / + 12)
	225	0.64 ± 0.01	0.80 ± 0.06	0.74 ± 0.04	557 ± 28	963 ± 31	225 (- 5 / + 5)
NG6	50	0.26 ± 0.06	0.28 ± 0.03	0.22 ± 0.01	1022 ± 51	1377 ± 58	432 (- 170 / + 534)
	100	0.39 ± 0.03	0.41 ± 0.09	0.35 ± 0.02	902 ± 45	1139 ± 27	381 (- 61 / + 83)
	150	0.52 ± 0.05	0.51 ± 0.10	0.47 ± 0.03	1219 ± 61	1229 ± 29	515 (- 124 / + 255)
	225	0.67 ± 0.04	0.66 ± 0.15	0.59 ± 0.03	1101 ± 55	1078 ± 34	465 (- 81 / + 128)
NG7	50	0.44 ± 0.07	0.46 ± 0.06	0.39 ± 0.02	926 ± 46	1135 ± 38	385 (- 118 / + 258)
	100	0.64 ± 0.09	0.60 ± 0.07	0.54 ± 0.03	1010 ± 51	826 ± 33	420 (- 163 / + 308)
	150	0.66 ± 0.09	0.62 ± 0.10	0.56 ± 0.03	973 ± 49	813 ± 30	404 (- 146 / + 355)
	225	0.68 ± 0.07	0.61 ± 0.09	0.58 ± 0.03	1235 ± 62	758 ± 28	513 (- 196 / + 146)
NG8	50	0.53 ± 0.01	0.53 ± 0.05	0.46 ± 0.03	806 ± 40	883 ± 17	199 (- 9 / + 9)
	100	0.64 ± 0.02	0.67 ± 0.07	0.59 ± 0.03	865 ± 43	1017 ± 19	213 (- 14 / + 16)
	150	0.68 ± 0.02	0.63 ± 0.08	0.60 ± 0.04	1429 ± 71	1105 ± 27	352 (- 43 / + 63)
	225	0.77 ± 0.01	0.69 ± 0.10	0.67 ± 0.04	1491 ± 75	936 ± 30	367 (- 43 / + 70)
NG10	50	0.48 ± 0.03	0.44 ± 0.04	0.37 ± 0.02	1404 ± 70	1113 ± 24	389 (- 76 / + 164)
	100	0.64 ± 0.02	0.58 ± 0.06	0.50 ± 0.03	1329 ± 66	955 ± 22	368 (- 55 / + 96)
	150	0.68 ± 0.03	0.59 ± 0.08	0.53 ± 0.03	2010 ± 101	1032 ± 28	557 (- 157 / + 147)
	225	0.73 ± 0.02	0.58 ± 0.09	0.53 ± 0.03	1867 ± 93	925 ± 33	517 (- 39 / + 25)
NG11	50	0.43 ± 0.01*	0.51 ± 0.03	0.44 ± 0.03	826 ± 41	1345 ± 42	286 (- 4 / + 4)

	100	0.68 ± 0.01	0.75 ± 0.10	0.59 ± 0.03	720 ± 36	963 ± 27	249 (- 12 / + 13)
	150	0.69 ± 0.02	0.73 ± 0.26	0.21 ± 0.01	764 ± 38	938 ± 28	265 (- 22 / + 25)
	225	0.74 ± 0.08	0.73 ± 0.27	0.61 ± 0.04	963 ± 48	926 ± 41	334 (- 88 / + 217)
BUT.1	**50**	0.24 ± 0.03	0.41 ± 0.03	0.30 ± 0.02	517 ± 26	1515 ± 49	197 (- 28 / + 31)
	100	0.41 ± 0.06	0.45 ± 0.12	0.40 ± 0.02	801 ± 40	1112 ± 58	305 (- 81 / + 136)
	150	0.38 ± 0.02	0.28 ± 0.10	0.26 ± 0.01	1667 ± 83	985 ± 45	635 (- 40 / + 24)
	225	0.65 ± 0.01	0.76 ± 0.37	0.68 ± 0.04	508 ± 25	779 ± 37	193 (- 8 / + 9)
BUT.2	**50**	0.34 ± 0.07	0.49 ± 0.04	0.43 ± 0.02	573 ± 29	1327 ± 47	219 (- 61 / + 82)
	100	0.52 ± 0.06	0.73 ± 0.12	0.66 ± 0.04	474 ± 24	1015 ± 39	181 (- 32 / + 39)
	150	0.52 ± 0.03	0.63 ± 0.08	0.59 ± 0.03	633 ± 32	1047 ± 45	242 (- 29 / + 34)
	225	0.68 ± 0.02	0.76 ± 0.06	0.73 ± 0.04	596 ± 30	814 ± 42	227 (- 12 / + 13)
BUT.3	**50**	0.33 ± 0.02	0.48 ± 0.01	0.39 ± 0.02	514 ± 26	1171 ± 39	174 (- 14 / + 15)
	100	0.50 ± 0.01	0.63 ± 0.05	0.55 ± 0.03	514 ± 26	923 ± 27	174 (- 8 / + 9)
	150	0.57 ± 0.01	0.75 ± 0.06	0.65 ± 0.04	539 ± 27	1011 ± 34	182 (- 4 / + 4)
	225	0.67 ± 0.01	0.77 ± 0.07	0.71 ± 0.04	609 ± 30	890 ± 36	206 (- 5 / + 5)
BUT.4	**50**	0.32 ± 0.02	0.48 ± 0.01	0.40 ± 0.02	442 ± 22	1079 ± 21	154 (- 15 / + 16)
	100	0.44 ± 0.01	0.61 ± 0.03	0.52 ± 0.03	488 ± 24	1039 ± 25	170 (- 7 / + 7)
	150	0.49 ± 0.01	0.67 ± 0.04	0.59 ± 0.03	578 ± 29	1194 ± 33	201 (- 6 / + 6)
	225	0.62 ± 0.02	0.72 ± 0.03	0.66 ± 0.04	696 ± 35	1063 ± 35	242 (- 13 / + 14)
BUT.5	**50**	0.22 ± 0.07	0.41 ± 0.09	0.24 ± 0.01	414 ± 21	1422 ± 52	181 (- 71 / + 93)
	100	0.38 ± 0.06	0.73 ± 0.42	0.60 ± 0.03	350 ± 17	1183 ± 49	152 (- 33 / + 38)
	150	0.46 ± 0.05	0.70 ± 0.21	0.58 ± 0.03	493 ± 25	1199 ± 45	215 (- 33 / + 37)
	225	0.53 ± 0.03	0.53 ± 0.11	0.50 ± 0.03	970 ± 48	1021 ± 45	423 (- 56 / + 76)
SU-9	**50**	0.26 ± 0.01	0.37 ± 0.04	0.32 ± 0.02	476 ± 24	1110 ± 27	160 (- 5 / + 5)
	100	0.42 ± 0.01*	0.58 ± 0.05	0.51 ± 0.03	429 ± 21	908 ± 26	144 (- 2 / + 2)
	150	0.48 ± 0.02	0.66 ± 0.06	0.61 ± 0.04	495 ± 25	1008 ± 34	167 (- 9 / + 10)
	225	0.60 ± 0.03	0.71 ± 0.04	0.67 ± 0.04	560 ± 28	886 ± 34	189 (- 16 / + 18)
BAR-1	**50**	0.24 ± 0.03	0.29 ± 0.04	0.25 ± 0.01	681 ± 34	1168 ± 31	229 (- 44 / + 58)
	100	0.38 ± 0.03	0.53 ± 0.03	0.48 ± 0.03	456 ± 23	965 ± 30	153 (- 21 / + 24)
	150	0.42 ± 0.02	0.57 ± 0.05	0.55 ± 0.03	509 ± 25	1056 ± 36	171 (- 16 / + 17)
	225	0.55 ± 0.02	0.66 ± 0.05	0.63 ± 0.04	563 ± 28	909 ± 36	189 (- 14 / + 15)
RA-K01	**50**	0.37 ± 0.02	0.28 ± 0.05	0.23 ± 0.01	2493 ± 125	1416 ± 42	579 (- 46 / + 26)
	100	0.59 ± 0.01	0.55 ± 0.05	0.48 ± 0.03	1301 ± 65	1036 ± 28	302 (- 31 / + 42)
	150	0.65 ± 0.02	0.64 ± 0.10	0.54 ± 0.03	1021 ± 51	1058 ± 33	237 (- 24 / + 29)
	225	0.74 ± 0.01	0.73 ± 0.07	0.60 ± 0.03	973 ± 49	923 ± 34	226 (- 10 / + 11)
RA-K02	**50**	0.47 ± 0.02	0.47 ± 0.03	0.42 ± 0.02	898 ± 45	976 ± 13	193 (- 23 / + 29)
	100	0.58 ± 0.02	0.61 ± 0.06	0.57 ± 0.03	815 ± 41	976 ± 11	175 (- 16 / + 19)
	150	0.62 ± 0.03	0.61 ± 0.06	0.60 ± 0.03	1129 ± 56	1137 ± 22	243 (- 30 / + 40)
	225	0.76 ± 0.02	0.76 ± 0.08	0.71 ± 0.04	959 ± 48	991 ± 30	206 (- 14 / + 16)
RA-K03	**50**	0.47 ± 0.01	0.44 ± 0.03	0.38 ± 0.02	1359 ± 68	1086 ± 25	293 (- 27 / + 35)

	100	0.59 ± 0.01	0.62 ± 0.06	0.58 ± 0.03	867 ± 43	1032 ± 24	187 (- 11 / + 12)
	150	0.67 ± 0.01	0.72 ± 0.06	0.69 ± 0.04	926 ± 46	1165 ± 27	199 (- 6 / + 6)
	225	0.73 ± 0.01	0.66 ± 0.06	0.64 ± 0.04	1442 ± 72	1035 ± 34	310 (- 20 / + 25)
RA-K04	**50**	0.56 ± 0.04	0.46 ± 0.06	0.35 ± 0.02	2303 ± 115	1052 ± 17	505 (- 127 / + 77)
	100	0.67 ± 0.03	0.63 ± 0.08	0.54 ± 0.03	1180 ± 59	944 ± 12	259 (- 38 / + 62)
	150	0.71 ± 0.01	0.68 ± 0.08	0.57 ± 0.03	1188 ± 59	1076 ± 24	260 (- 17 / + 20)
	225	0.81 ± 0.01	0.76 ± 0.09	0.61 ± 0.04	1145 ± 57	941 ± 27	251 (- 7 / + 8)
RA-K05	**50**	0.49 ± 0.02	0.53 ± 0.05	0.45 ± 0.03	701 ± 35	922 ± 16	175 (- 16 / + 19)
	100	0.67 ± 0.02	0.73 ± 0.06	0.67 ± 0.04	697 ± 35	920 ± 12	174 (- 10 / + 12)
	150	0.74 ± 0.03	0.78 ± 0.09	0.74 ± 0.04	861 ± 43	1053 ± 22	215 (- 18 / + 21)
	225	0.82 ± 0.01	0.81 ± 0.14	0.76 ± 0.04	957 ± 48	954 ± 27	239 (- 10 / + 11)
RA-K06	**50**	0.62 ± 0.08	0.48 ± 0.06	0.44 ± 0.03	1624 ± 81	884 ± 19	507 (- 1 / + 50)
	100	0.70 ± 0.03	0.63 ± 0.09	0.53 ± 0.03	1390 ± 70	943 ± 14	434 (- 81 / + 199)
	150	0.74 ± 0.01	0.66 ± 0.08	0.54 ± 0.03	1642 ± 82	1064 ± 25	513 (- 43 / + 59)
	225	0.83 ± 0.01	0.75 ± 0.15	0.59 ± 0.03	1361 ± 68	940 ± 29	425 (- 31 / + 40)
CA14-4	**50**	0.31 ± 0.06	0.29 ± 0.06	0.27 ± 0.02	975 ± 49	795 ± 47	339 (- 157 / + 169)
	100	0.42 ± 0.07	0.28 ± 0.13	0.27 ± 0.02	1101 ± 55	685 ± 44	382 (- 94 / + 20)
	150	0.54 ± 0.01*	0.28 ± 0.22	0.28 ± 0.02	1232 ± 62	821 ± 18	428 (- inf / + inf)
	225	0.55 ± 0.01*	0.27 ± 0.16	0.27 ± 0.02	1219 ± 61	820 ± 32	423 (- inf / + inf)
CA14-7	**50**	0.31 ± 0.04	0.31 ± 0.04	0.29 ± 0.02	1090 ± 54	1174 ± 109	348 (- 101 / + 258)
	100	0.48 ± 0.01	0.60 ± 0.11	0.51 ± 0.03	491 ± 25	859 ± 33	157 (- 9 / + 9)
	150	0.50 ± 0.03	0.62 ± 0.11	0.62 ± 0.04	509 ± 25	886 ± 29	162 (- 20 / + 23)
	225	0.64 ± 0.01	0.76 ± 0.13	0.70 ± 0.04	524 ± 26	824 ± 33	167 (- 7 / + 8)
SJT01A	**50**	0.30 ± 0.01	0.32 ± 0.02	0.26 ± 0.02	855 ± 43	1100 ± 19	232 (- 14 / + 16)
	100	0.44 ± 0.01	0.47 ± 0.02	0.41 ± 0.02	892 ± 45	1157 ± 24	242 (- 8 / + 9)
	150	0.55 ± 0.01*	0.57 ± 0.02	0.53 ± 0.03	1036 ± 52	1241 ± 32	280 (- 3 / + 3)
	225	0.68 ± 0.01	0.64 ± 0.01	0.61 ± 0.04	1206 ± 60	1040 ± 34	327 (- 14 / + 16)
SJT03	**50**	0.29 ± 0.01	0.36 ± 0.02	0.29 ± 0.02	540 ± 27	994 ± 23	187 (- 16 / + 18)
	100	0.37 ± 0.02	0.48 ± 0.01	0.42 ± 0.02	602 ± 30	1130 ± 26	208 (- 16 / + 18)
	150	0.47 ± 0.01	0.56 ± 0.02	0.52 ± 0.03	754 ± 38	1191 ± 31	261 (- 13 / + 14)
	225	0.63 ± 0.02	0.64 ± 0.02	0.61 ± 0.04	881 ± 44	989 ± 33	304 (- 20 / + 23)
SJT05	**50**	0.27 ± 0.01	0.34 ± 0.02	0.28 ± 0.02	557 ± 28	1062 ± 20	146 (- 6 / + 6)
	100	0.37 ± 0.01	0.47 ± 0.02	0.41 ± 0.02	664 ± 33	1199 ± 29	174 (- 9 / + 10)
	150	0.48 ± 0.01	0.52 ± 0.01	0.49 ± 0.03	971 ± 49	1263 ± 37	254 (- 16 / + 17)
	225	0.63 ± 0.01*	0.60 ± 0.02	0.57 ± 0.03	1157 ± 58	1023 ± 36	303 (- 7 / + 7)
SJT07	**50**	0.28 ± 0.01*	0.36 ± 0.02	0.29 ± 0.02	492 ± 25	970 ± 17	157 (- 3 / + 3)
	100	0.36 ± 0.01*	0.46 ± 0.01	0.41 ± 0.02	588 ± 29	1098 ± 23	188 (- 3 / + 3)
	150	0.46 ± 0.01*	0.53 ± 0.01	0.49 ± 0.03	795 ± 40	1177 ± 29	254 (- 2 / + 2)
	225	0.61 ± 0.01	0.62 ± 0.02	0.59 ± 0.03	925 ± 46	1001 ± 33	296 (- 10 / + 10)
SJT 08	**50**	0.26 ± 0.01	0.23 ± 0.03	0.21 ± 0.01	1371 ± 69	1001 ± 24	403 (- 46 / + 70)

	100	0.38 ± 0.01	0.47 ± 0.03	0.41 ± 0.02	622 ± 31	1100 ± 31	183 (- 11 / + 12)
	150	0.48 ± 0.01	0.56 ± 0.04	0.53 ± 0.03	759 ± 38	1182 ± 36	223 (- 7 / + 8)
	225	0.61 ± 0.01*	0.65 ± 0.04	0.61 ± 0.04	834 ± 42	1005 ± 37	245 (- 5 / + 5)
SJT10	**50**	0.30 ± 0.02	0.26 ± 0.04	0.22 ± 0.01	2527 ± 126	1042 ± 25	768 (- 355 / + 124)
	100	0.45 ± 0.01	0.54 ± 0.04	0.48 ± 0.03	649 ± 32	1082 ± 28	197 (- 10 / + 11)
	150	0.54 ± 0.01	0.59 ± 0.07	0.55 ± 0.03	842 ± 42	1139 ± 32	256 (- 12 / + 13)
	225	0.67 ± 0.01	0.67 ± 0.03	0.64 ± 0.04	921 ± 46	967 ± 35	280 (- 16 / + 18)
SJT11	**50**	0.24 ± 0.01	0.23 ± 0.05	0.20 ± 0.01	1189 ± 59	1171 ± 31	273 (- 21 / + 25)
	100	0.39 ± 0.02	0.49 ± 0.03	0.43 ± 0.02	677 ± 34	1188 ± 31	155 (- 16 / + 18)
	150	0.51 ± 0.03	0.58 ± 0.03	0.54 ± 0.03	823 ± 41	1219 ± 40	189 (- 19 / + 22)
	225	0.66 ± 0.01	0.65 ± 0.02	0.62 ± 0.04	989 ± 49	1001 ± 38	227 (- 12 / + 14)
SJT12	**50**	0.29 ± 0.02	0.30 ± 0.04	0.26 ± 0.02	934 ± 47	1116 ± 29	266 (- 44 / + 63)
	100	0.43 ± 0.01	0.48 ± 0.02	0.43 ± 0.03	741 ± 37	1088 ± 28	211 (- 8 / + 9)
	150	0.51 ± 0.01	0.58 ± 0.03	0.55 ± 0.03	787 ± 39	1145 ± 34	224 (- 11 / + 12)
	225	0.64 ± 0.01	0.66 ± 0.02	0.62 ± 0.04	887 ± 44	977 ± 35	253 (- 13 / + 15)

* Uncertainties < 0.005.

Table S6: *Samples with their reference thrust, geographical distance to the Main Frontal Thrust (MFT), and stratigraphic burial depth and associated maximum burial temperature, derived from the stratigraphic location of the sample today, and cross-section reconstruction.*

Sample	Reference thrust sheet	Geographical distance to MFT [km]	Stratigraphic burial depth [km]	Maximum burial temperature [°C]	Reference cross-section
NG1	MFT	-2.2	4.2	104	Hirschmiller et al., 2014 Mugnier et al., 1995
NG2	MFT 2	3.4	4.7	114	
NG3	MFT 2	4.8	3.9	97	
NG4	MFT 2	5.8	3.3	86	
NG5	MFT 2	7.0	2.6	73	
NG6	IST	9.2	3.0	80	
NG7	IST	12.4	2.5	70	
NG8	IST 2	19.6	4.0	100	
NG10	IST 2	24.5	3.6	92	
NG11	IST 2	25.0	2.9	78	
BUT.1	MFT	1.6	4.7	114	No cross-section published, J. Lavé measurements
BUT.2	MFT	2.2	4.5	110	
BUT.3	MFT	3.1	4.1	101	
BUT.4	MFT	3.8	3.6	92	
BUT.5	MFT	4.5	3.1	82	
SU-9	MFT	1.5	5.0	120	Lavé and Avouac, 2000 Lavé and Avouac, 2001
BAR-1	MFT	1.5	5.0	120	
RA-K01	IST	15.0	3.3	86	Hirschmiller et al., 2014
RA-K02	IST	15.6	2.7	74	
RA-K03	IST	16.6	2.1	62	
RA-K04	IST	16.5	1.3	46	
RA-K05	IST	19.0	0.8	36	
RA-K06	IST	19.8	0.3	26	
CA14-4	MFT	3.3	4.0	100	Lavé and Avouac, 2001
CA14-7	MFT	3.8	3.5	90	
SJT01A	MFT	1.8	1.9	67.1*	Coutand et al., 2016 Hirschmiller et al., 2014
SJT03	MFT	3.1	1.6	67.1*	
SJT05	MFT	3.8	1.3	67.1*	
SJT07	MFT	3.7	0.9	67.1*	
SJT08	MFT	3.6	0.6	67.1*	
SJT10	MFT	4.0	0.3	67.1*	
SJT11	MFT	4.3	0.2	92.4*	
SJT12	MFT	4.6	0.1	92.4*	

*From vitrinite reflectance data, Coutand et al., 2016.

Table S7: *Samples with their IRSL signal specific exhumation rate, and their sample specific exhumation rate, i.e., the average of the non-saturated IRSL signal specific exhumation rates.*

Sample	IRSL signal specific exhumation rate [mm/yr]				Sample specific = average exhumation rate [mm/yr]
	IRSL.50	IRSL.100	IRSL.150	IRSL.225	
NG1	-	-	7.1 (- 1.4 / + 1.5)	-	7.1 ± 1.5
NG2	5.2 (- 0.8 / + 0.9)	-	5.6 (- 1.1 / + 1.1)	-	5.4 ± 0.3
NG3	3.0 (- 1.2 / + 1.3)	5.5 (- 0.8 / + 0.9)	-	-	4.3 ± 1.8
NG4	2.6 (- 0.6 / + 0.6)	3.0 (- 0.6 / + 0.6)	5.0 (- 0.7 / + 0.8)	4.3 (- 0.9 / + 0.9)	3.7 ± 1.1
NG5	6.2 (- 0.7 / + 0.8)	7.8 (- 1.4 / + 1.8)	7.5 (- 0.8 / + 0.8)	6.6 (- 0.9 / + 0.9)	7.0 ± 0.8
NG6	-	-	-	-	-
NG7	-	-	-	-	-
NG8	-	-	-	-	-
NG10	-	-	-	-	-
NG11	3.0 (- 0.6 / + 0.6)	-	-	-	3.0 ± 0.6
BUT.1	3.7 (- 0.9 / + 1.2)	-	-	6.2 (- 1.2 / + 1.1)	5.0 ± 1.8
BUT.2	6.2 (- 2.5 / + 3.6)	8.8 (- 2.2 / + 2.6)	7.1 (- 1.2 / + 1.4)	8.8 (- 1.3 / + 1.4)	7.7 ± 1.3
BUT.3	4.8 (- 0.6 / + 0.8)	6.1 (- 0.9 / + 1.0)	5.9 (- 0.8 / + 0.9)	6.7 (- 1.2 / + 1.2)	5.9 ± 0.8
BUT.4	6.2 (- 1.0 / + 1.1)	6.1 (- 0.7 / + 0.9)	5.9 (- 0.7 / + 0.8)	5.6 (- 0.9 / + 1.0)	6.0 ± 0.3
BUT.5	2.3 (- 2.3 / + 3.8)	8.9 (- 2.4 / + 3.5)	5.4 (- 1.2 / + 1.5)	-	5.5 ± 3.3
SU-9	7.6 (- 0.9 / + 1.0)	8.2 (- 1.0 / + 1.1)	10.0 (- 1.1 / + 1.2)	9.5 (- 1.3 / + 1.4)	8.8 ± 1.1
BAR-1	5.1 (- 1.9 / + 2.1)	9.6 (- 1.8 / + 2.2)	12.6 (- 1.4 / + 1.6)	9.9 (- 1.3 / + 1.5)	9.3 ± 3.1
RA-K01	-	-	-	-	-
RA-K02	-	-	-	-	-
RA-K03	-	-	10.7 (- 2.5 / + 2.9)	-	10.7 ± 2.7
RA-K04	-	-	-	-	-
RA-K05	-	-	-	-	-
RA-K06	-	-	-	-	-
CA14-4	-	-	-	-	-
CA14-7	-	5.0 (- 1.0 / + 1.0)	-	8.4 (- 1.2 / + 1.4)	6.7 ± 2.4
SJT01A	-	-	-	-	-
SJT03	3.3 (- 0.7 / + 0.7)	5.2 (- 0.7 / + 0.8)	5.7 (- 0.9 / + 0.9)	-	4.7 ± 1.3
SJT05	4.3 (- 0.9 / + 0.9)	5.8 (- 0.9 / + 0.9)	5.6 (- 1.1 / + 1.2)	-	5.2 ± 0.8
SJT07	4.3 (- 0.8 / + 0.8)	6.1 (- 0.8 / + 1.0)	6.3 (- 1.1 / + 1.1)	-	5.6 ± 1.1
SJT08	-	5.5 (- 0.9 / + 0.9)	7.7 (- 1.2 / + 1.3)	-	6.6 ± 1.6
SJT10	-	5.4 (- 0.9 / + 0.9)	5.7 (- 1.1 / + 1.1)	-	5.6 ± 0.2
SJT11	-	6.6 (- 1.2 / + 1.3)	7.7 (- 1.3 / + 1.4)	-	7.2 ± 0.8
SJT12	-	5.3 (- 1.0 / + 1.1)	7.2 (- 1.1 / + 1.2)	-	6.3 ± 1.3

Note: No exhumation rate is available for saturated IRSL signals.

Table S8: *Samples with their averaged apparent age, exhumation rate, and thrust slip rates with a fixed dip angle of 30°, and with a dip angle range between 25 and 45°.*

Sample	Apparent age [ka]	Exhumation rate [mm/yr]	Thrust slip rate [mm/yr]	
			Fixed dip angle: 30°	Dip angle range: 25-45°
NG1	201 ± 25	7.1 ± 1.5	14.2 ± 2.9	8.0-20.2
NG2	211 ± 5	5.4 ± 0.3	10.8 ± 0.6	7.2-13.4
NG3	167 ± 67	4.3 ± 1.8	8.5 ± 3.5	3.5-14.2
NG4	198 ± 44	3.7 ± 1.1	7.5 ± 2.2	3.7-11.5
NG5	174 ± 38	7.0 ± 0.8	14.1 ± 1.5	8.9-18.4
NG6	-	-	-	-
NG7	-	-	-	-
NG8	-	-	-	-
NG10	-	-	-	-
NG11	286 ± 4	3.0 ± 0.6	6.0 ± 1.2	3.4-8.5
BUT.1	195 ± 2	5.0 ± 1.8	9.9 ± 3.5	4.5-15.9
BUT.2	217 ± 26	7.7 ± 1.3	15.5 ± 2.6	9.1-21.3
BUT.3	184 ± 15	5.9 ± 0.8	11.8 ± 1.6	7.2-15.8
BUT.4	191 ± 39	6.0 ± 0.3	11.9 ± 0.5	8.0-14.7
BUT.5	183 ± 31	5.5 ± 3.3	11.1 ± 6.6	3.2-20.9
SU-9	165 ± 18	8.8 ± 1.1	17.7 ± 2.2	10.9-23.5
BAR-1	186 ± 32	9.3 ± 3.1	18.6 ± 6.2	8.8-29.4
RA-K01	-	-	-	-
RA-K02	-	-	-	-
RA-K03	199 ± 6	10.7 ± 2.7	21.4 ± 5.4	11.3-31.7
RA-K04	-	-	-	-
RA-K05	-	-	-	-
RA-K06	-	-	-	-
CA14-4	-	-	-	-
CA14-7	162 ± 7	6.7 ± 2.4	13.4 ± 4.8	6.1-21.5
SJT01A	-	-	-	-
SJT03	219 ± 38	4.7 ± 1.3	9.5 ± 2.5	4.9-14.2
SJT05	191 ± 56	5.2 ± 0.8	10.5 ± 1.6	6.2-14.3
SJT07	200 ± 50	5.6 ± 1.1	11.1 ± 2.2	6.3-15.8
SJT08	203 ± 28	6.6 ± 1.6	13.2 ± 3.1	7.1-19.3
SJT10	227 ± 41	5.6 ± 0.2	11.1 ± 0.4	7.5-13.6
SJT11	172 ± 24	7.2 ± 0.8	14.3 ± 1.6	9.0-18.8
SJT12	218 ± 9	6.3 ± 1.3	12.5 ± 2.7	6.9-18.0

Note: No value is available for samples that are saturated for all the 4 IRSL signals; apparent ages, exhumation rates, and thrust slip rates are thus empty for these samples.

Table S9: A. *Compilation of Global Positioning System (GPS) derived geodetic convergence rates from the literature, and* ***B.*** *their references.*

A.

Segment		Longitude [°E]	Convergence [mm/yr]	Years of survey	Ref
West-central Nepal		83.5 ± 1.5	20.6 ± 1.6	1999-2015	Li et al., 2019
Central Nepal		85.5 ± 1.5	17.4 ± 0.3	1999-2015	Li et al., 2019
Eastern Nepal		87.5 ± 1.5	16.9 ± 0.9	1999-2015	Li et al., 2019
West-central Nepal		80.9 ± 1.9	21.6 ± 1.7	1996-2015	Sreejith et al., 2018
Central Nepal		84.9 ± 2.2	17.2 ± 2.1	1996-2015	Sreejith et al., 2018
Eastern Nepal		93.9 ± 3.3	15.1 ± 1.4	1996-2015	Sreejith et al., 2018
Eastern Kashmir		75.0 ± 1.0	12 ± 1	1991-2012	Bilham et al., 2017
Kangra		77.0 ± 1.0	17 ± 2	1991-2012	Bilham et al., 2017
Gahrwal		79.5 ± 0.5	18 ± 2	1991-2012	Bilham et al., 2017
Kumaun		81.0 ± 1.0	20 ± 1	1991-2012	Bilham et al., 2017
Western Nepal		83.3 ± 1.3	20 ± 1	1991-2012	Bilham et al., 2017
Central Nepal		85.5 ± 1.0	19 ± 1	1991-2012	Bilham et al., 2017
Eastern Nepal, Sikkim		87.5 ± 1.0	18 ± 1	1991-2012	Bilham et al., 2017
Sikkim, Western Bhutan		89.8 ± 1.3	17 ± 1	1991-2012	Bilham et al., 2017
Eastern Bhutan		92.3 ± 1.3	16 ± 3	1991-2012	Bilham et al., 2017
Arunachal Plateau		94.5 ± 2.0	17 ± 5	1991-2012	Bilham et al., 2017
Bhutan		90.5 ± 1.5	17 ± 2	1991-2016	Marechal et al., 2016
74-75°E		74.5 ± 1.0	13.3 ± 1.7	1991-2012	Stevens and Avouac, 2015
75-79°E		77.0 ± 1.5	18.5 ± 1.8	1991-2012	Stevens and Avouac, 2015
Western Nepal		81.0 ± 2.5	20.2 ± 1.1	1991-2012	Stevens and Avouac, 2015
Central Nepal		85.0 ± 1.5	19.4 ± 1.4	1991-2012	Stevens and Avouac, 2015
Eastern Nepal + Western Bhutan		89.0 ± 2.5	17.6 ± 0.9	1991-2012	Stevens and Avouac, 2015
Eastern Bhutan + Assam		93.5 ± 2.0	21.2 ± 2	1991-2012	Stevens and Avouac, 2015
Eastern Nepal	85-86°E	85.5 ± 0.5	18 ± 1	1991-2012	Vernant et al., 2014
Sikkim	87.2-88.8°E	88.0 ± 0.8	17 ± 1	1991-2012	Vernant et al., 2014
Western Bhutan	89-90°E	89.5 ± 0.5	16.5 ± 1.5	1991-2012	Vernant et al., 2014
Central Bhutan	90.4-91.4°E	90.9 ± 0.5	15.0 ± 1.5	1991-2012	Vernant et al., 2014
Eastern Bhutan	91.5-93°E	92.3 ± 0.8	17 ± 1	1991-2012	Vernant et al., 2014
Western Assam	92-94°E	93.0 ± 1.0	14 ± 1	1991-2012	Vernant et al., 2014
Arunachal	94-95°E	94.5 ± 0.5	11.5 ± 1.0	1991-2012	Vernant et al., 2014
Eastern Assam	>95°E	96.0 ± 1.0	14 ± 2	1991-2012	Vernant et al., 2014
West of Thakkola graben	~80-83°E	81.3 ± 2.3	20.5 ± 1.0	1991-2009	Ader et al., 2012
East of Thakkola graben	~83.5-88°E	85.8 ± 2.3	17.8 ± 0.5	1991-2009	Ader et al., 2012

B. References

Ader, T., Avouac, J.P., Liu-Zeng, J., Lyon-Caen, H., Bollinger, L., Galetzka, J., Genrich, J., Thomas, M., Chanard, K., Sapkota, S.N., Rajaure, Su., Shrestha, P., Ding, L., and Flouzat, M., 2012. Convergence rate across the Nepal Himalaya

and interseismic coupling on the Main Himalayan Thrust: Implications for seismic hazard. Journal of Geophysical Research: Solid Earth, 117(B4), B04403, doi:10.1029/2011JB009071

Bilham, R., Mencin, D., Bendick, R., and Bürgmann, R., 2017. Implications for elastic energy storage in the Himalaya from the Gorkha 2015 earthquake and other incomplete ruptures of the Main Himalayan Thrust. Quaternary International, 462, 3–21, doi:10.1016/j.quaint.2016.09.055

Li, S., Wang, Q., Chen, G., He, P., Ding, K., Chen, Y., and Zou, R., 2019. Interseismic Coupling in the Central Nepalese Himalaya: Spatial Correlation with the 2015 Mw 7.9 Gorkha Earthquake. Pure and Applied Geophysics, 176(9), 3893–3911, doi:10.1007/s00024-019-02121-7

Marechal, A., Mazzotti, S., Cattin, R., Cazes, G., Vernant, P., Drukpa, D., Thinley, K., Tarayoun, A., Le Roux-Mallouf, R., Thapa, B.B., and Pelgay, P., 2016. Evidence of interseismic coupling variations along the Bhutan Himalayan arc from new GPS data. Geophysical Research Letters, 43(24), 12–399, doi:10.1002/2016GL071163

Sreejith, K.M., Sunil, P.S., Agrawal, R., Saji, A.P., Rajawat, A.S., and Ramesh, D.S., 2018. Audit of stored strain energy and extent of future earthquake rupture in central Himalaya. Scientific reports, 8(1), 1–9, doi:10.1038/s41598-018-35025-y

Stevens, V.L., and Avouac, J.P., 2015. Interseismic coupling on the main Himalayan thrust. Geophysical Research Letters, 42(14), 5828–5837, doi:10.1002/2015GL064845

Vernant, P., Bilham, R., Szeliga, W., Drukpa, D., Kalita, S., Bhattacharyya, A.K., Gaur, V.K., Pelgay, P., Cattin, R., and Berthet, T., 2014. Clockwise rotation of the Brahmaputra Valley relative to India: Tectonic convergence in the eastern Himalaya, Naga Hills, and Shillong Plateau. Journal of Geophysical Research: Solid Earth, 119(8), 6558–6571, doi:10.1002/2014JB011196

Table S10: *Compilation of literature data used in Fig. 3B for* ***A.*** *the Holocene and late Quaternary, and* ***B.*** *the Miocene-Pliocene, and* ***C.*** *their references.*

A.

Transect	Longitude [°E]	Rock uplift rate [mm/yr]	Age [ka]	Thrust slip rate [mm/yr]	Method	Reference
Dehra Dun [a]	77.8 ± 0.5	6.9 ± 1.8	< 2.5	13.8 ± 3.6	Vertical uplift rate: ^{14}C dating of terraces	Wesnousky et al., 1999
Uttarakhand [b]	78.0 ± 1.3	4-6	~ 1.5	-	Vertical uplift rate: ^{14}C age of trench exposure	Kumar et al., 2006
KAR [c]	81.3 ± 0.2	~12	~300	~24*	Exhumation rate: apatite fission-track thermochronology	van der Beek et al., 2006
Bakaya/ Bagmati [d]	85.2 ± 0.5	~10-15	≤ 9.2	21.5 ± 1.5	Rock uplift rate derived from river incision: ^{14}C dating of terraces	Lavé and Avouac, 2000
Sir Khola [e]	85.6 ± 0.1	8.5 ± 1.5	< 2.5	20.1 ± 3.5*		
RA-B [e]	85.9 ± 0.1	~10 ± 1.5	< 2.5	18.4 ± 2.8*	Apparent uplift rate derived from river incision: ^{14}C and ^{10}Be dating of terraces	Bollinger et al., 2014
RA-P [e]	85.9 ± 0.1	12.4 ± 2.3	< 2.5	17.5 ± 3.3*		
Sarpang [f]	90.3 ± 0.1	8.8 ± 2.1	< 6.5	20.8 ± 8.8	Vertical slip rate: ^{10}Be dating of terraces	Berthet et al., 2014

*calculated for this study from the published rock uplift rates and thrust angles.

B.

Transect	Longitude [°E]	Rock uplift rate [mm/yr]	Age [Ma]	Shortening rate [mm/yr]	Method	Reference
All Himalayas	80 ± 7	-	15-20	12.5 ± 2.5	Flexural rigidity + age of sediments	Lyon-Caen and Molnar, 1985
All Himalayas	80 ± 7	-	15-20	18 ± 7	Flexural rigidity + age of sediments	Molnar, 1988
Western Nepal	82 ± 2	-	~11	19 ± 5	Total area balancing + age	Mugnier et al., 2004
Arunachal Pradesh, NE India	92.5 ± 0.5	-	13-14	25-30	Thermokinematic modelling of balanced cross-sections	Braza and McQuarrie, 2022
		-	10-13	18-20		
		-	6-10	25-35		
		-	0-6	9-15		

C. References

Berthet, T., Ritz, J.F., Ferry, M., Pelgay, P., Cattin, R., Drukpa, D., Braucher, R., and Hetényi, G., 2014. Active tectonics of the eastern Himalaya: new constraints from the first tectonic geomorphology study in southern Bhutan. Geology, 42(5), 427–430, doi:10.1130/G35162.1

Bollinger, L., Sapkota, S.N., Tapponnier, P., Klinger, Y., Rizza, M., van der Woerd, J., Tiwari, D.R., Pandey, R., Bitri, A., and Bes de Berc, S., 2014. Estimating the return times of great Himalayan earthquakes in eastern Nepal: Evidence from

the Patu and Bardibas strands of the Main Frontal Thrust. Journal of Geophysical Research: Solid Earth, 119(9), 7123–7163, doi:10.1002/2014JB010970

Braza, M., and McQuarrie, N., 2022. Determining the tempo of exhumation in the eastern Himalaya: Part 1. Geometry, kinematics and predicted cooling ages. Basin Research, 34(1), 141–169, doi:10.1111/bre.12615

Kumar, S., Wesnousky, S.G., Rockwell, T.K., Briggs, R.W., Thakur, V.C., and Jayangondaperumal, R., 2006. Paleoseismic evidence of great surface rupture earthquakes along the Indian Himalaya. Journal of Geophysical Research: Solid Earth, 111(B3), doi:10.1029/2004JB003309

Lavé, J., and Avouac, J.P., 2000. Active folding of fluvial terraces across the Siwaliks Hills, Himalayas of central Nepal. Journal of Geophysical Research: Solid Earth, 105(B3), 5735–5770, doi:10.1029/1999JB900292

Lyon-Caen, H., and Molnar, P., 1985. Gravity anomalies, flexure of the Indian plate, and the structure, support and evolution of the Himalaya and Ganga Basin. Tectonics, 4(6), 513–538, doi:10.1029/TC004i006p00513

Molnar, P., 1988. A review of geophysical constraints on the deep structure of the Tibetan Plateau, the Himalaya and the Karakoram, and their tectonic implications. Philosophical Transactions of the Royal Society of London. Series A, Mathematical and Physical Sciences 326(1589), 33–88, https://doi.org/10.1098/rsta.1988.0080

Mugnier, J.L., Huyghe, P., Leturmy, P., and Jouanne, F., 2004. Episodicity and rates of thrust-sheet motion in the Himalayas (Western Nepal). In K.R. McClay, ed., Thrust tectonics and hydrocarbon systems: AAPG Memoir 82, 91–114, doi:10.1306/M82813C6

van der Beek, P., Robert, X., Mugnier, J.L., Bernet, M., Huyghe, P., and Labrin, E. (2006). Late Miocene–Recent exhumation of the central Himalaya and recycling in the foreland basin assessed by apatite fission-track thermochronology of Siwalik sediments, Nepal. Basin Research, 18(4), 413–434, doi:10.1111/j.1365-2117.2006.00305.x

Wesnousky, S.G., Kumar, S., Mohindra, R., and Thakur, V.C., 1999. Uplift and convergence along the Himalayan Frontal Thrust of India. Tectonics, 18(6), 967–976, doi:10.1029/1999TC900026

Table S11: *Percentage of convergence taken by the Sub-Himalayan FTB thrusts during the late Quaternary (last 200 k.y.).*

				Fixed angle: 30°		**Angle range: 25-45°**	
Transect	**Thrust sheet**	**Longitude [°E]**	**Local geodetic convergence rate [mm/yr]**	**Thrust slip rate [mm/yr]**	**Convergence accommodated [%]**	**Thrust slip rate [mm/yr]**	**Convergence accommodated [%]**
NG.2-5	MFT	81.7	20.6 ± 0.7	*10.2 ± 2.9 **	*50 ± 14*	*5.1 – 15.5 **	*25 – 75*
NG.11	IST	81.7	20.6 ± 0.7	*6.0 ± 1.2 **	*29 ± 6*	*3.4 – 8.5 **	*17 – 41*
NG.2-11	Sub-H. FTB	81.7	20.6 ± 0.7	16.2 ± 3.0 *****	79 ± 15	8.5 – 24.0 *****	41 – 117
BUT	MFT	83.5	19.4 ± 1.4	12.0 ± 2.1	62 ± 12	7.0 – 16.7	36 – 86
SU/BAR	MFT	85.2	18.1 ± 0.9	18.1 ± 0.7	100 ± 6	12.3 – 22.2	68 – 122
RA-K03	IST	85.9	18.1 ± 0.9	21.4 ± 5.4	118 ± 30	11.3 – 31.7	62 – 175
CA14-7	MFT	87.2	17.5 ± 0.5	13.4 ± 4.8	77 ± 28	6.1 – 21.5	35 – 123
SJT	MFT	91.5	17.8 ± 2.0	11.7 ± 1.7	66 ± 12	7.1 – 15.9	40 – 90

*thrust slip rate for the NG transect is the sum of the MFT and IST thrust sheet values (data in italic).

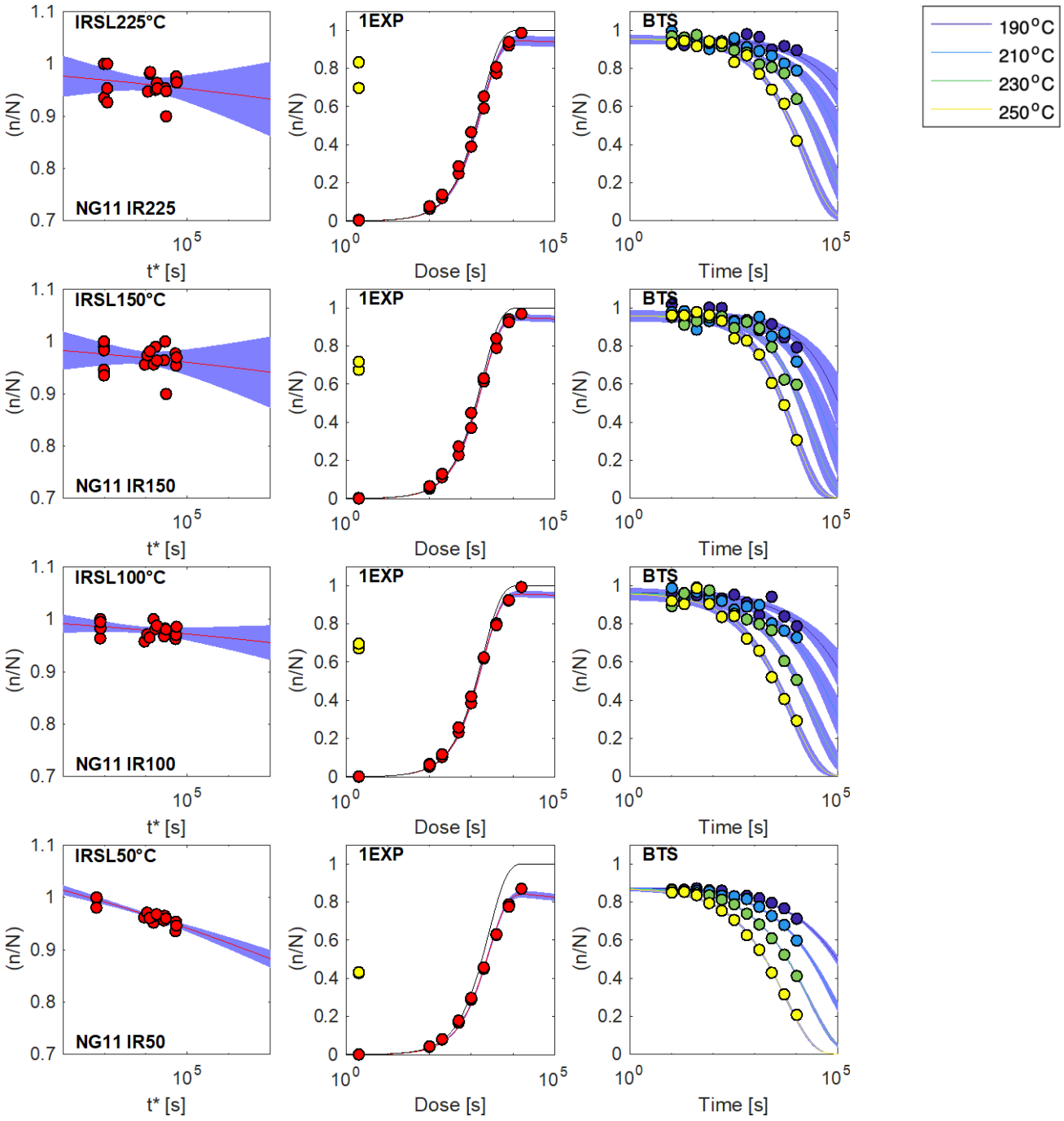
IRSL225°C
NG11 IR225
1EXP
BTS
IRSL150°C
NG11 IR150
IRSL100°C
NG11 IR100
IRSL50°C
NG11 IR50
(n/N)
t* [s]
Dose [s]
Time [s]
190°C
210°C
230°C
250°C

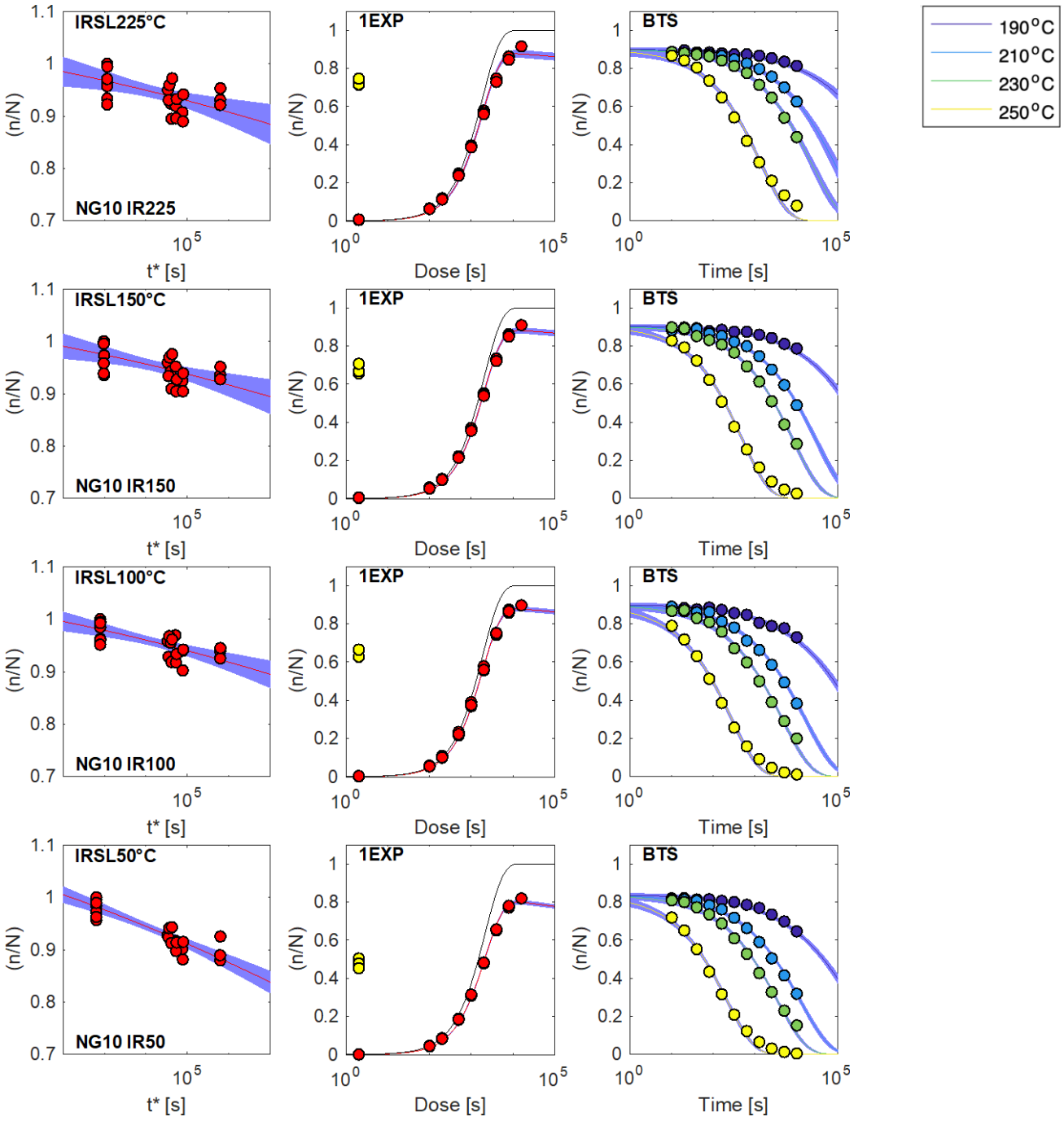
IRSL225°C
NG10 IR225
IRSL150°C
NG10 IR150
IRSL100°C
NG10 IR100
IRSL50°C
NG10 IR50
1EXP
BTS
(n/N)
t* [s]
Dose [s]
Time [s]
190°C
210°C
230°C
250°C

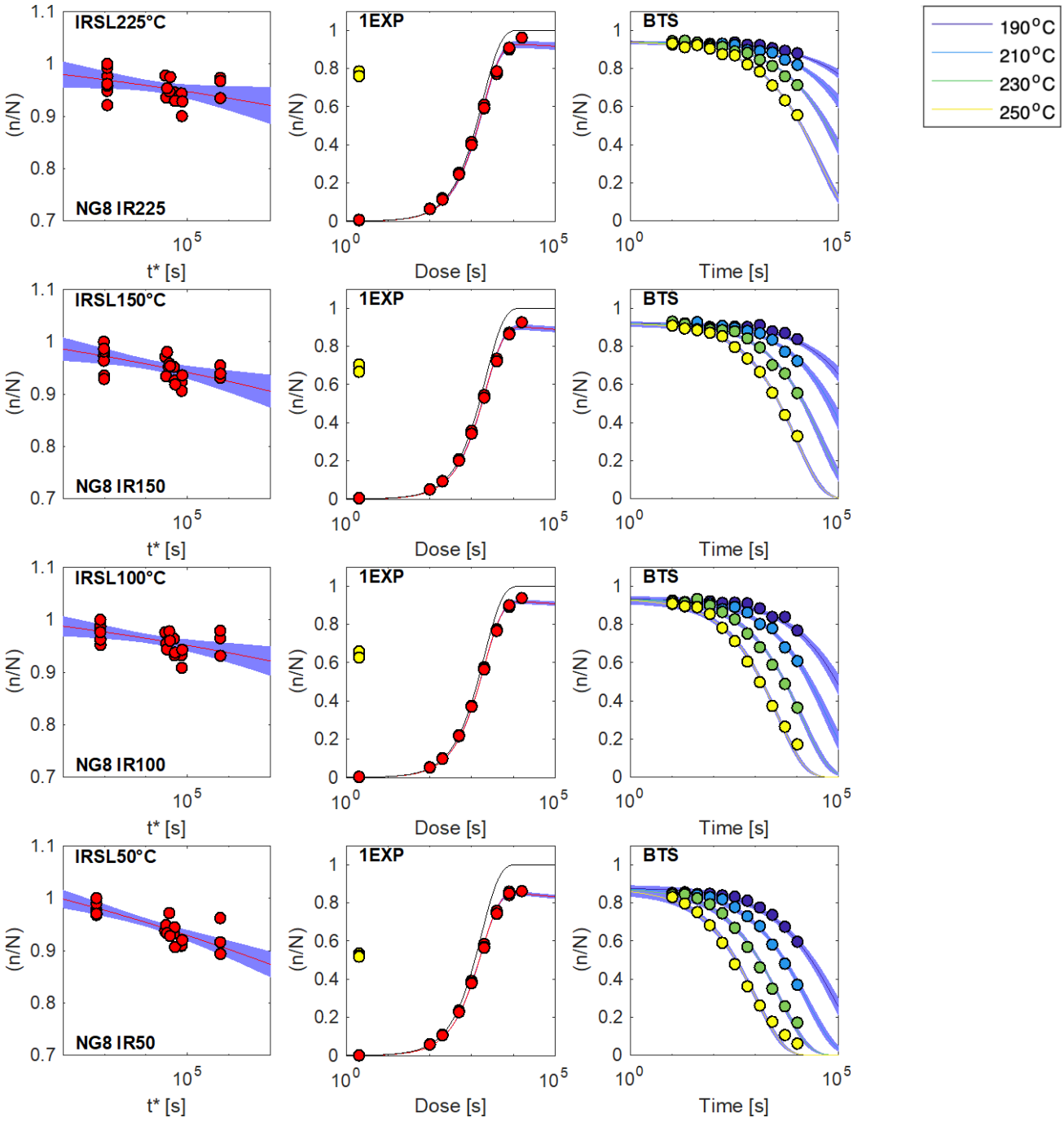
IRSL225°C
NG8 IR225
1EXP
BTS
IRSL150°C
NG8 IR150
IRSL100°C
NG8 IR100
IRSL50°C
NG8 IR50
(n/N)
t* [s]
Dose [s]
Time [s]
190°C
210°C
230°C
250°C

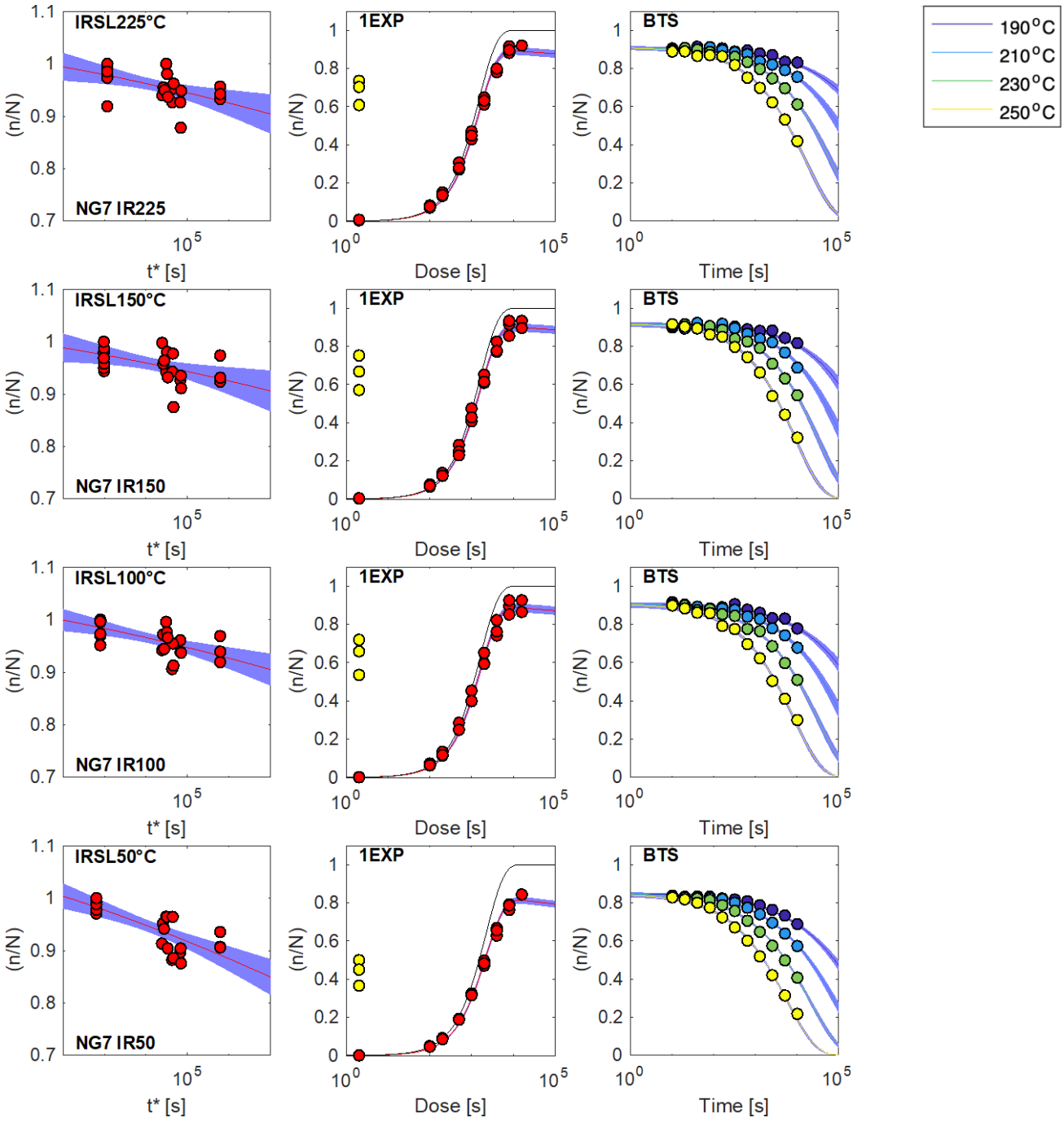
IRSL225°C
NG7 IR225
IRSL150°C
NG7 IR150
IRSL100°C
NG7 IR100
IRSL50°C
NG7 IR50
1EXP
BTS
(n/N)
t* [s]
Dose [s]
Time [s]
190°C
210°C
230°C
250°C

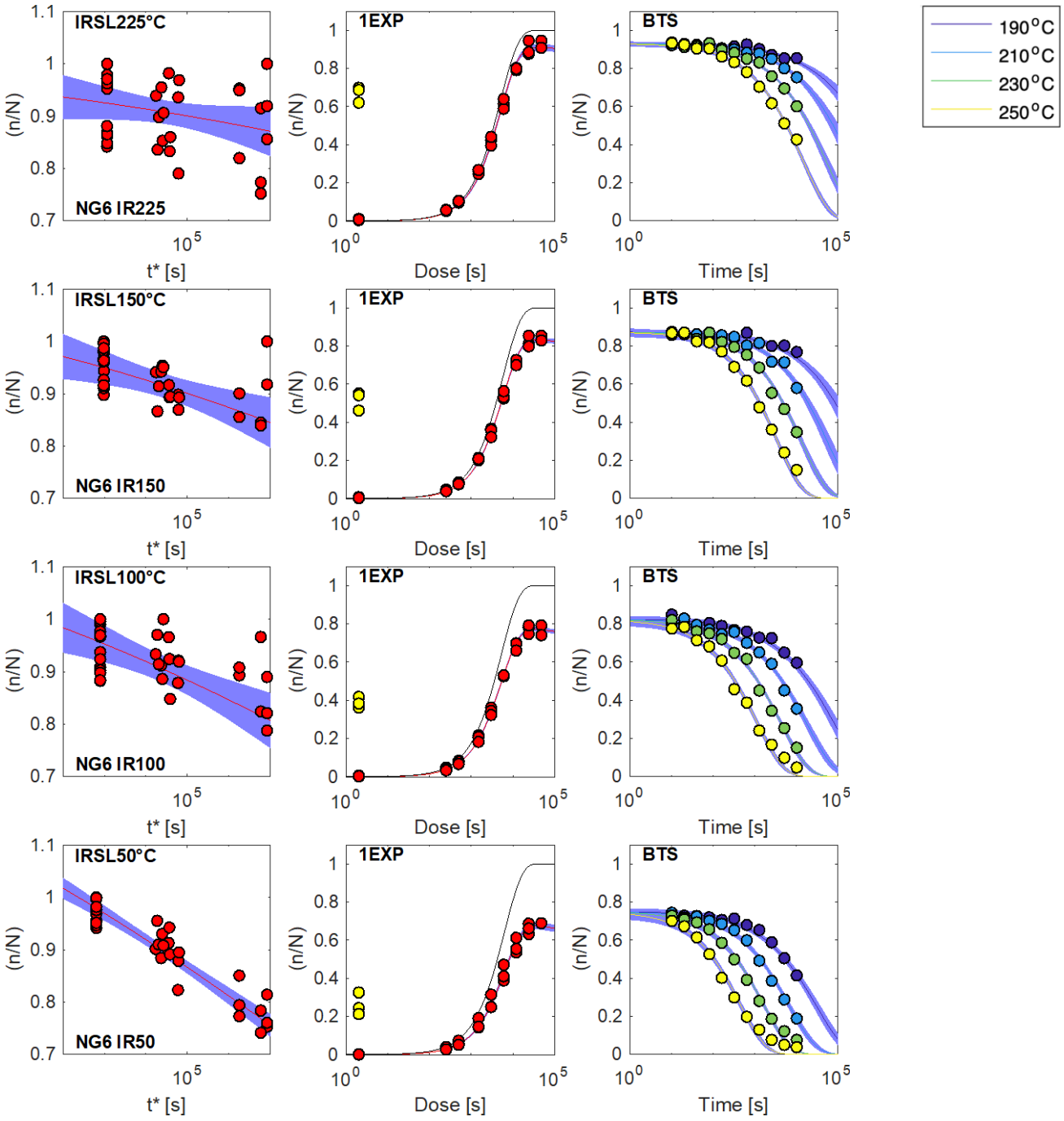
IRSL225°C
NG6 IR225
IRSL150°C
NG6 IR150
IRSL100°C
NG6 IR100
IRSL50°C
NG6 IR50
1EXP
BTS
(n/N)
t* [s]
Dose [s]
Time [s]
190°C
210°C
230°C
250°C

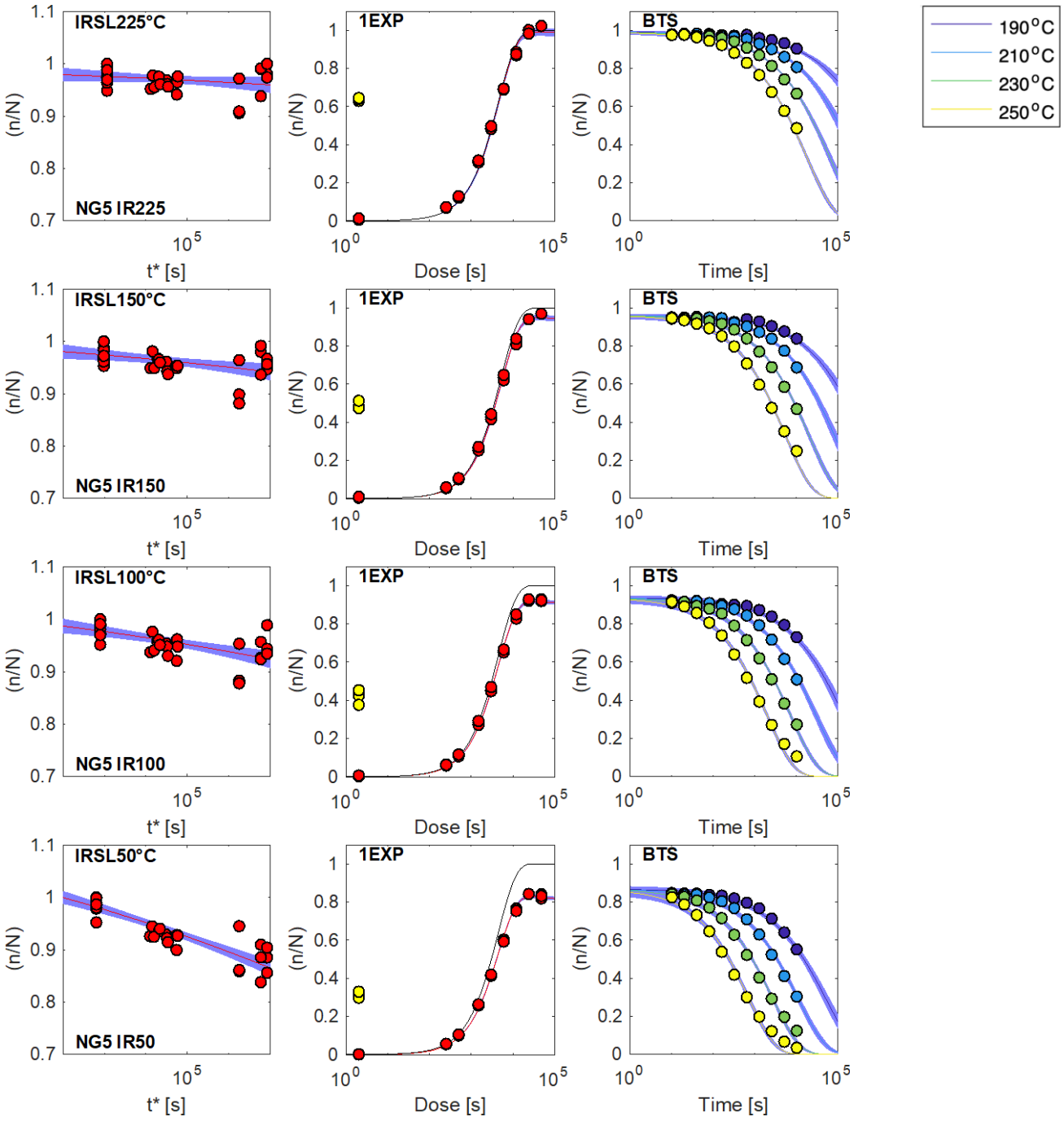
IRSL225°C
NG5 IR225
1EXP
BTS
IRSL150°C
NG5 IR150
IRSL100°C
NG5 IR100
IRSL50°C
NG5 IR50
(n/N)
t* [s]
Dose [s]
Time [s]
190°C
210°C
230°C
250°C

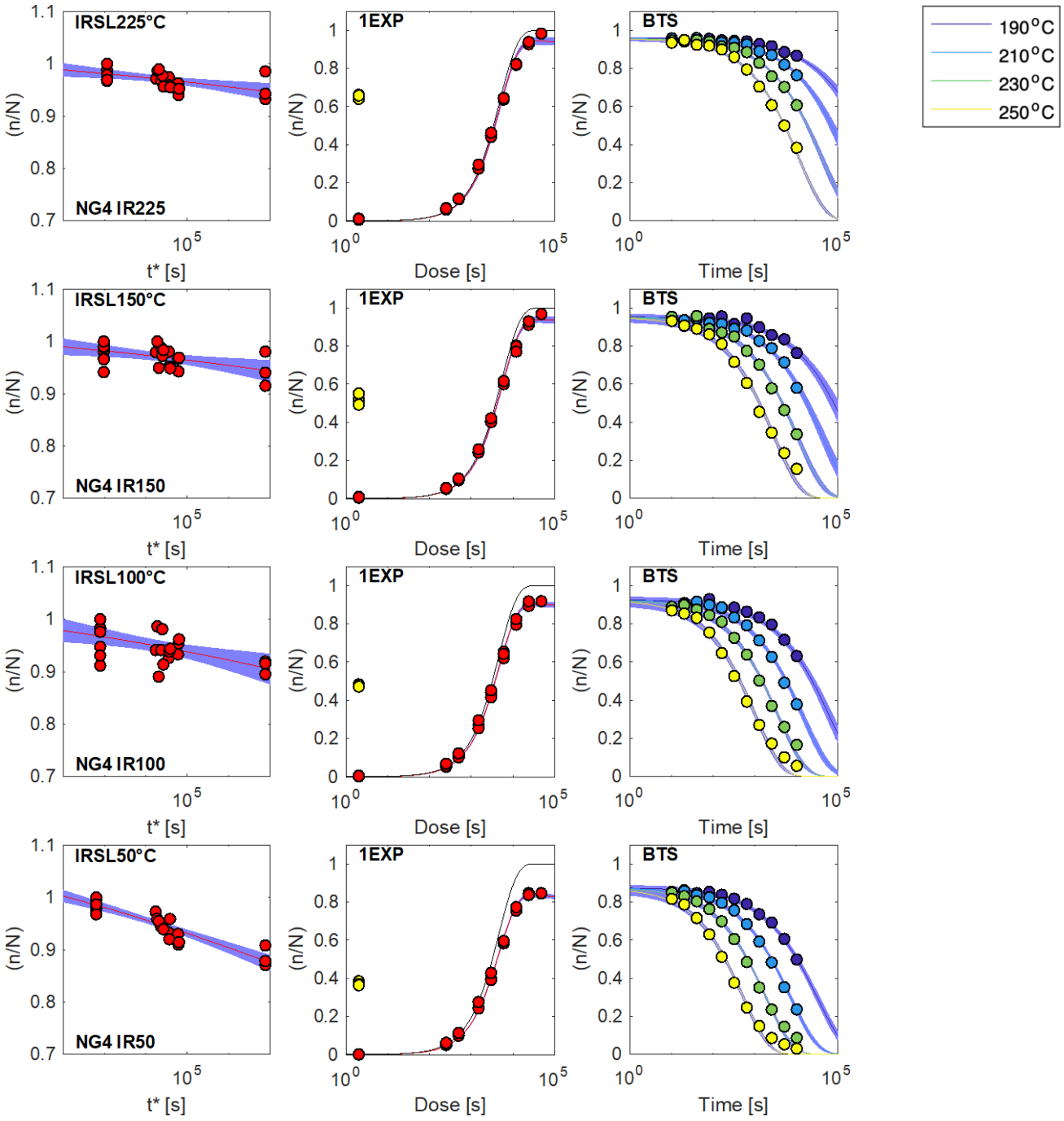
IRSL225°C
NG4 IR225
IRSL150°C
NG4 IR150
IRSL100°C
NG4 IR100
IRSL50°C
NG4 IR50
1EXP
BTS
(n/N)
t* [s]
Dose [s]
Time [s]
190°C
210°C
230°C
250°C

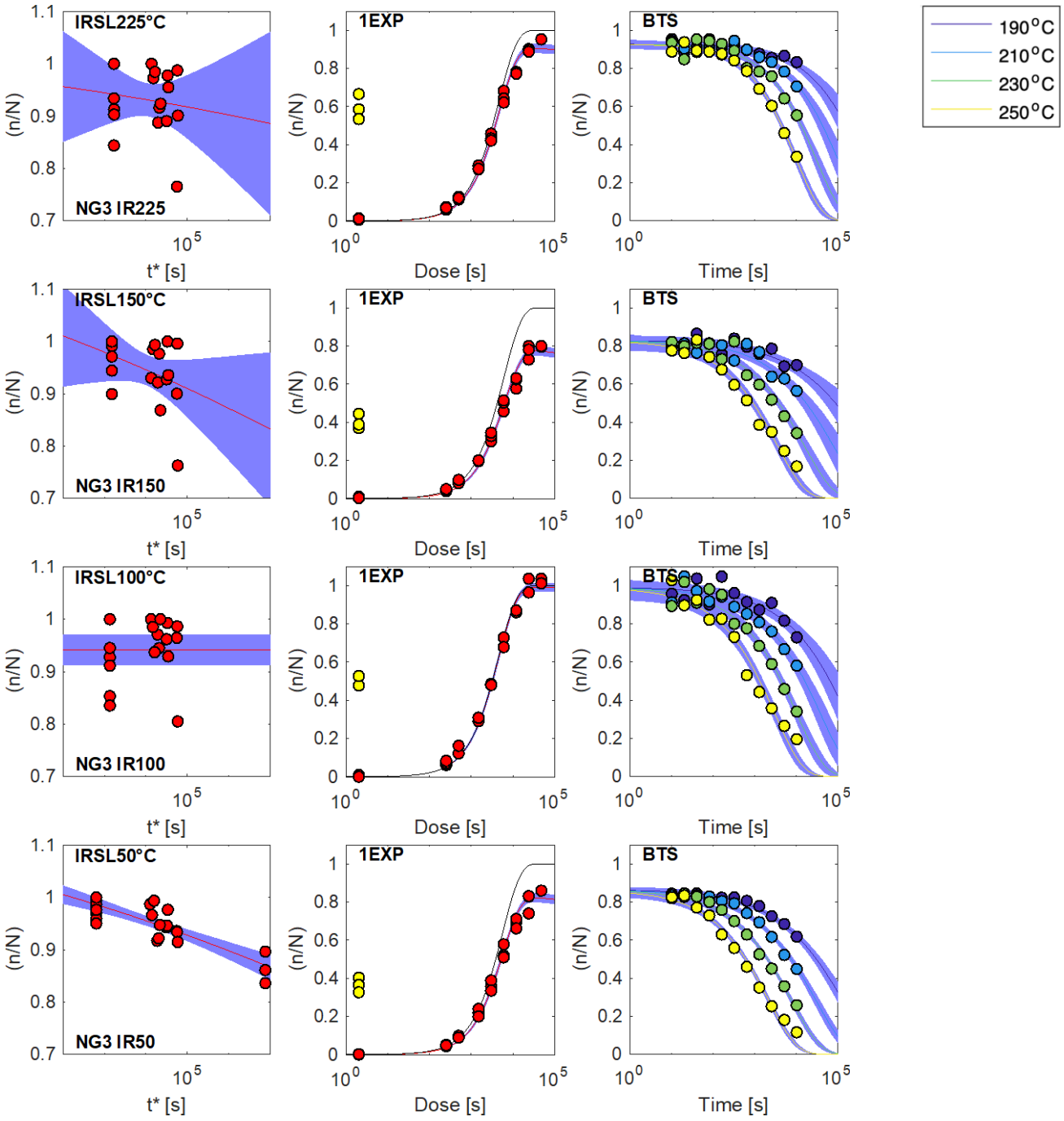
IRSL225°C
NG3 IR225
IRSL150°C
NG3 IR150
IRSL100°C
NG3 IR100
IRSL50°C
NG3 IR50
1EXP
BTS
(n/N)
t* [s]
Dose [s]
Time [s]
190°C
210°C
230°C
250°C

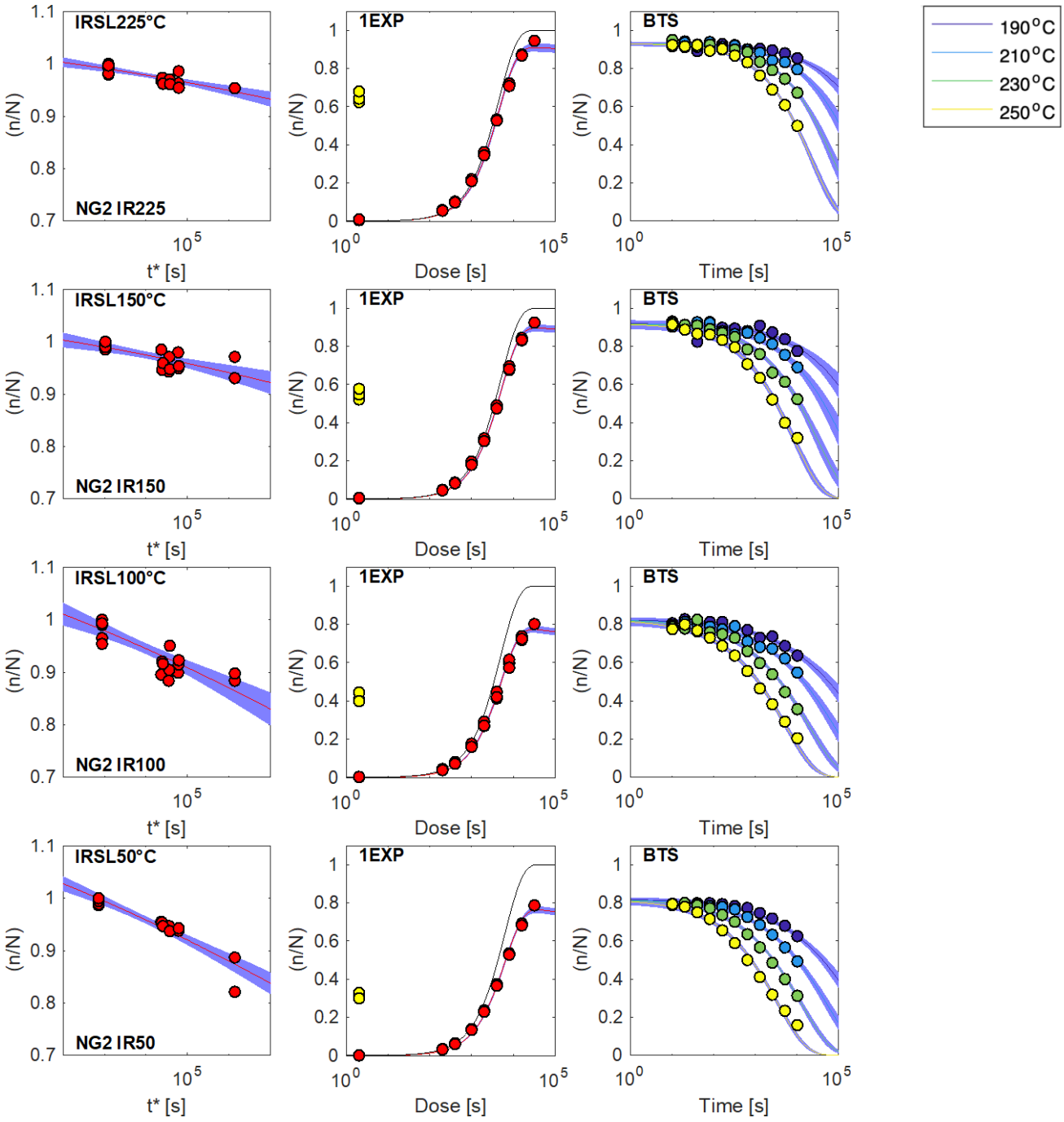
IRSL225°C
NG2 IR225
IRSL150°C
NG2 IR150
IRSL100°C
NG2 IR100
IRSL50°C
NG2 IR50
1EXP
BTS
(n/N)
t* [s]
Dose [s]
Time [s]
190°C
210°C
230°C
250°C

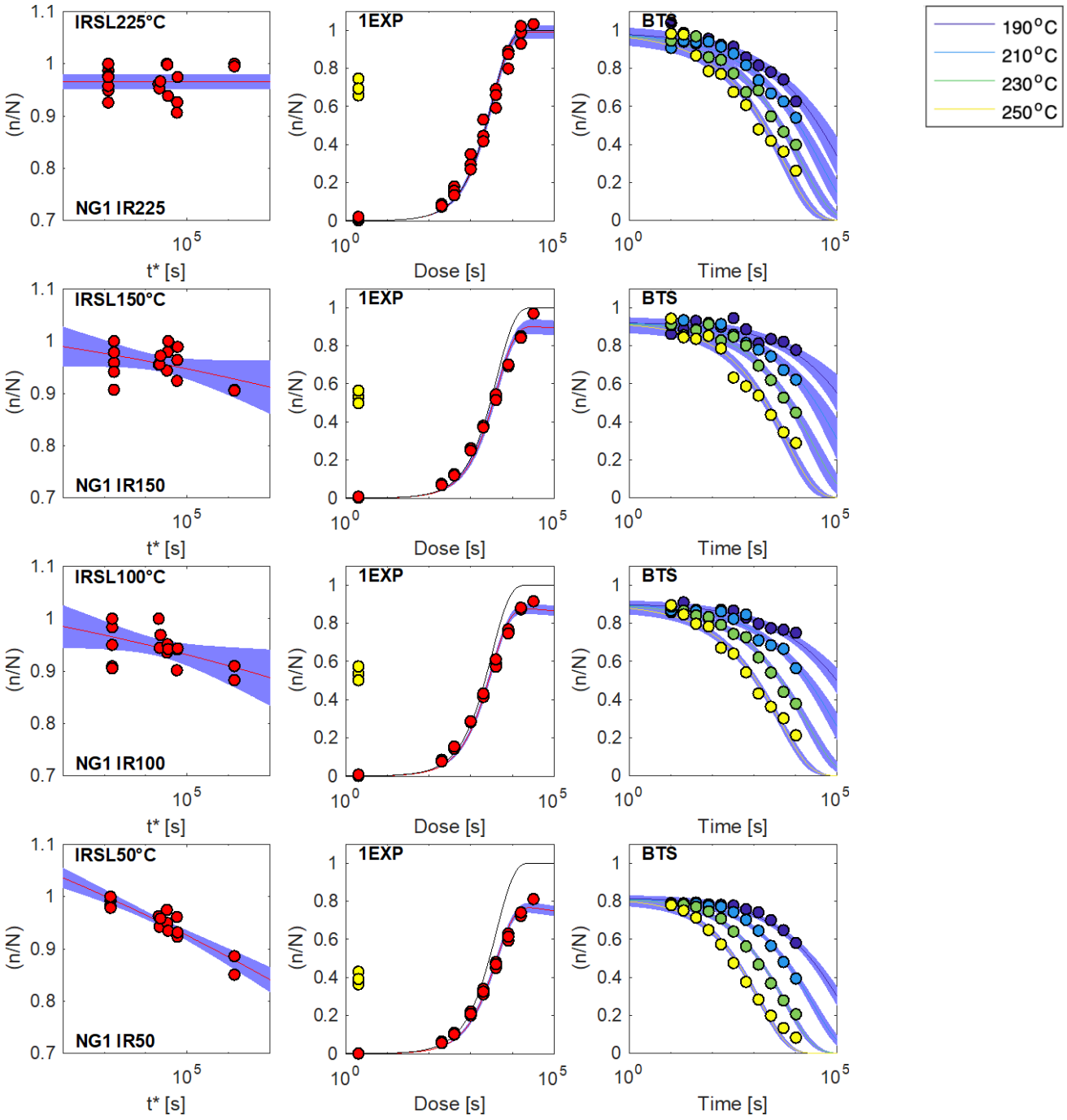

Fig. S3.1: *Luminescence measurement and model fit results for all samples of the NG transect. (A, D, G, J) Anomalous fading data fitted using equations 3 and 4 of King et al. (2016), for the IRSL at 50, 100, 150, and 225 °C respectively. (B, E, H, K) Luminescence dose response accounting for fading, fitted using equation 5 of King et al. (2016). The black solid line is the unfaded dose response curve, and the yellow dots represent the $\tilde{n}_{nat}$ values of each aliquot. (C, F, I, L) Isothermal decay data fitted with the BTS model, using equations 6 and 7 of King et al. (2016).*

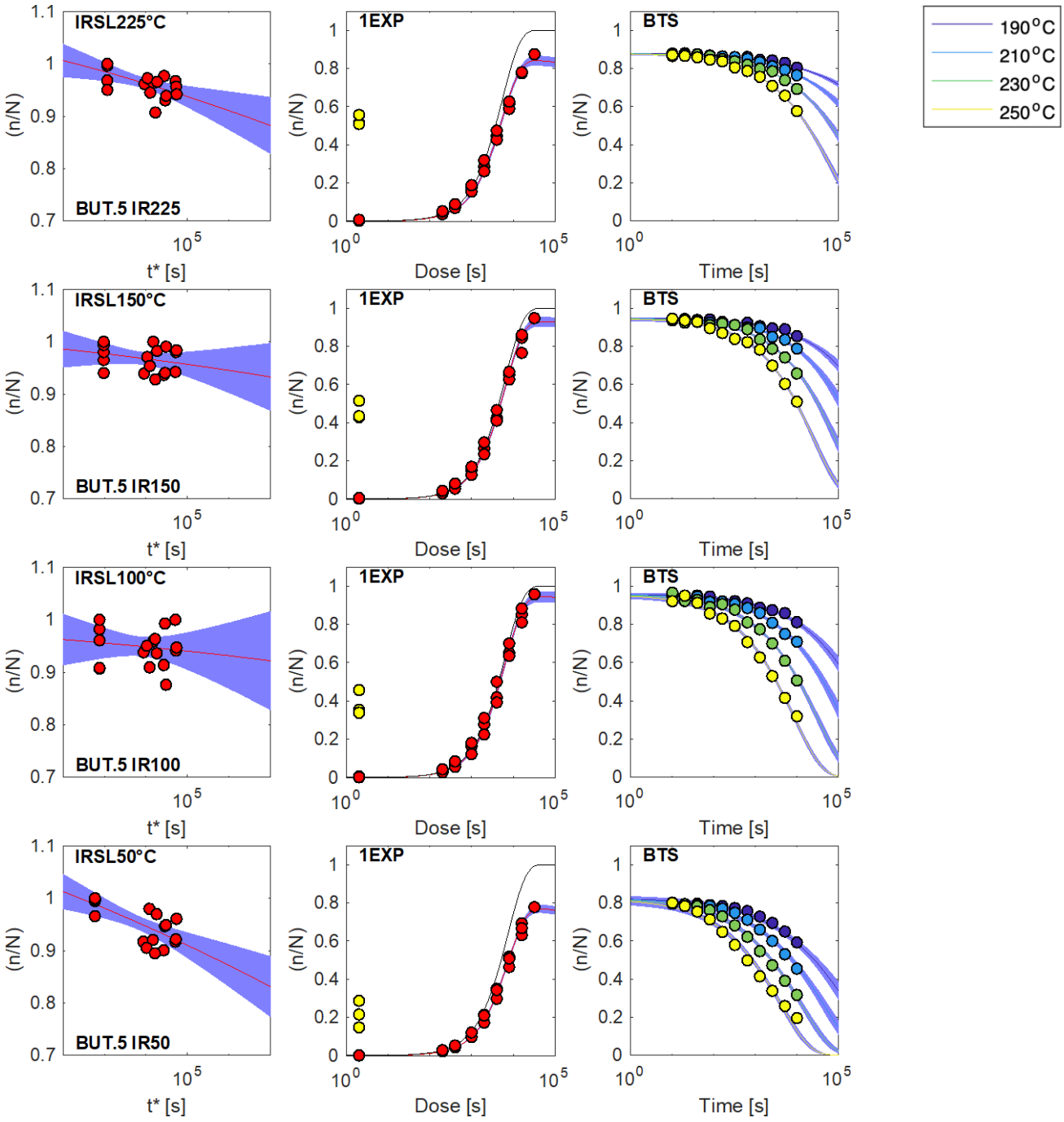
IRSL225°C
BUT.5 IR225
1EXP
BTS
IRSL150°C
BUT.5 IR150
IRSL100°C
BUT.5 IR100
IRSL50°C
BUT.5 IR50
(n/N)
t* [s]
Dose [s]
Time [s]
190°C
210°C
230°C
250°C

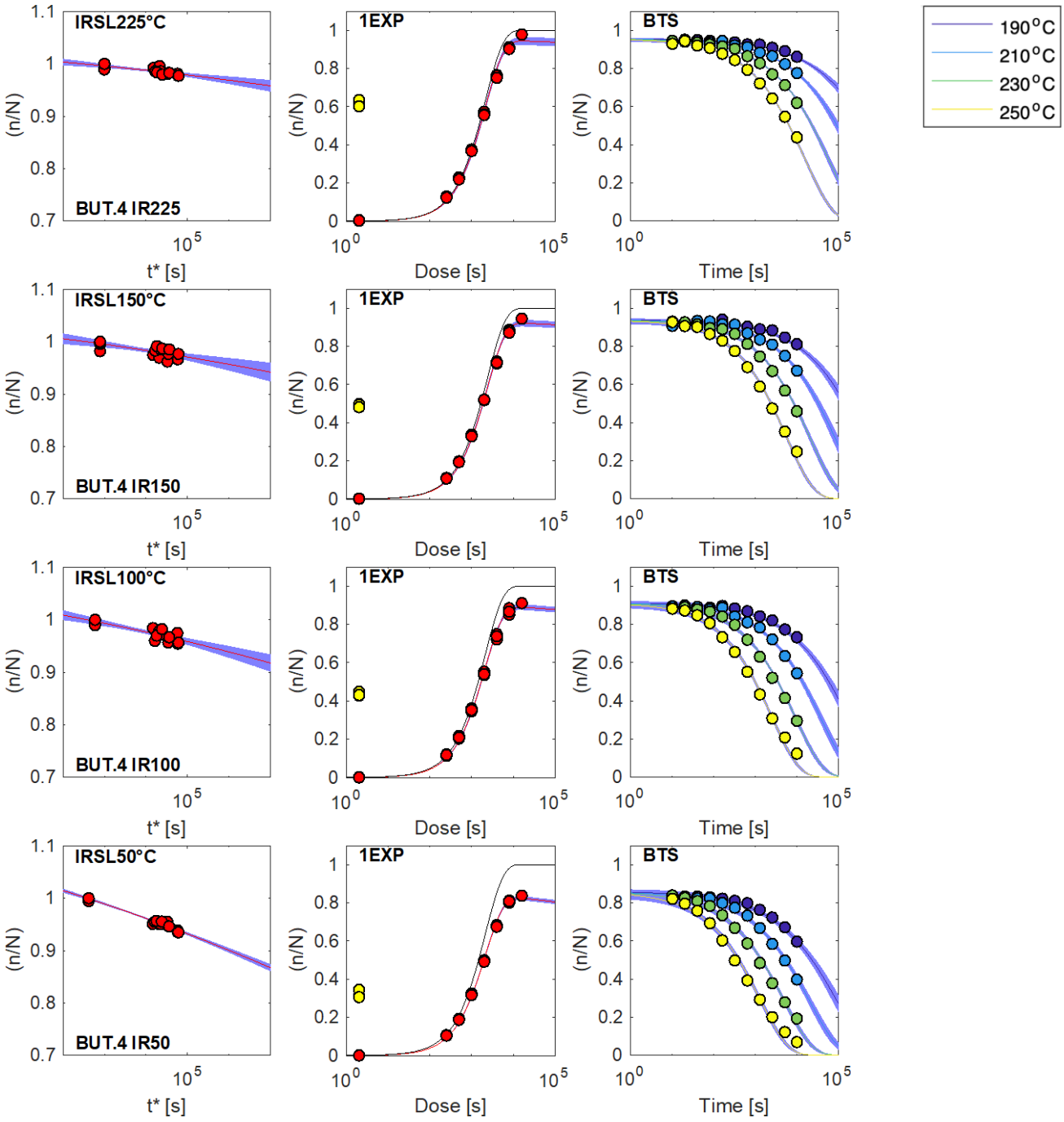
IRSL225°C
1EXP
BTS
BUT.4 IR225
IRSL150°C
BUT.4 IR150
IRSL100°C
BUT.4 IR100
IRSL50°C
BUT.4 IR50
(n/N)
t* [s]
Dose [s]
Time [s]
190°C
210°C
230°C
250°C

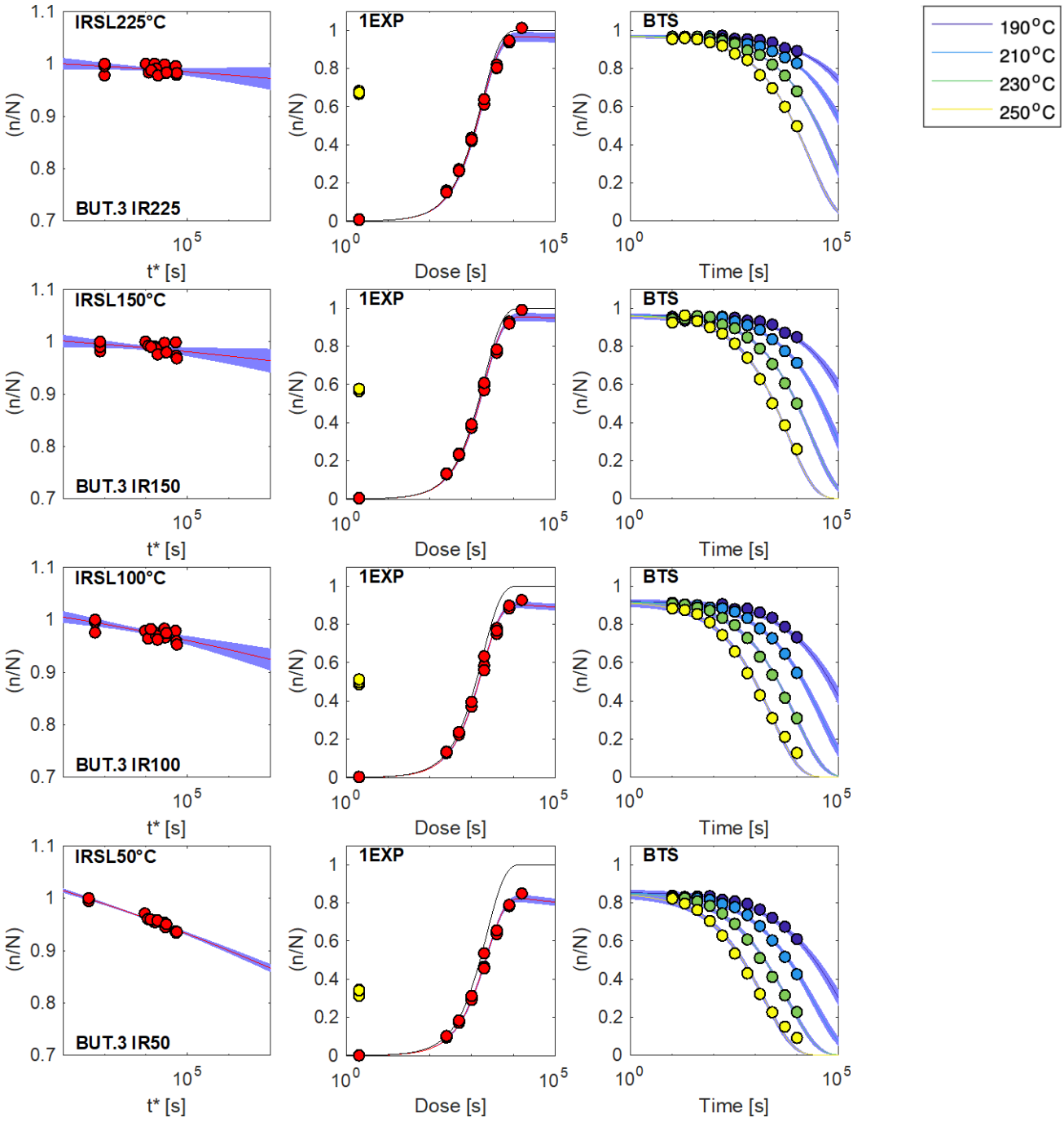
IRSL225°C
BUT.3 IR225
1EXP
BTS
IRSL150°C
BUT.3 IR150
IRSL100°C
BUT.3 IR100
IRSL50°C
BUT.3 IR50
(n/N)
t* [s]
Dose [s]
Time [s]
190°C
210°C
230°C
250°C

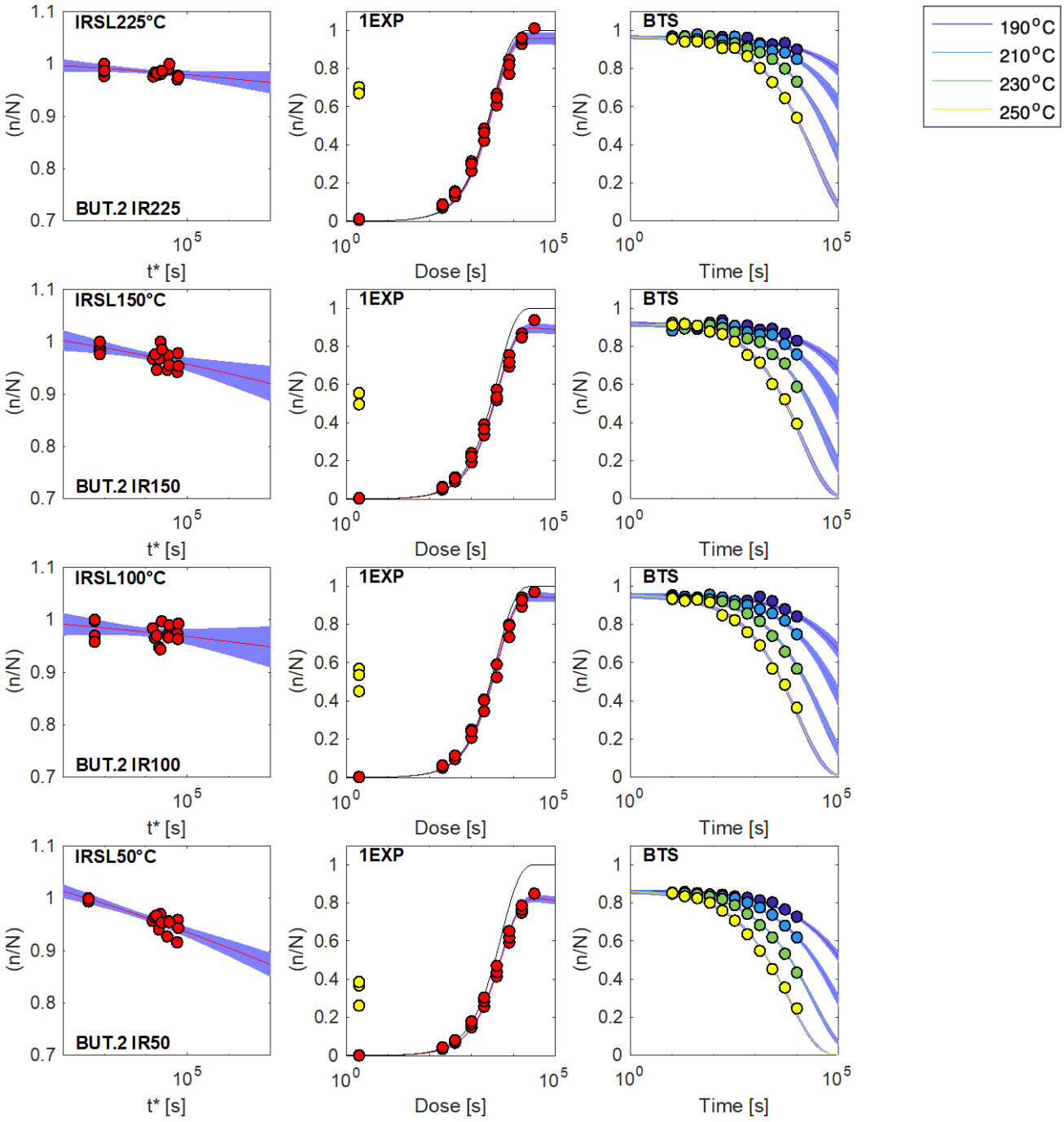
IRSL225°C
1EXP
BTS
BUT.2 IR225
IRSL150°C
BUT.2 IR150
IRSL100°C
BUT.2 IR100
IRSL50°C
BUT.2 IR50
(n/N)
t* [s]
Dose [s]
Time [s]
190°C
210°C
230°C
250°C

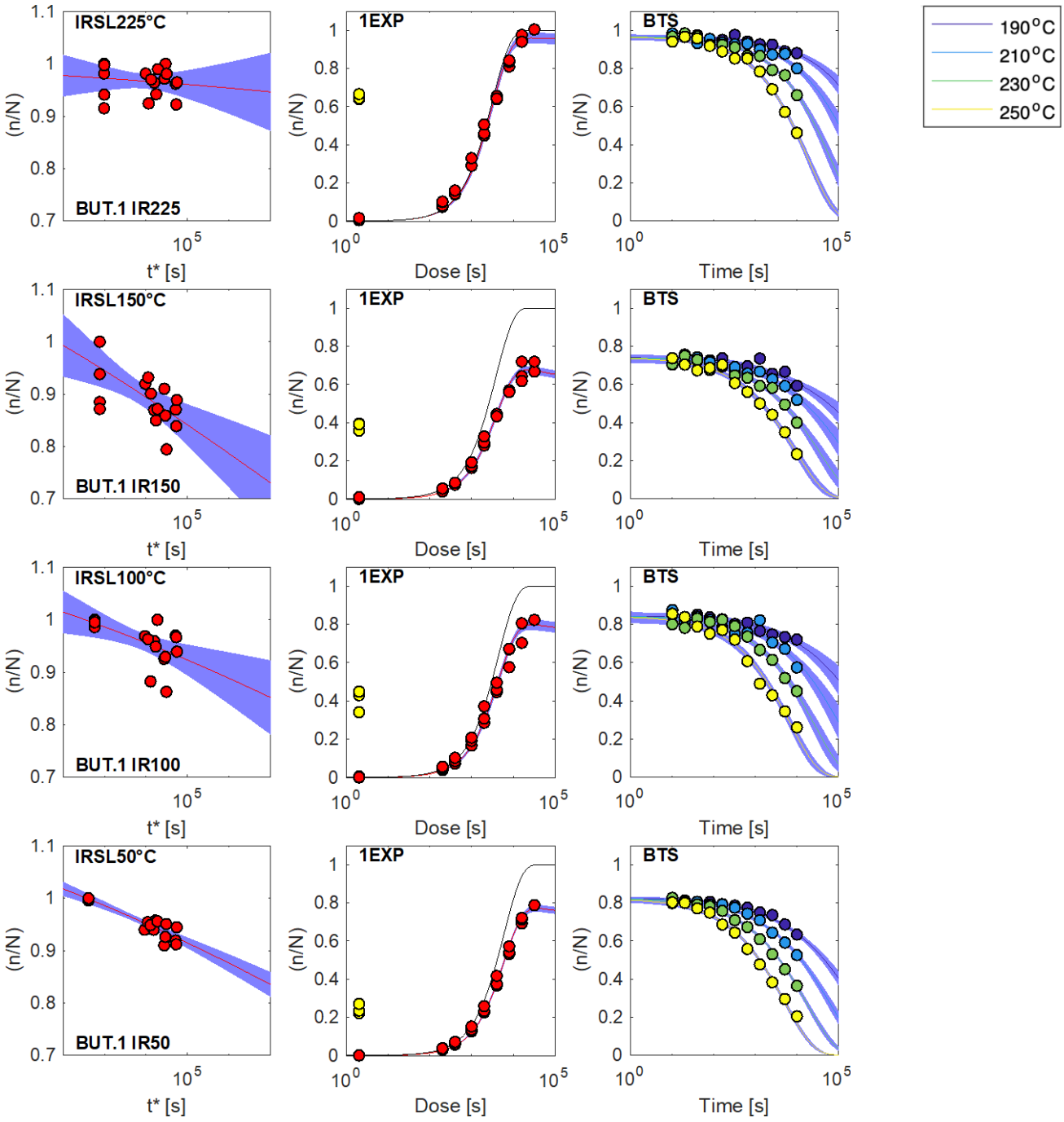

Fig. S3.2: *Luminescence measurement and model fit results for all samples of the BUT transect. (A, D, G, J) Anomalous fading data fitted using equations 3 and 4 of King et al. (2016), for the IRSL at 50, 100, 150, and 225 °C respectively. (B, E, H, K) Luminescence dose response accounting for fading, fitted using equation 5 of King et al. (2016). The black solid line is the unfaded dose response curve, and the yellow dots represent the $\tilde{n}_{nat}$ values of each aliquot. (C, F, I, L) Isothermal decay data fitted with the BTS model, using equations 6 and 7 of King et al. (2016).*

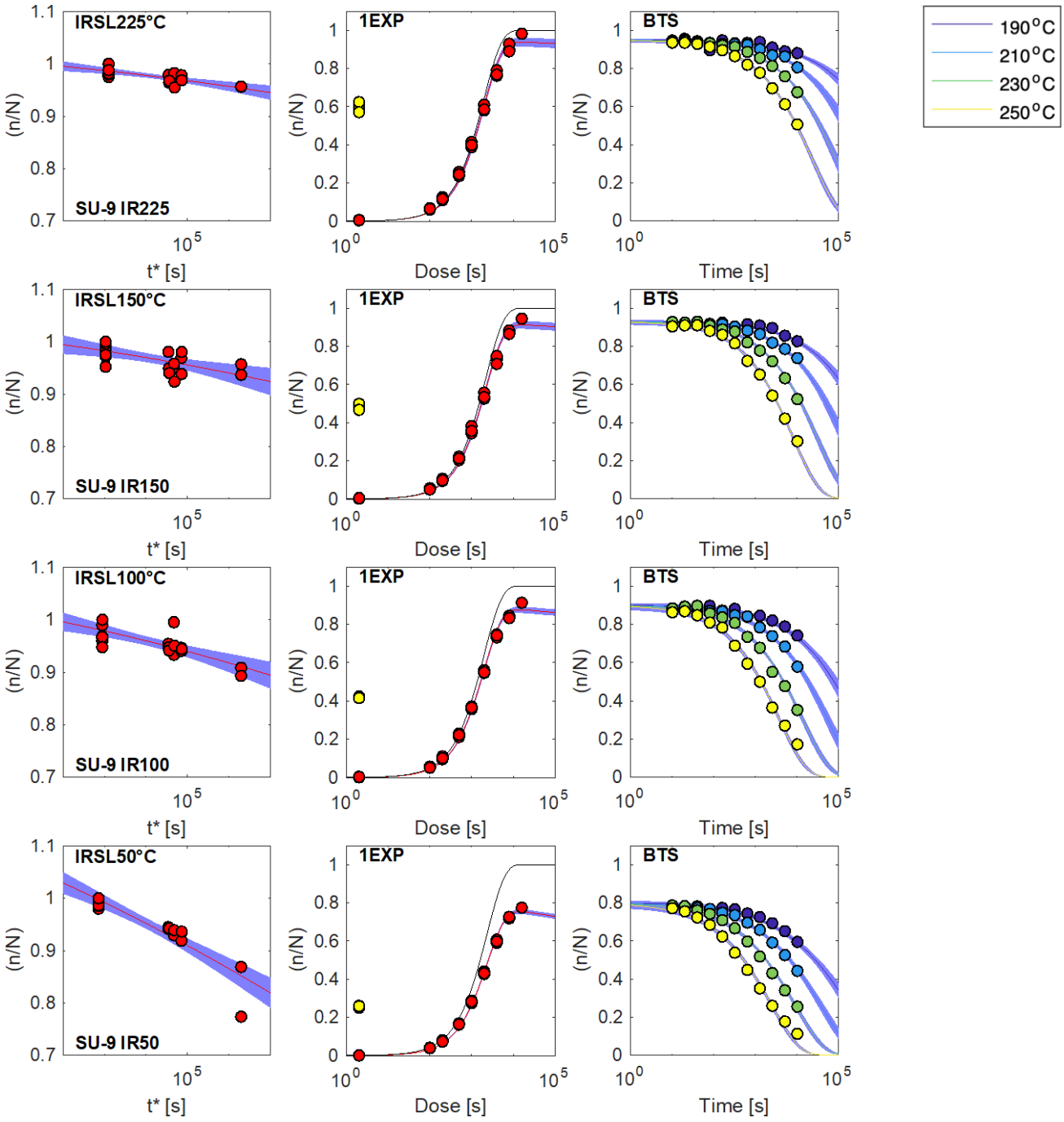
IRSL225°C
SU-9 IR225
1EXP
BTS
IRSL150°C
SU-9 IR150
IRSL100°C
SU-9 IR100
IRSL50°C
SU-9 IR50
(n/N)
t* [s]
Dose [s]
Time [s]
190°C
210°C
230°C
250°C

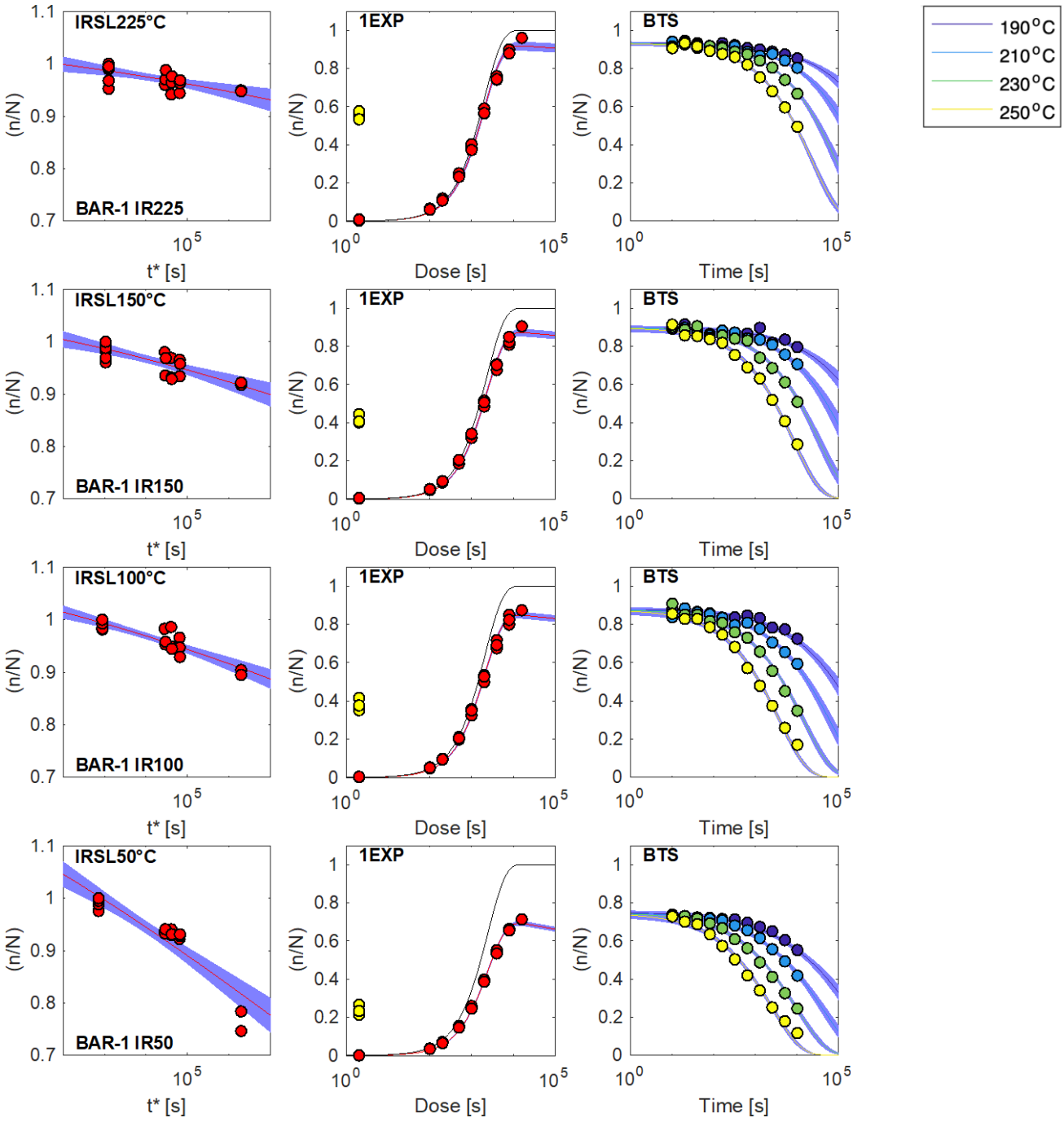

Fig. S3.3: *Luminescence measurement and model fit results of the samples SU-9 and BAR-1. (A, D, G, J) Anomalous fading data fitted using equations 3 and 4 of King et al. (2016), for the IRSL at 50, 100, 150, and 225 °C respectively. (B, E, H, K) Luminescence dose response accounting for fading, fitted using equation 5 of King et al. (2016). The black solid line is the unfaded dose response curve, and the yellow dots represent the $\tilde{n}_{nat}$ values of each aliquot. (C, F, I, L) Isothermal decay data fitted with the BTS model, using equations 6 and 7 of King et al. (2016).*

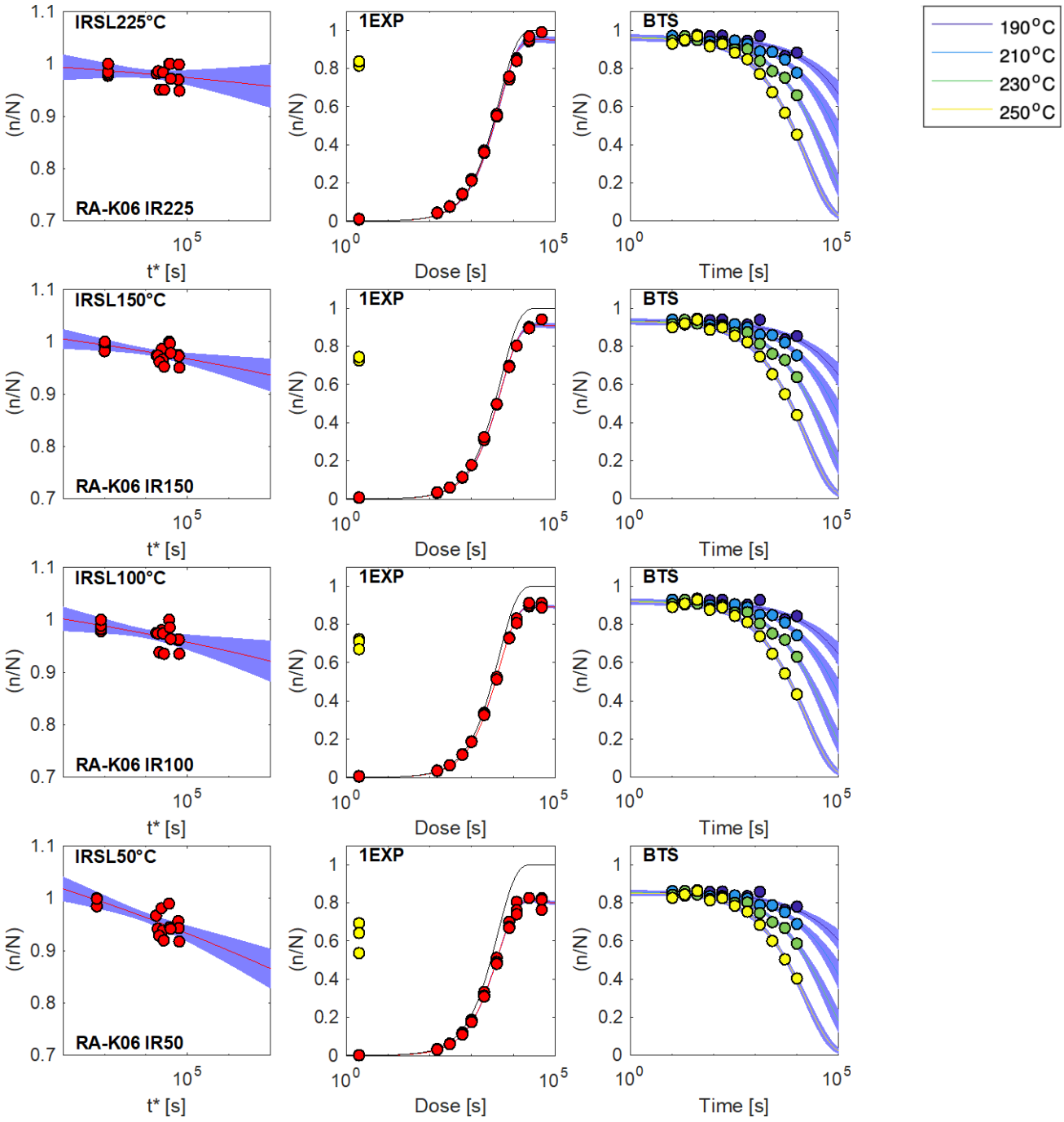
IRSL225°C
RA-K06 IR225
1EXP
BTS
IRSL150°C
RA-K06 IR150
IRSL100°C
RA-K06 IR100
IRSL50°C
RA-K06 IR50
(n/N)
t* [s]
Dose [s]
Time [s]
190°C
210°C
230°C
250°C

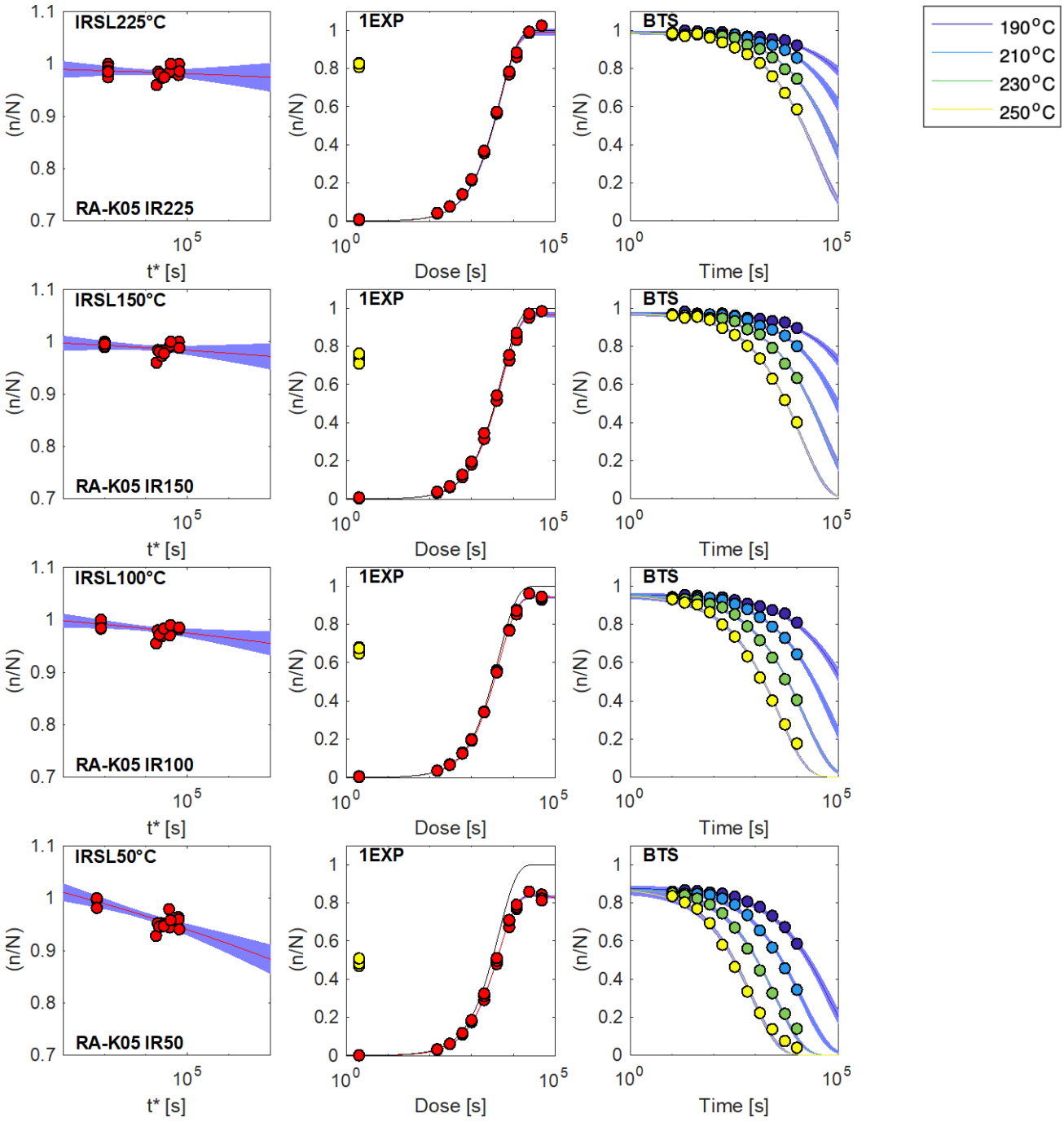
IRSL225°C
RA-K05 IR225
1EXP
BTS
IRSL150°C
RA-K05 IR150
IRSL100°C
RA-K05 IR100
IRSL50°C
RA-K05 IR50
(n/N)
t* [s]
Dose [s]
Time [s]
190°C
210°C
230°C
250°C

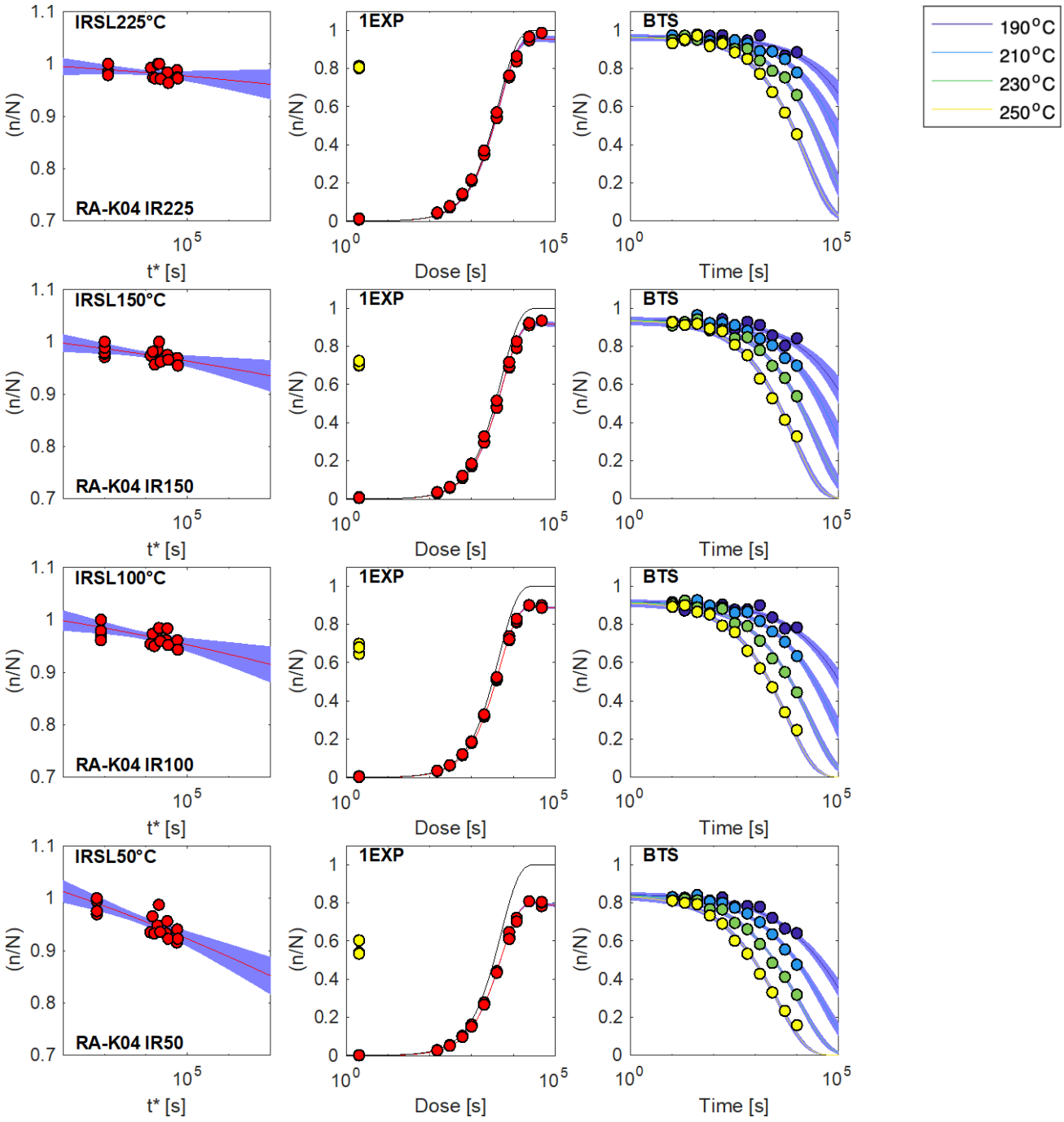
IRSL225°C
1EXP
BTS
RA-K04 IR225
IRSL150°C
RA-K04 IR150
IRSL100°C
RA-K04 IR100
IRSL50°C
RA-K04 IR50
(n/N)
t* [s]
Dose [s]
Time [s]
190°C
210°C
230°C
250°C

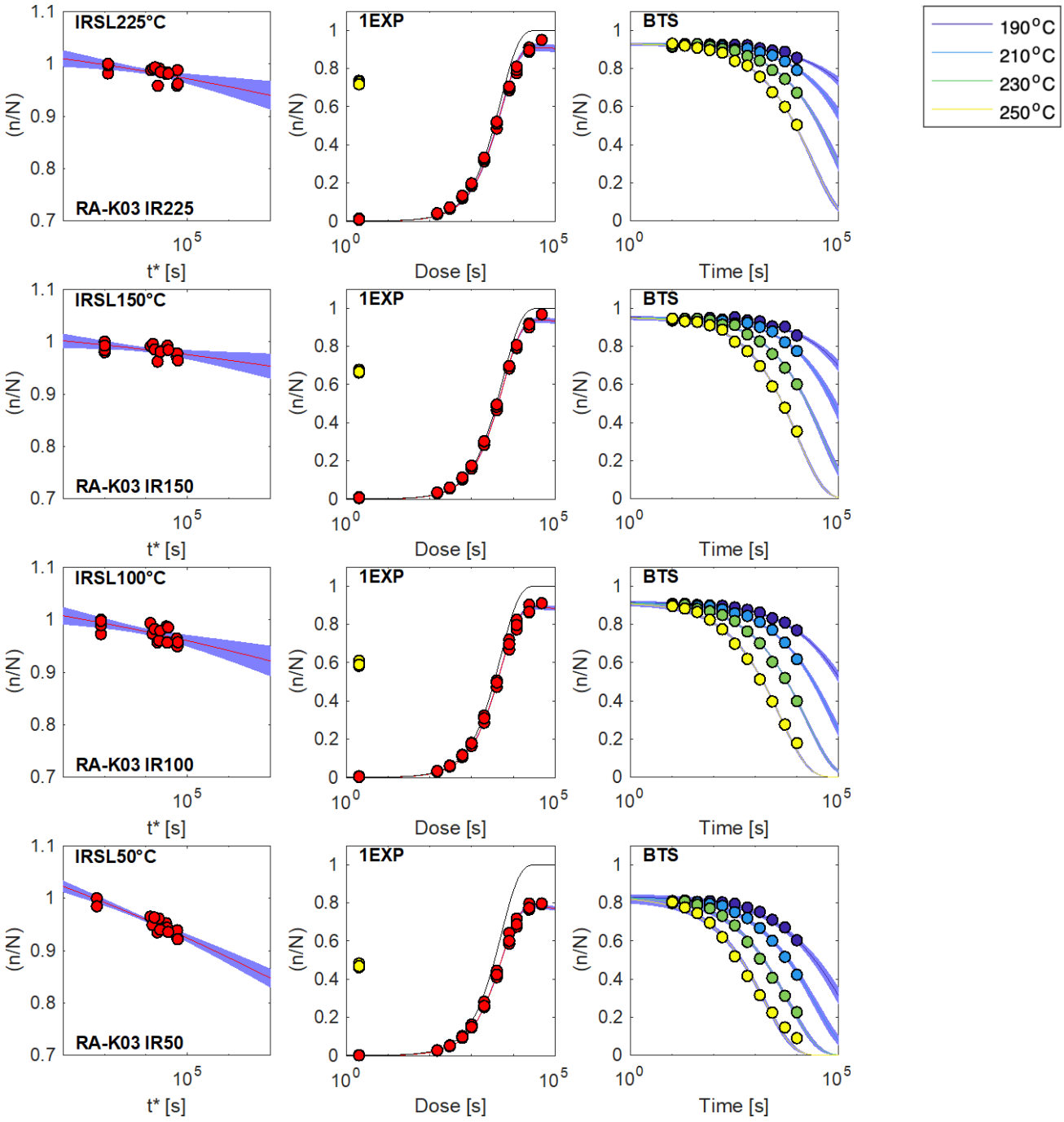
IRSL225°C
1EXP
BTS
RA-K03 IR225
IRSL150°C
RA-K03 IR150
IRSL100°C
RA-K03 IR100
IRSL50°C
RA-K03 IR50
(n/N)
t* [s]
Dose [s]
Time [s]
190°C
210°C
230°C
250°C

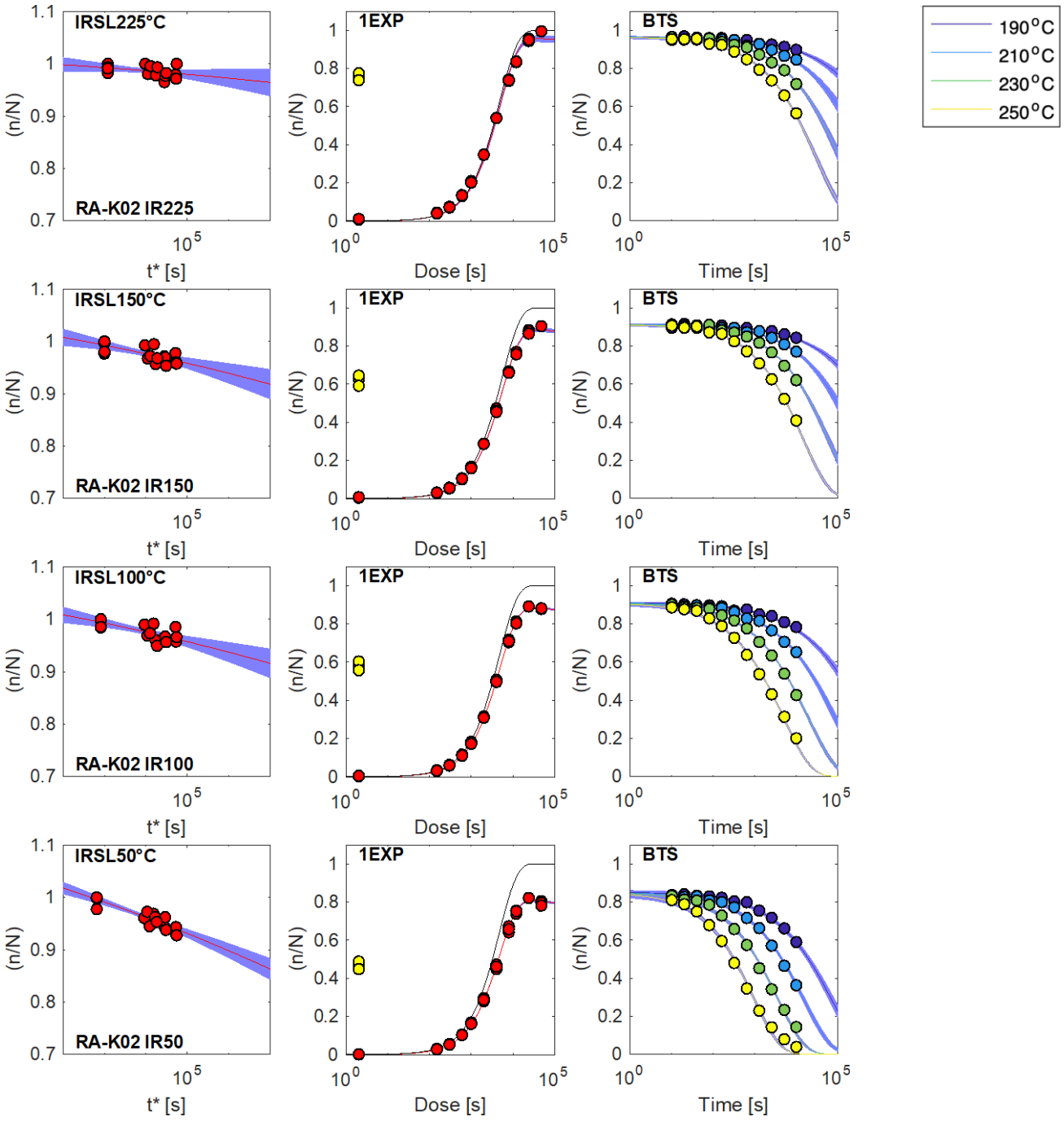
IRSL225°C
RA-K02 IR225
1EXP
BTS
IRSL150°C
RA-K02 IR150
IRSL100°C
RA-K02 IR100
IRSL50°C
RA-K02 IR50
(n/N)
t* [s]
Dose [s]
Time [s]
190°C
210°C
230°C
250°C

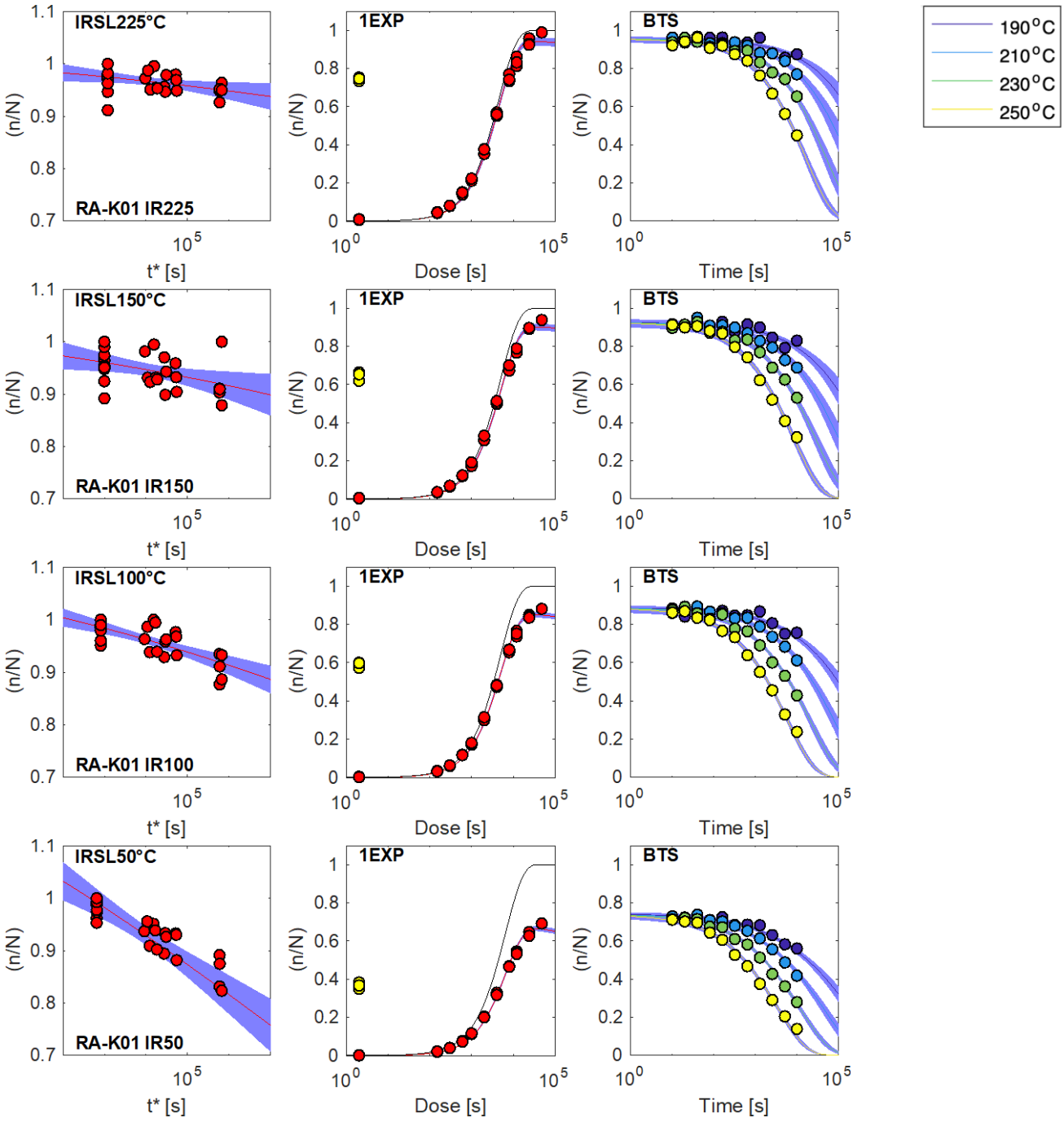

Fig. S3.4: *Luminescence measurement and model fit results for all samples of the RA-K transect. (A, D, G, J) Anomalous fading data fitted using equations 3 and 4 of King et al. (2016), for the IRSL at 50, 100, 150, and 225 °C respectively. (B, E, H, K) Luminescence dose response accounting for fading, fitted using equation 5 of King et al. (2016). The black solid line is the unfaded dose response curve, and the yellow dots represent the $\tilde{n}_{nat}$ values of each aliquot. (C, F, I, L) Isothermal decay data fitted with the BTS model, using equations 6 and 7 of King et al. (2016).*

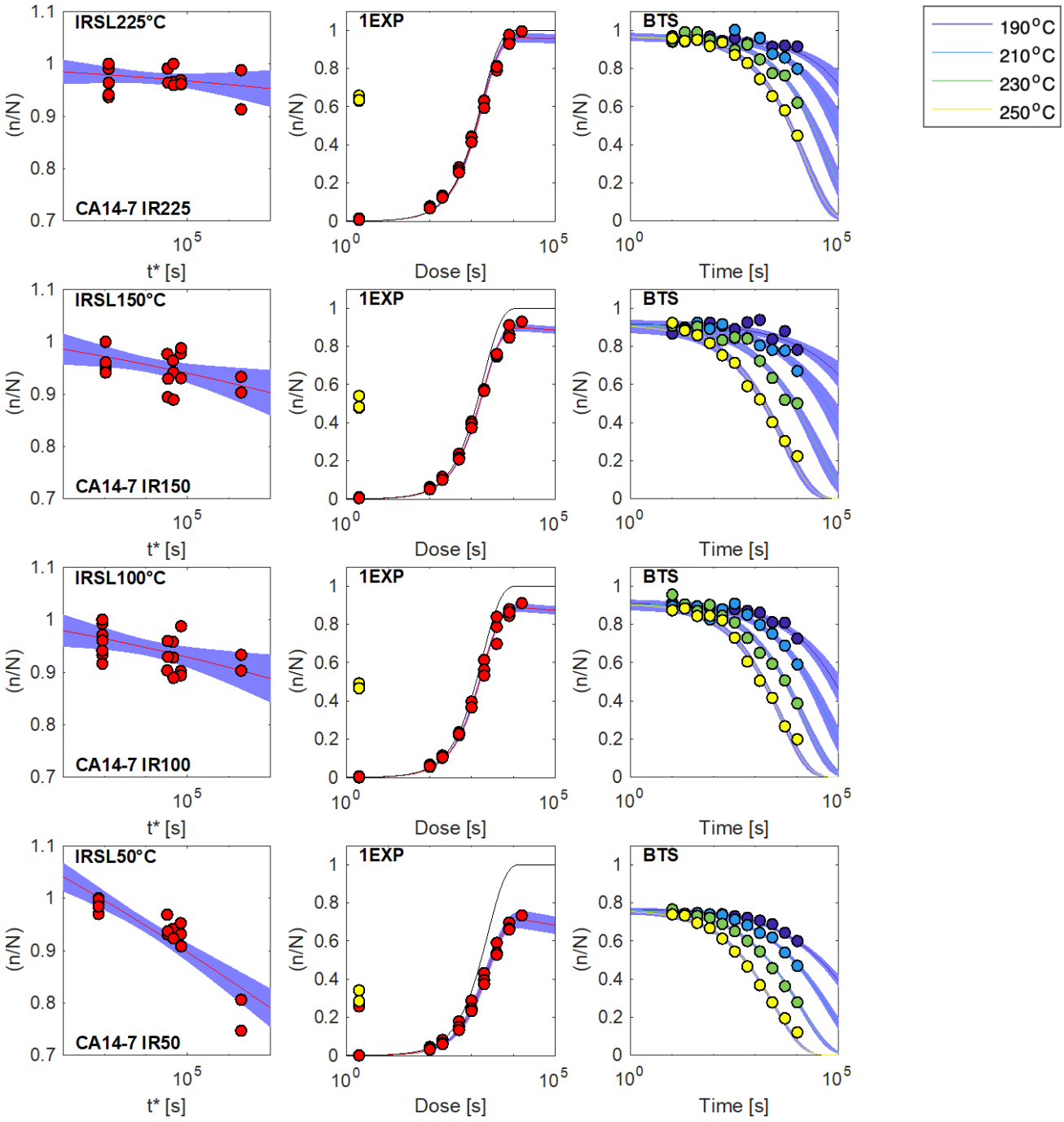
IRSL225°C
CA14-7 IR225
IRSL150°C
CA14-7 IR150
IRSL100°C
CA14-7 IR100
IRSL50°C
CA14-7 IR50
1EXP
BTS
(n/N)
t* [s]
Dose [s]
Time [s]
190°C
210°C
230°C
250°C

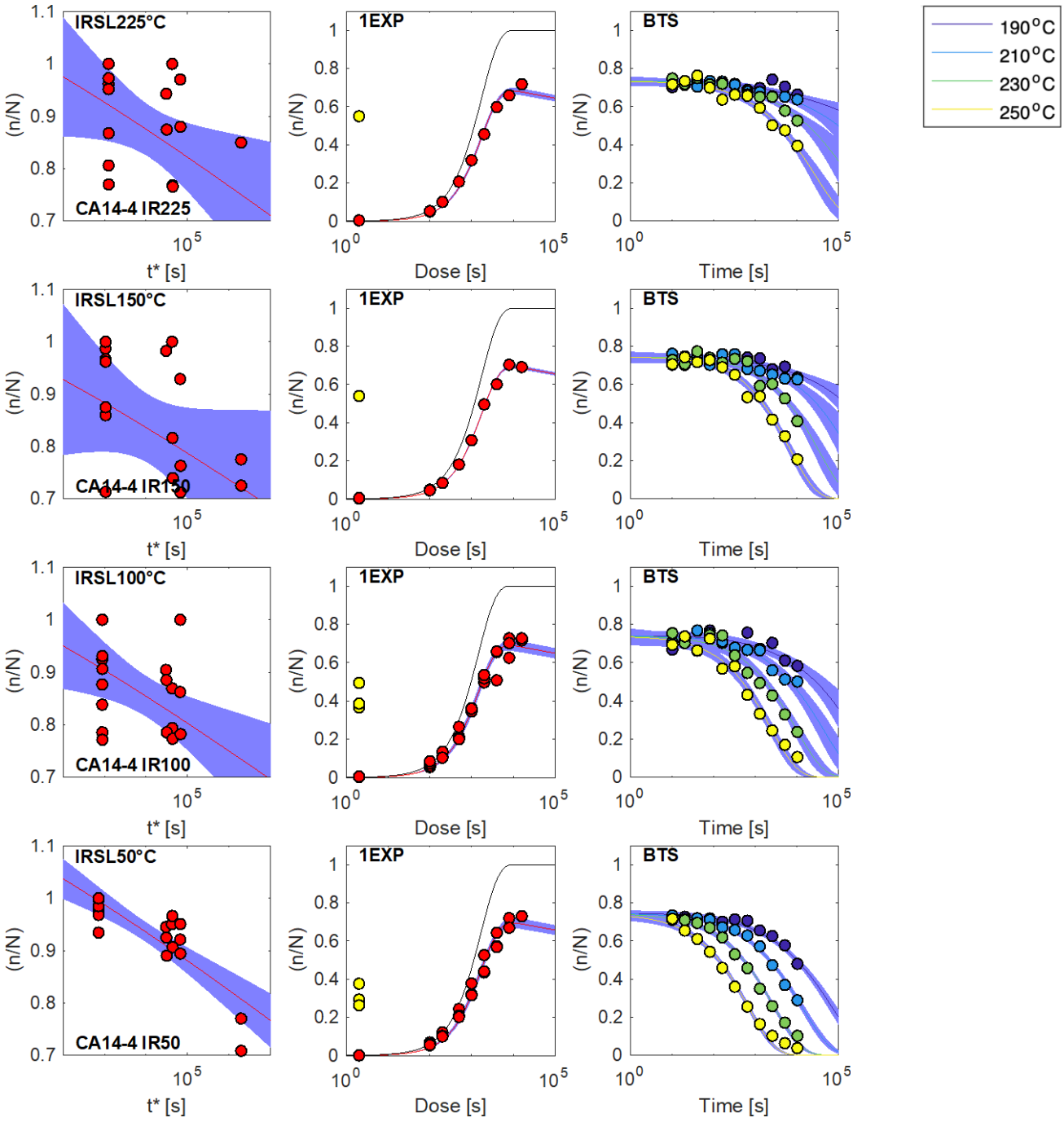

Fig. S3.5: *Luminescence measurement and model fit results for the samples CA14-4 and CA14-7. (A, D, G, J) Anomalous fading data fitted using equations 3 and 4 of King et al. (2016), for the IRSL at 50, 100, 150, and 225 °C respectively. (B, E, H, K) Luminescence dose response accounting for fading, fitted using equation 5 of King et al. (2016). The black solid line is the unfaded dose response curve, and the yellow dots represent the $\tilde{n}_{nat}$ values of each aliquot. (C, F, I, L) Isothermal decay data fitted with the BTS model, using equations 6 and 7 of King et al. (2016).*

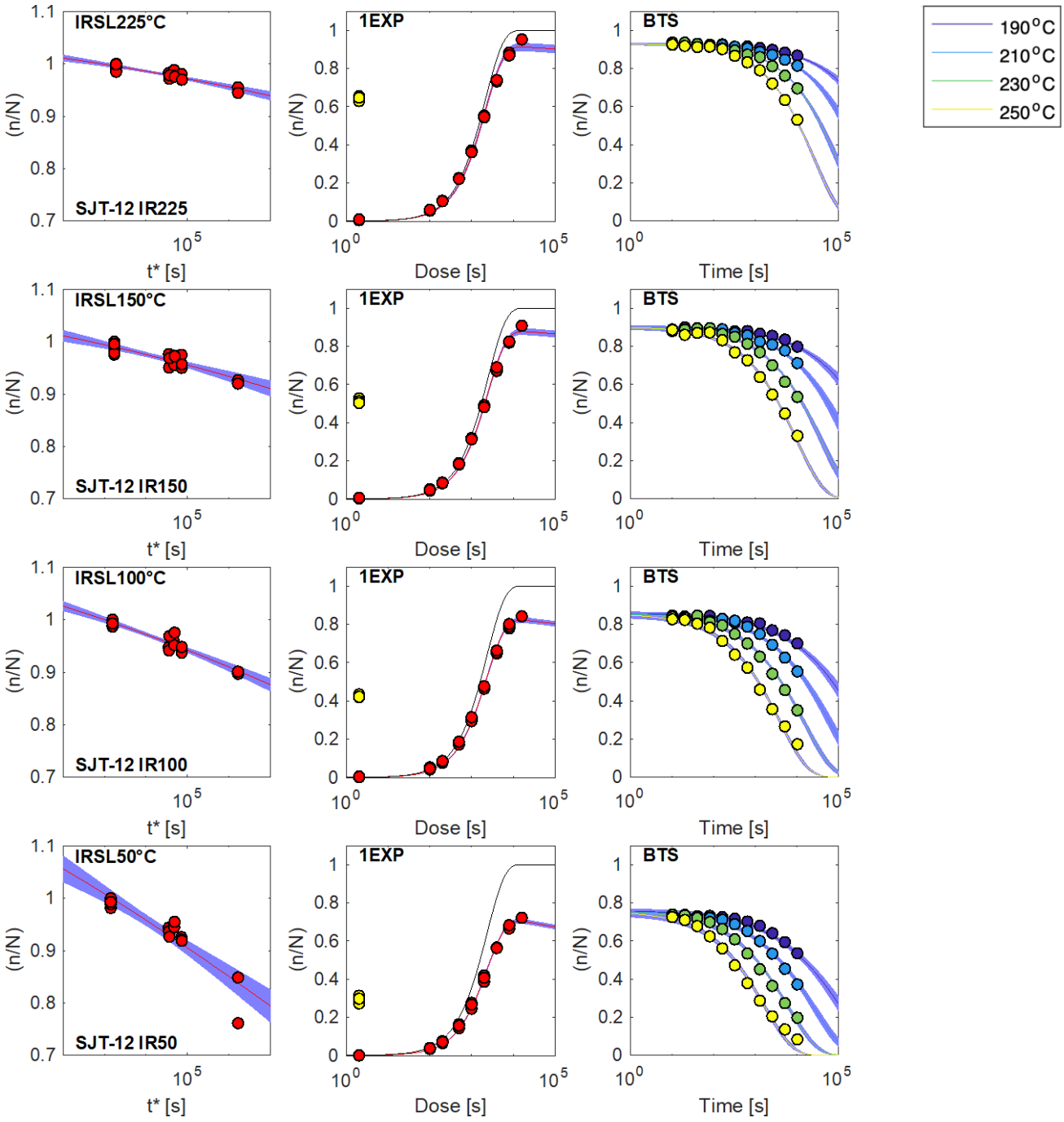
IRSL225°C
SJT-12 IR225
1EXP
BTS
IRSL150°C
SJT-12 IR150
IRSL100°C
SJT-12 IR100
IRSL50°C
SJT-12 IR50
(n/N)
t* [s]
Dose [s]
Time [s]
190°C
210°C
230°C
250°C

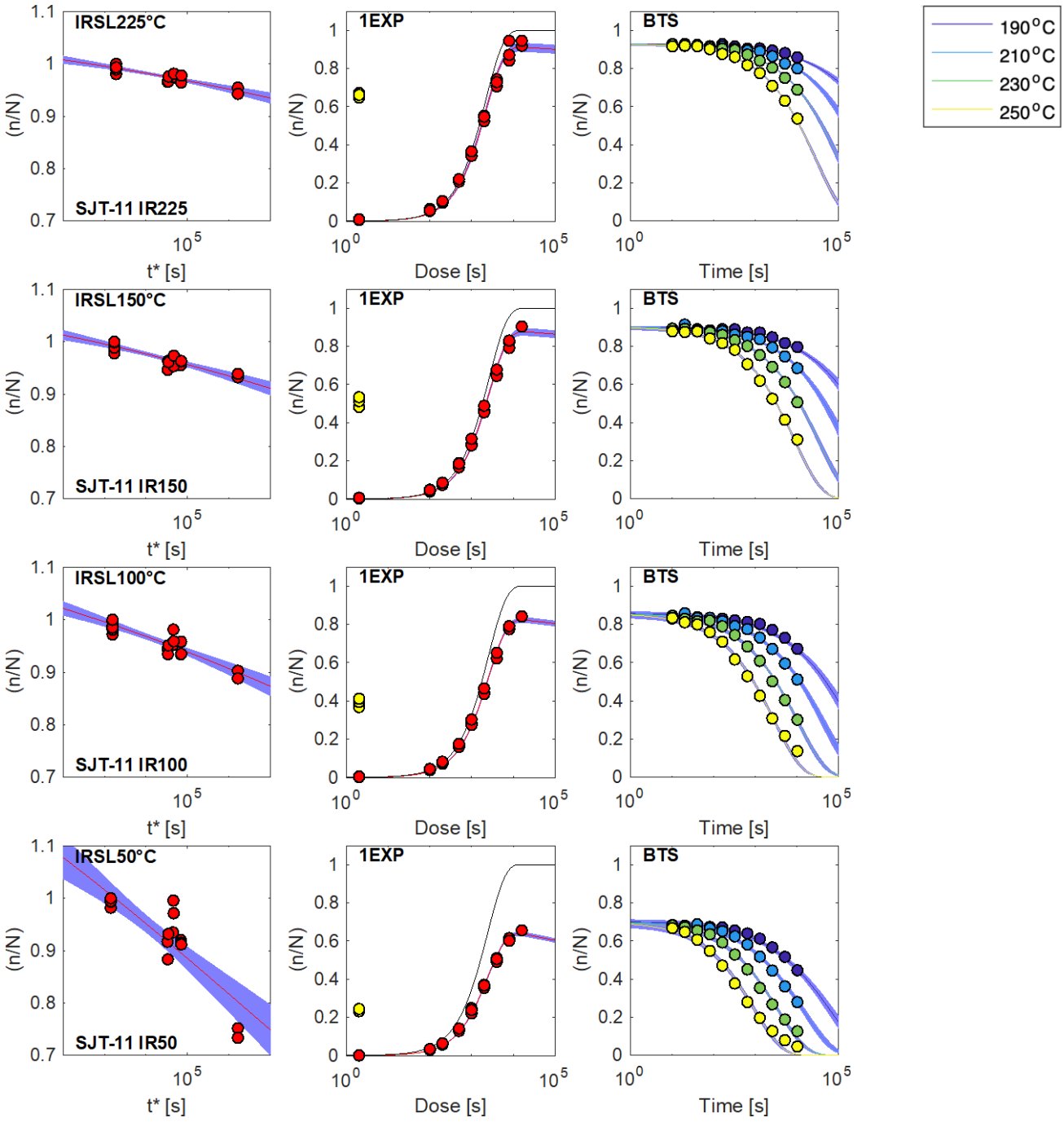
IRSL225°C
SJT-11 IR225
1EXP
BTS
IRSL150°C
SJT-11 IR150
IRSL100°C
SJT-11 IR100
IRSL50°C
SJT-11 IR50
(n/N)
t* [s]
Dose [s]
Time [s]
190°C
210°C
230°C
250°C

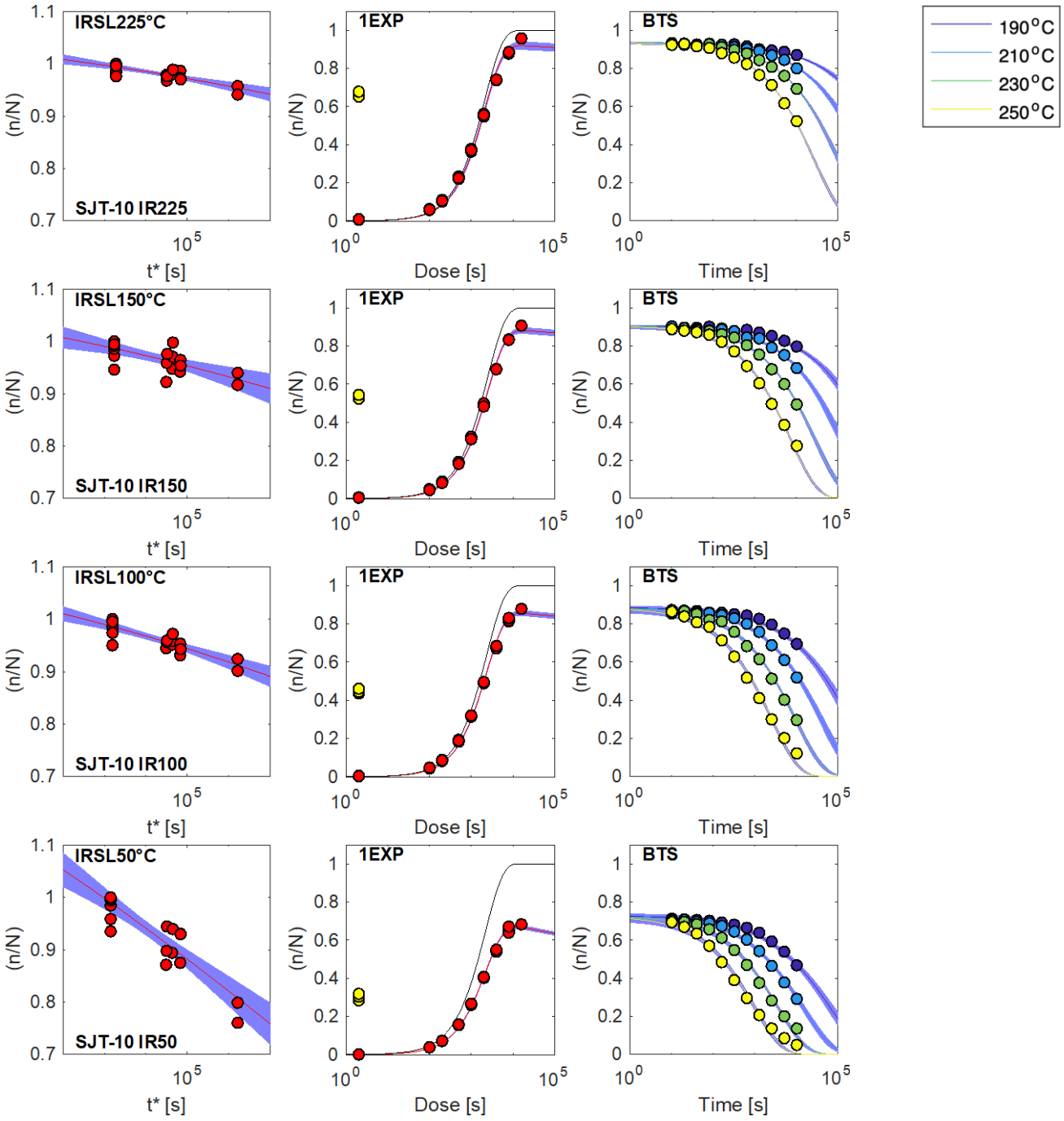
IRSL225°C
SJT-10 IR225
1EXP
BTS
IRSL150°C
SJT-10 IR150
IRSL100°C
SJT-10 IR100
IRSL50°C
SJT-10 IR50
(n/N)
t* [s]
Dose [s]
Time [s]
190°C
210°C
230°C
250°C

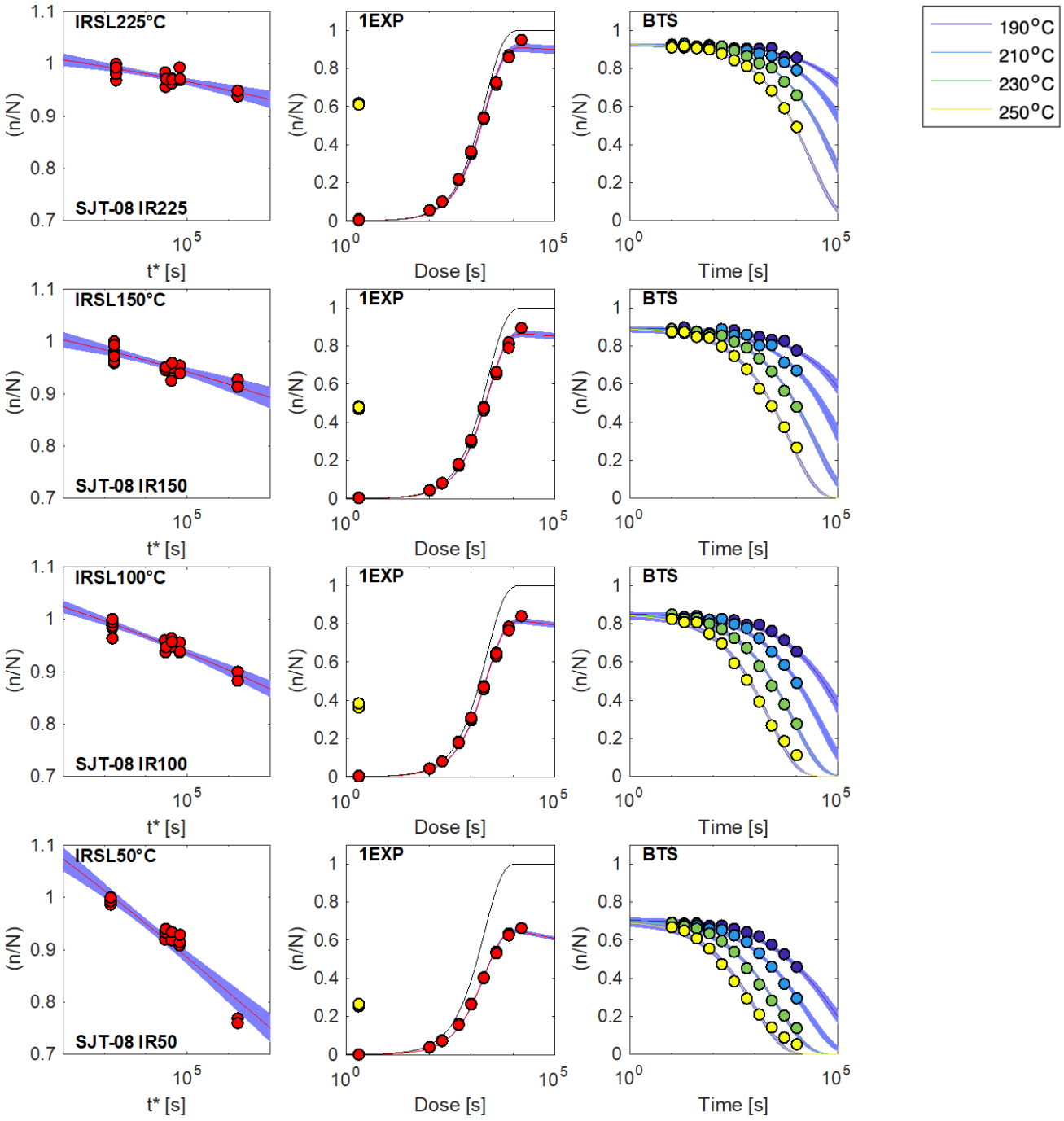
IRSL225°C
SJT-08 IR225
1EXP
BTS
IRSL150°C
SJT-08 IR150
IRSL100°C
SJT-08 IR100
IRSL50°C
SJT-08 IR50
(n/N)
t* [s]
Dose [s]
Time [s]
190°C
210°C
230°C
250°C

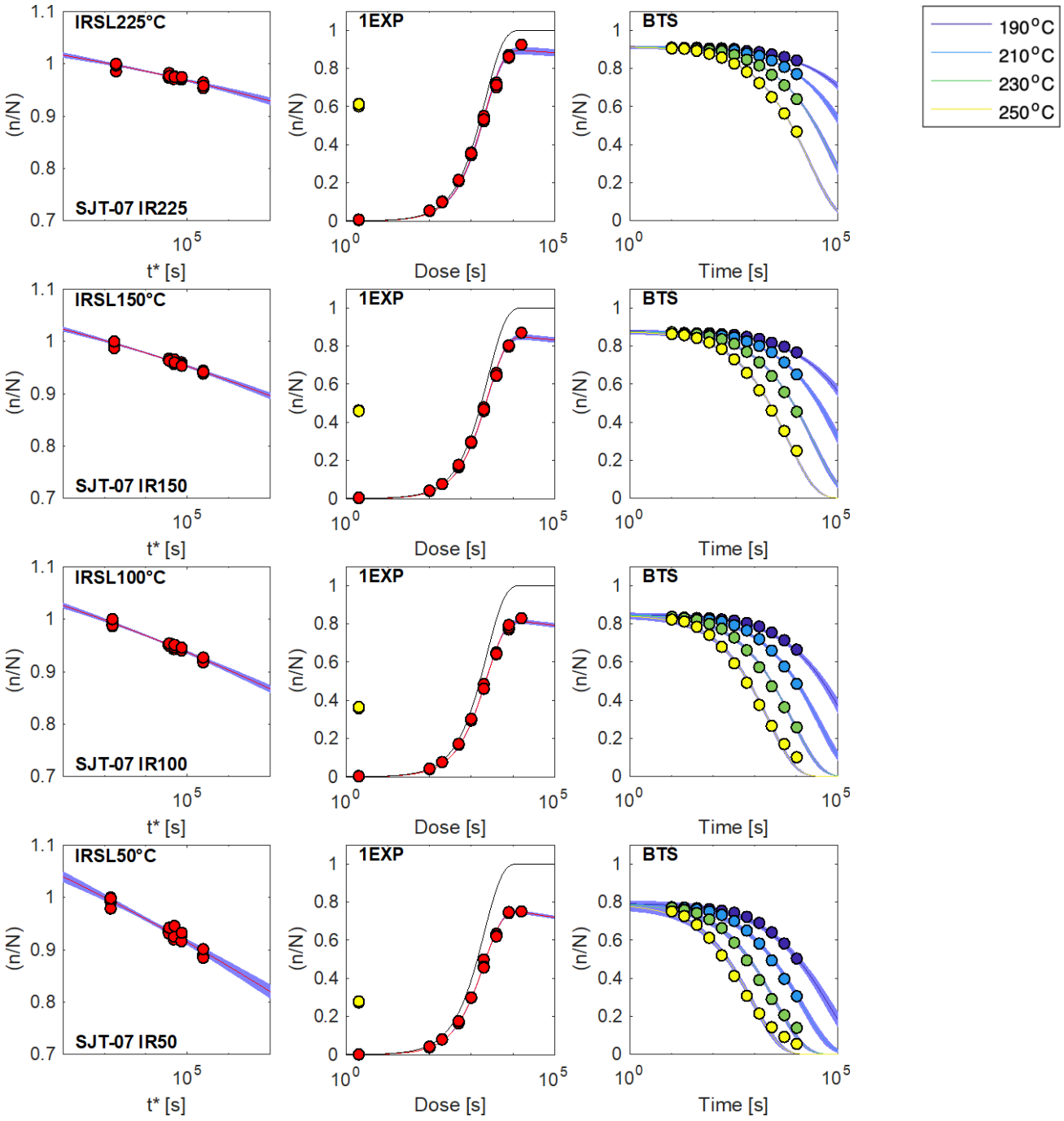
IRSL225°C
1EXP
BTS
SJT-07 IR225
IRSL150°C
SJT-07 IR150
IRSL100°C
SJT-07 IR100
IRSL50°C
SJT-07 IR50
(n/N)
t* [s]
Dose [s]
Time [s]
190°C
210°C
230°C
250°C

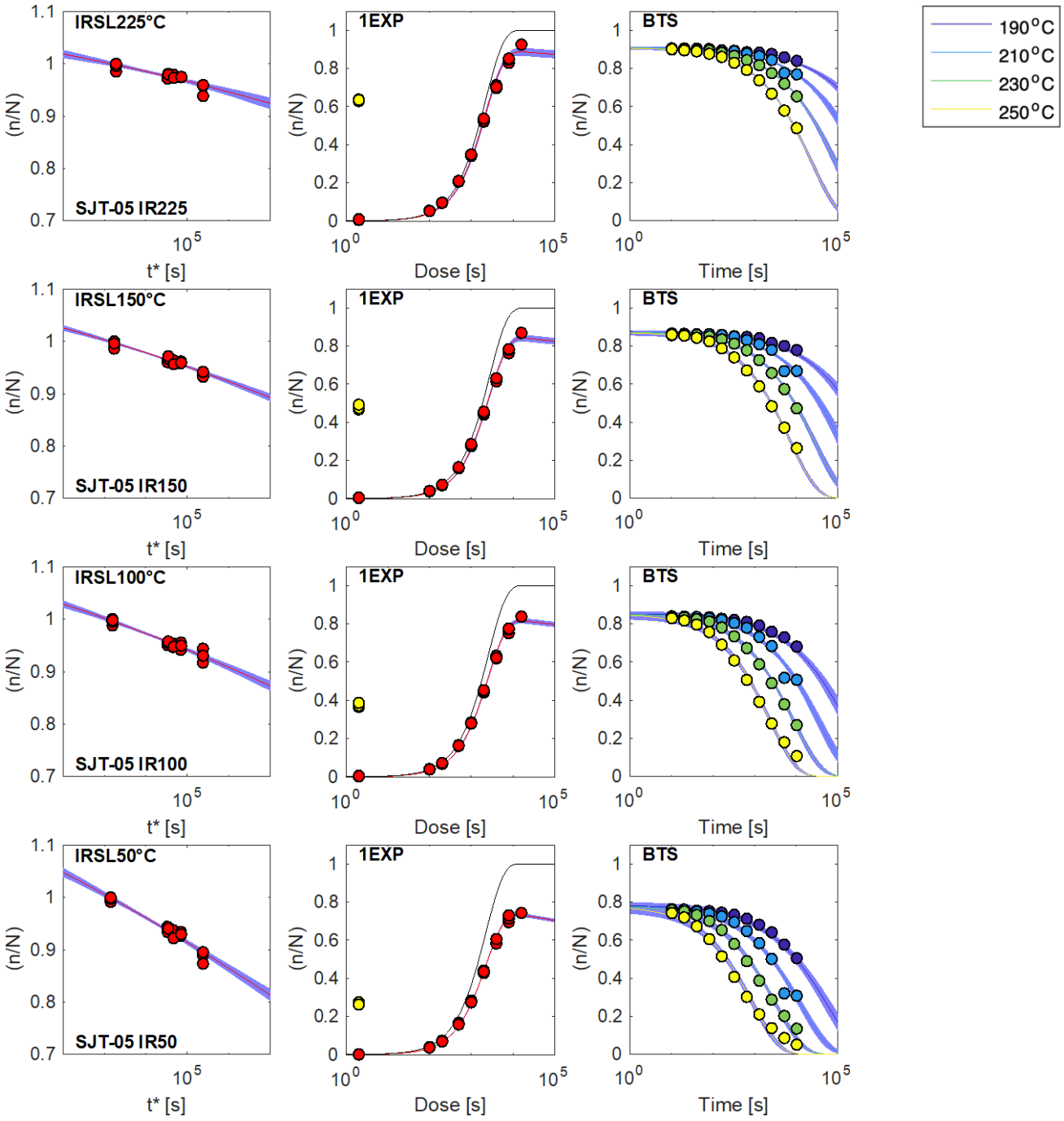
IRSL225°C
1EXP
BTS
SJT-05 IR225
IRSL150°C
SJT-05 IR150
IRSL100°C
SJT-05 IR100
IRSL50°C
SJT-05 IR50
(n/N)
t* [s]
Dose [s]
Time [s]
190°C
210°C
230°C
250°C

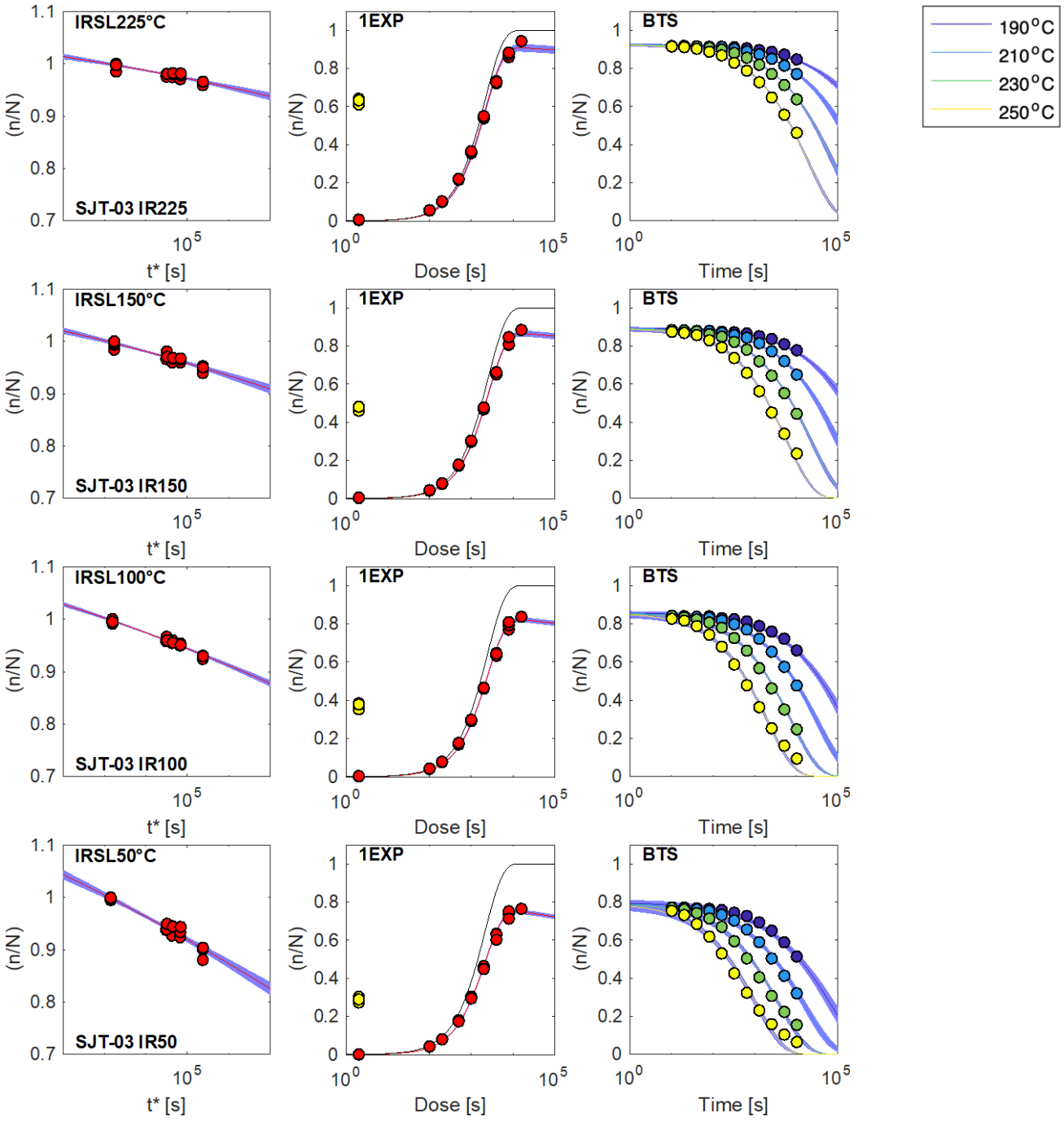
IRSL225°C
SJT-03 IR225
1EXP
BTS
IRSL150°C
SJT-03 IR150
IRSL100°C
SJT-03 IR100
IRSL50°C
SJT-03 IR50
(n/N)
t* [s]
Dose [s]
Time [s]
190°C
210°C
230°C
250°C

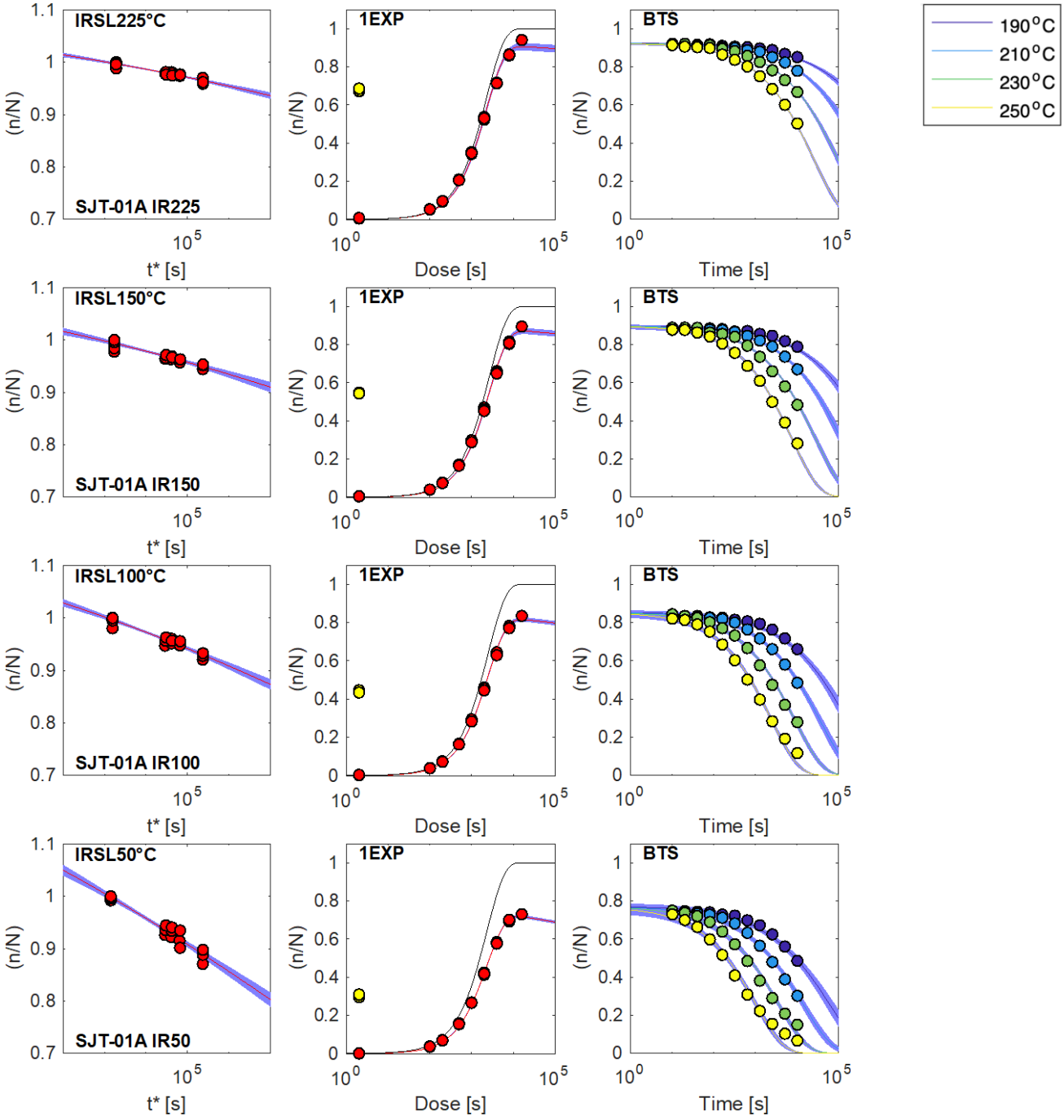

Fig. S3.6: *Luminescence measurement and model fit results for all samples of the SJT transect. (A, D, G, J) Anomalous fading data fitted using equations 3 and 4 of King et al. (2016), for the IRSL at 50, 100, 150, and 225 °C respectively. (B, E, H, K) Luminescence dose response accounting for fading, fitted using equation 5 of King et al. (2016). The black solid line is the unfaded dose response curve, and the yellow dots represent the $\tilde{n}_{nat}$ values of each aliquot. (C, F, I, L) Isothermal decay data fitted with the BTS model, using equations 6 and 7 of King et al. (2016).*

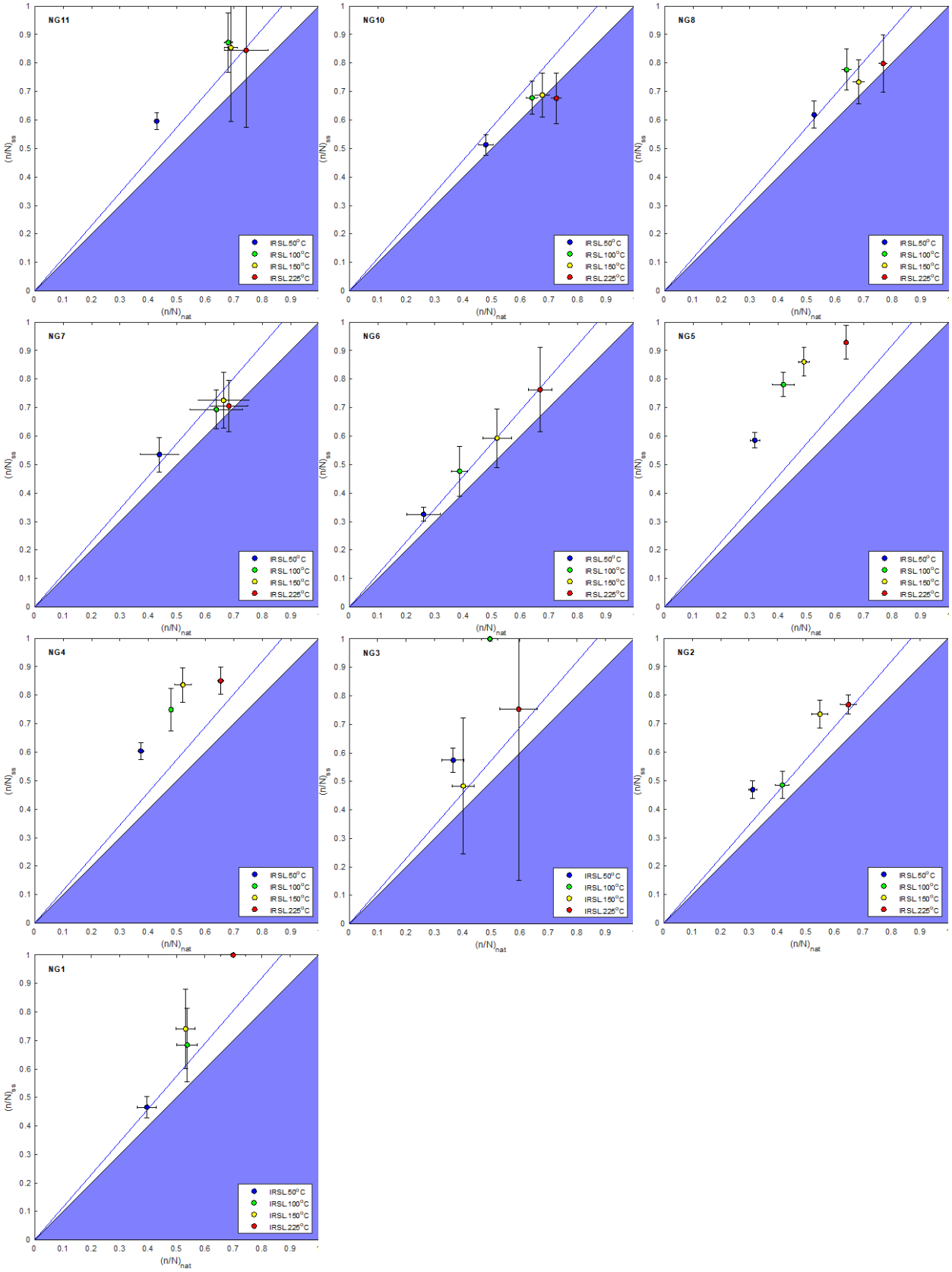

Fig. S4.1: *Steady-state saturation plots (Kars plots) for the NG transect, contrasting natural luminescence values, $\tilde{n}_{nat}$, with steady-state luminescence values, $\tilde{n}_{SS}$, predicted for each of the samples. The 1:1 line delimits saturated samples (blue area) to unsaturated samples (white area), with the saturation limit indicated by the blue line.*

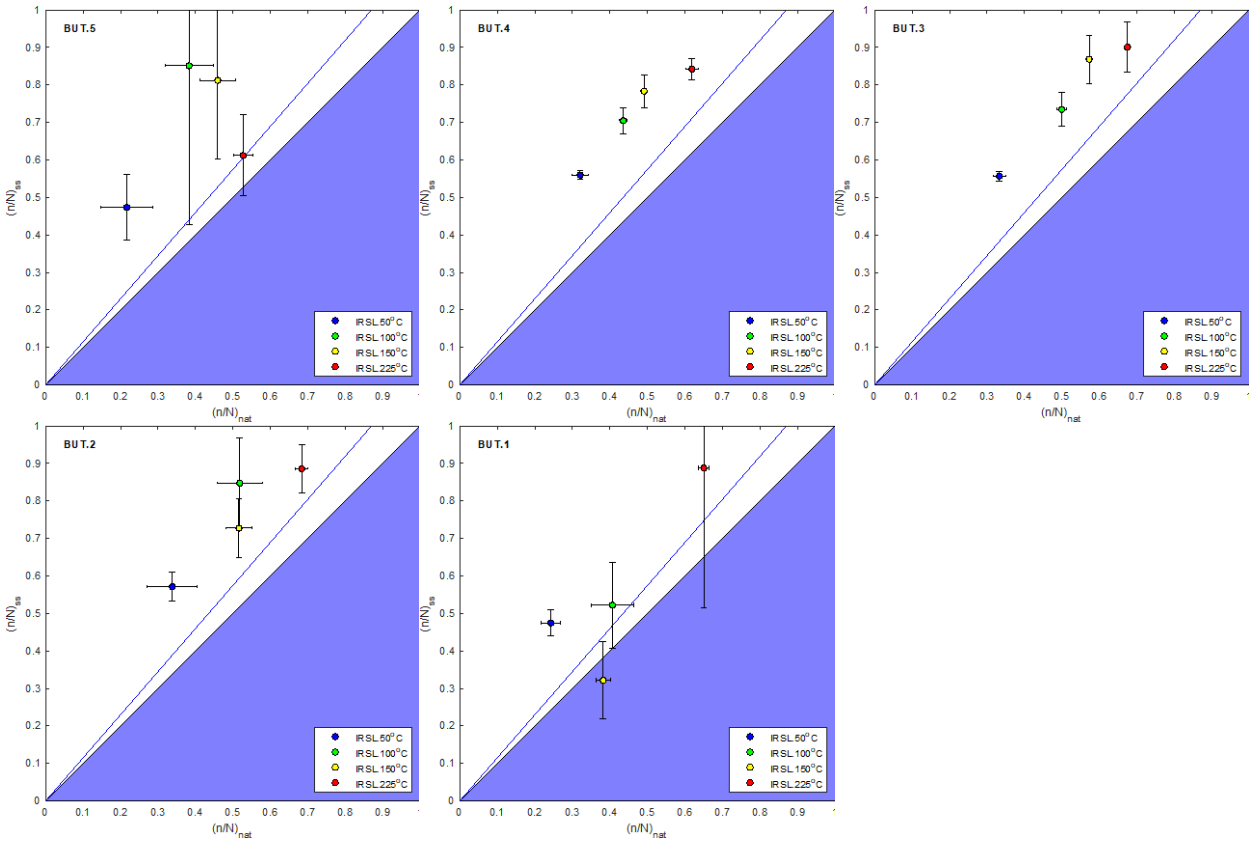

Fig. S4.2: *Steady-state saturation plots (Kars plots) for the BUT transect, contrasting natural luminescence values, $\tilde{n}_{nat}$, with steady-state luminescence values, $\tilde{n}_{SS}$, predicted for each of the samples. The 1:1 line delimits saturated samples (blue area) to unsaturated samples (white area), with the saturation limit indicated by the blue line.*

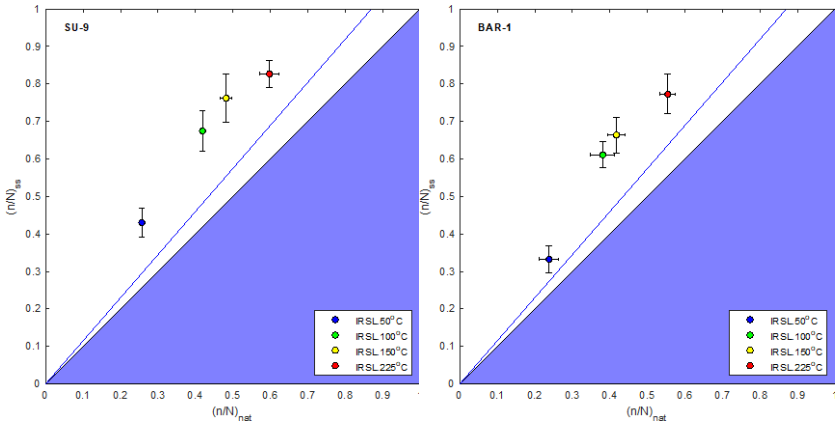

Fig. S4.3: *Steady-state saturation plots (Kars plots) for the SU-9 and BAR-1 samples, contrasting natural luminescence values, $\tilde{n}_{nat}$, with steady-state luminescence values, $\tilde{n}_{SS}$, predicted for each of the samples. The 1:1 line delimits saturated samples (blue area) to unsaturated samples (white area), with the saturation limit indicated by the blue line.*

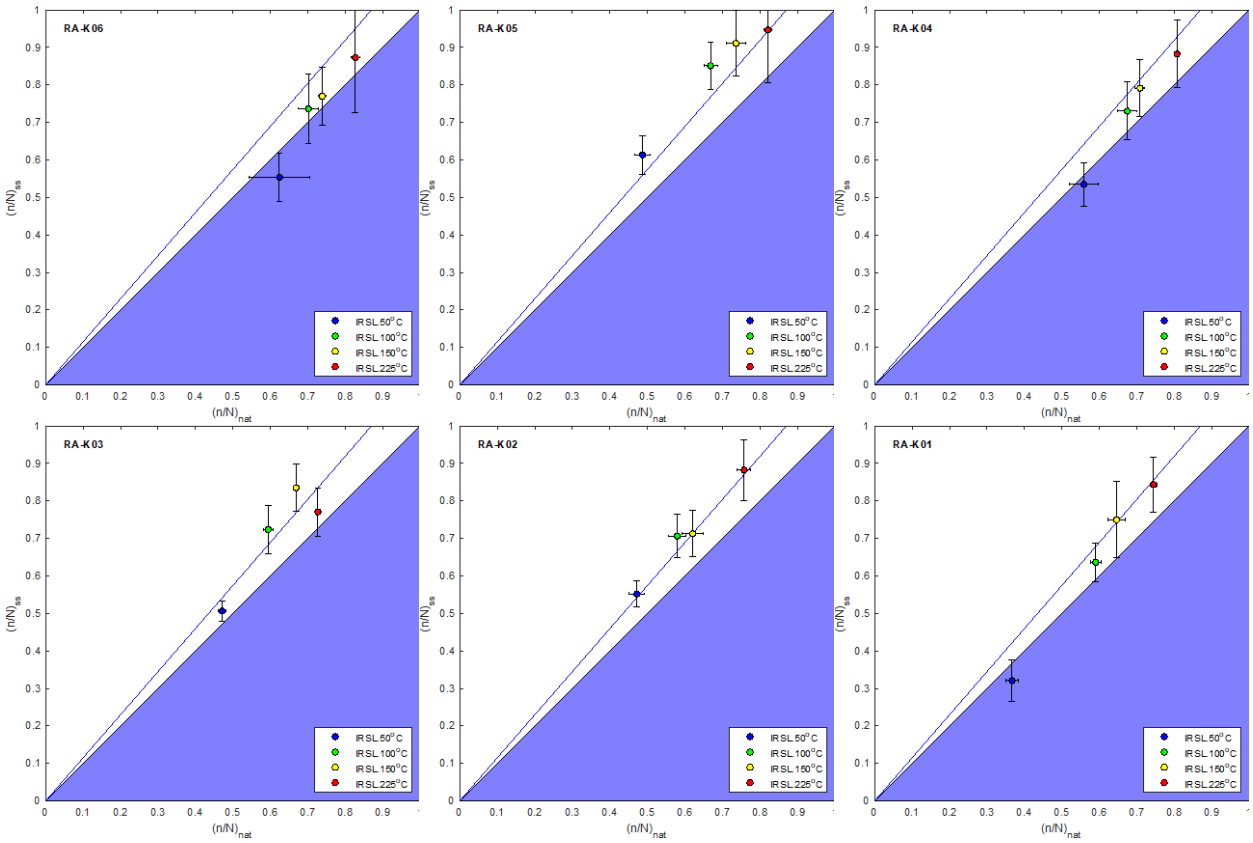

Fig. S4.4: *Steady-state saturation plots (Kars plots) for the RA-K transect, contrasting natural luminescence values, $\tilde{n}_{nat}$, with steady-state luminescence values, $\tilde{n}_{SS}$, predicted for each of the samples. The 1:1 line delimits saturated samples (blue area) to unsaturated samples (white area), with the saturation limit indicated by the blue line.*

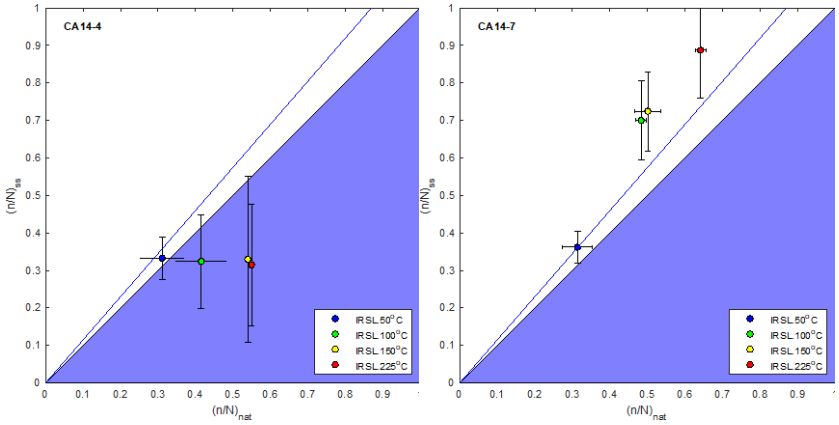

Fig. S4.5: *Steady-state saturation plots (Kars plots) for the CA14-4 and CA14-7 samples, contrasting natural luminescence values, $\tilde{n}_{nat}$, with steady-state luminescence values, $\tilde{n}_{SS}$, predicted for each of the samples. The 1:1 line delimits saturated samples (blue area) to unsaturated samples (white area), with the saturation limit indicated by the blue line.*

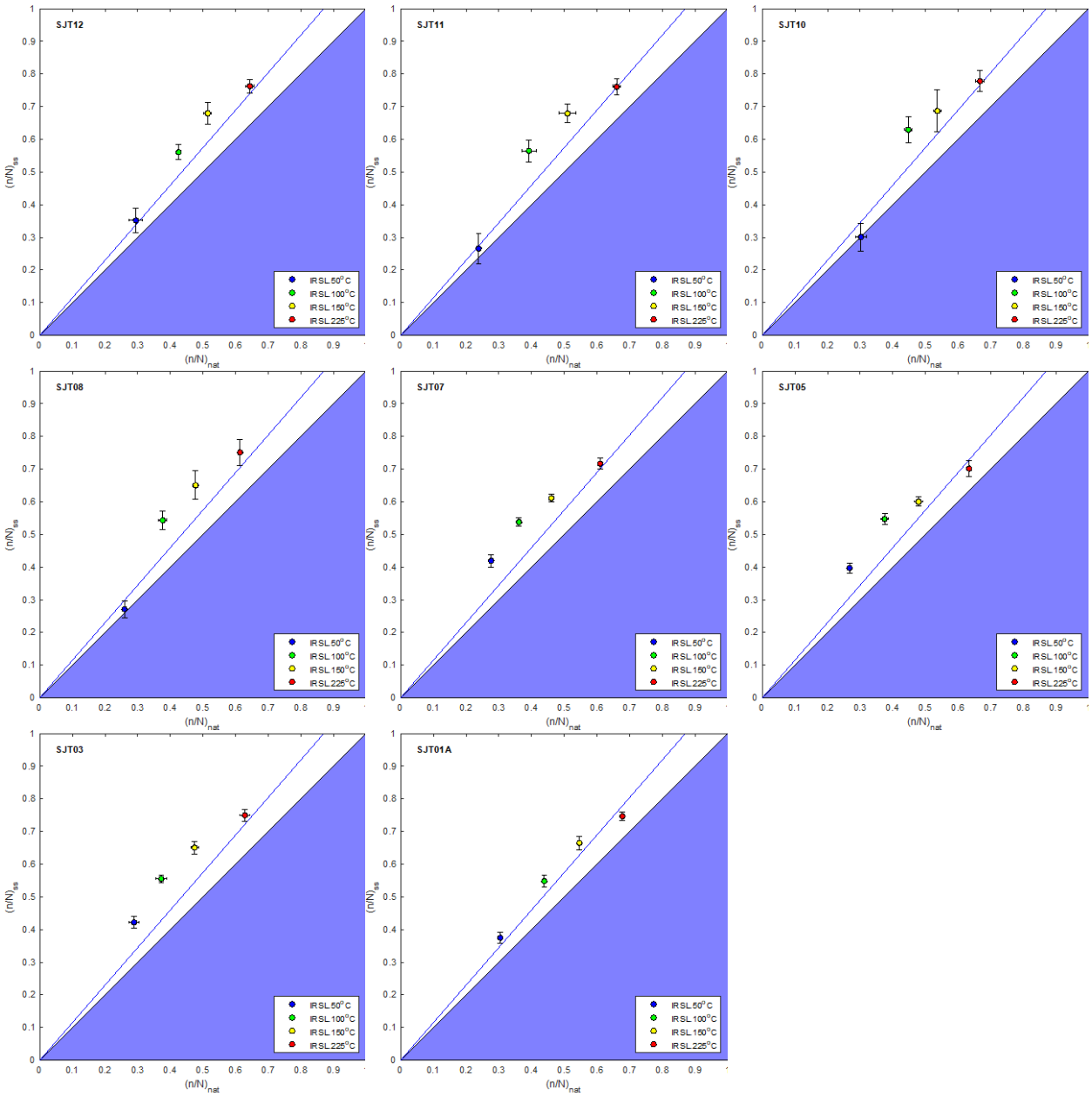

Fig. S4.6: *Steady-state saturation plots (Kars plots) for the SJT transect, contrasting natural luminescence values, $\tilde{n}_{nat}$, with steady-state luminescence values, $\tilde{n}_{SS}$, predicted for each of the samples. The 1:1 line delimits saturated samples (blue area) to unsaturated samples (white area), with the saturation limit indicated by the blue line.*

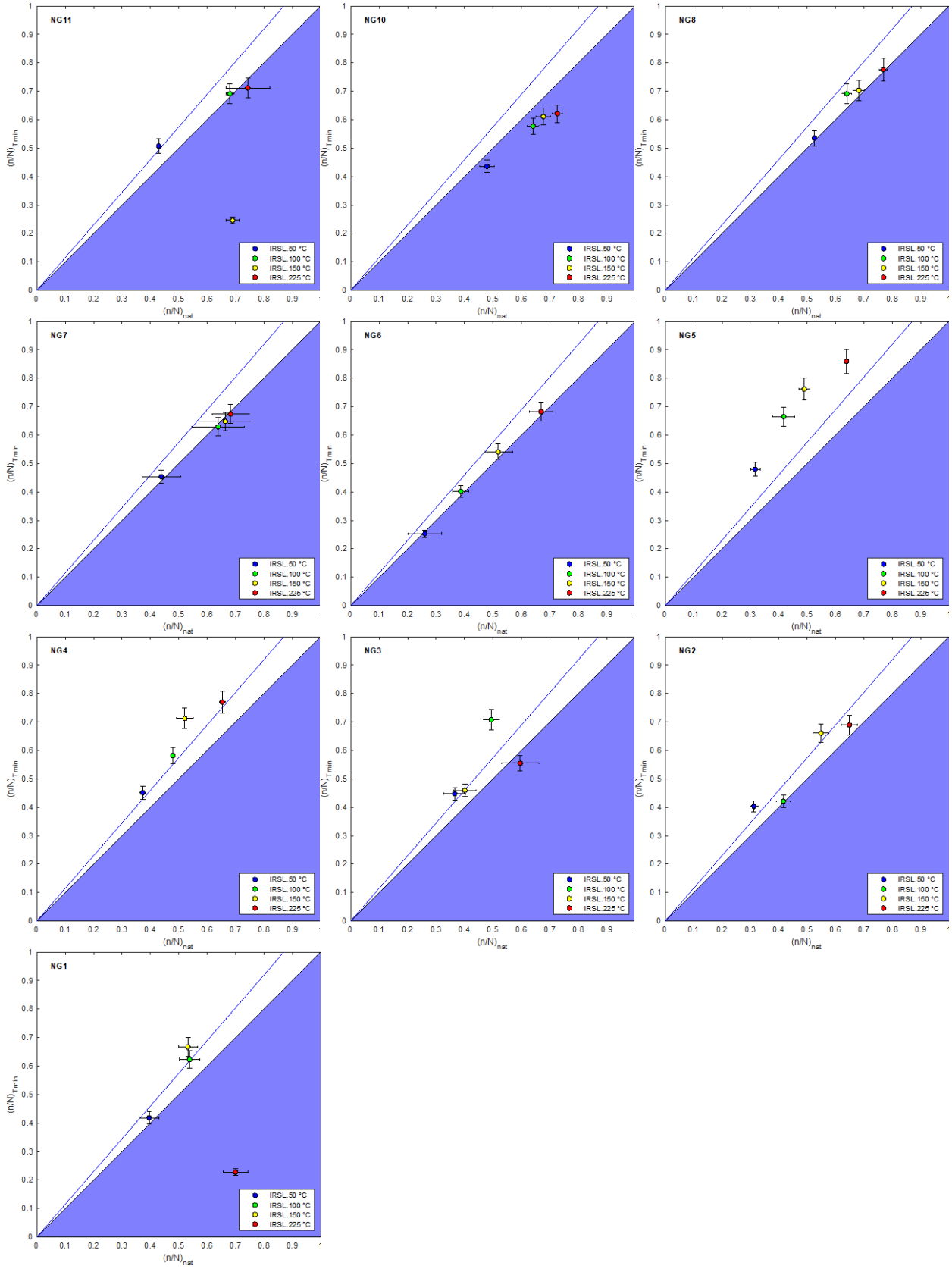

Fig. S5.1: *Surface temperature saturation plots for the NG transect, contrasting natural luminescence values, $\tilde{n}_{nat}$, with the luminescence values for a surface temperature of 20 °C, $\tilde{n}_{Tmin} = \tilde{n}_{20}$, predicted for each of the samples. The 1:1 line delimits saturated samples (blue area) to unsaturated samples (white area), with the saturation limit indicated by the blue line.*

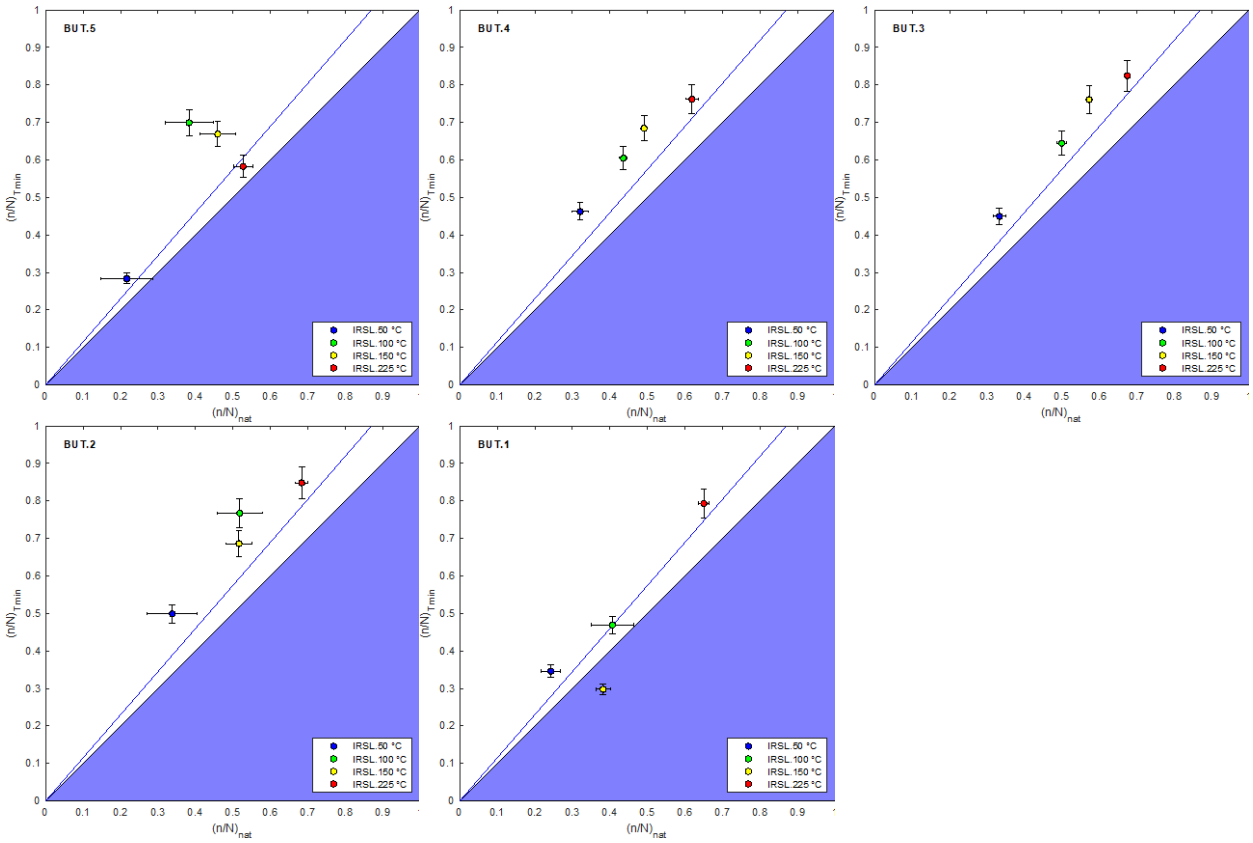

Fig. S5.2: *Surface temperature saturation plots for the BUT transect, contrasting natural luminescence values, $\tilde{n}_{nat}$, with the luminescence values for a surface temperature of 20 °C, $\tilde{n}_{Tmin} = \tilde{n}_{20}$, predicted for each of the samples. The 1:1 line delimits saturated samples (blue area) to unsaturated samples (white area), with the saturation limit indicated by the blue line.*

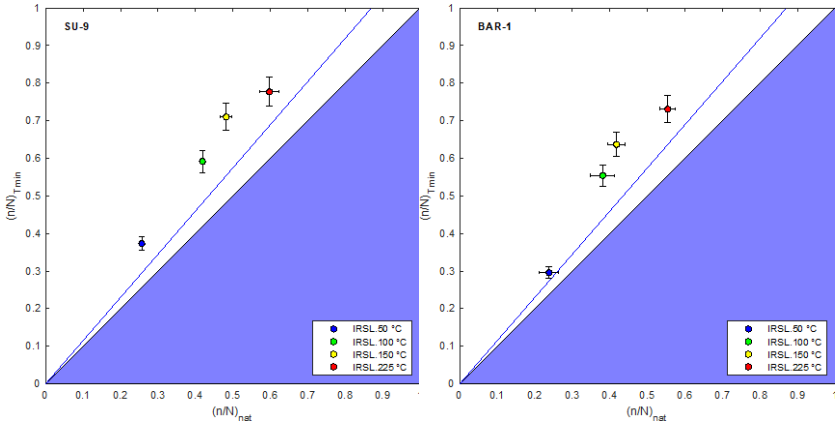

Fig. S5.3: *Surface temperature saturation plots for the SU-9 and BAR-1 samples, contrasting natural luminescence values, $\tilde{n}_{nat}$, with the luminescence values for a surface temperature of 20 °C, $\tilde{n}_{Tmin} = \tilde{n}_{20}$, predicted for each of the samples. The 1:1 line delimits saturated samples (blue area) to unsaturated samples (white area), with the saturation limit indicated by the blue line.*

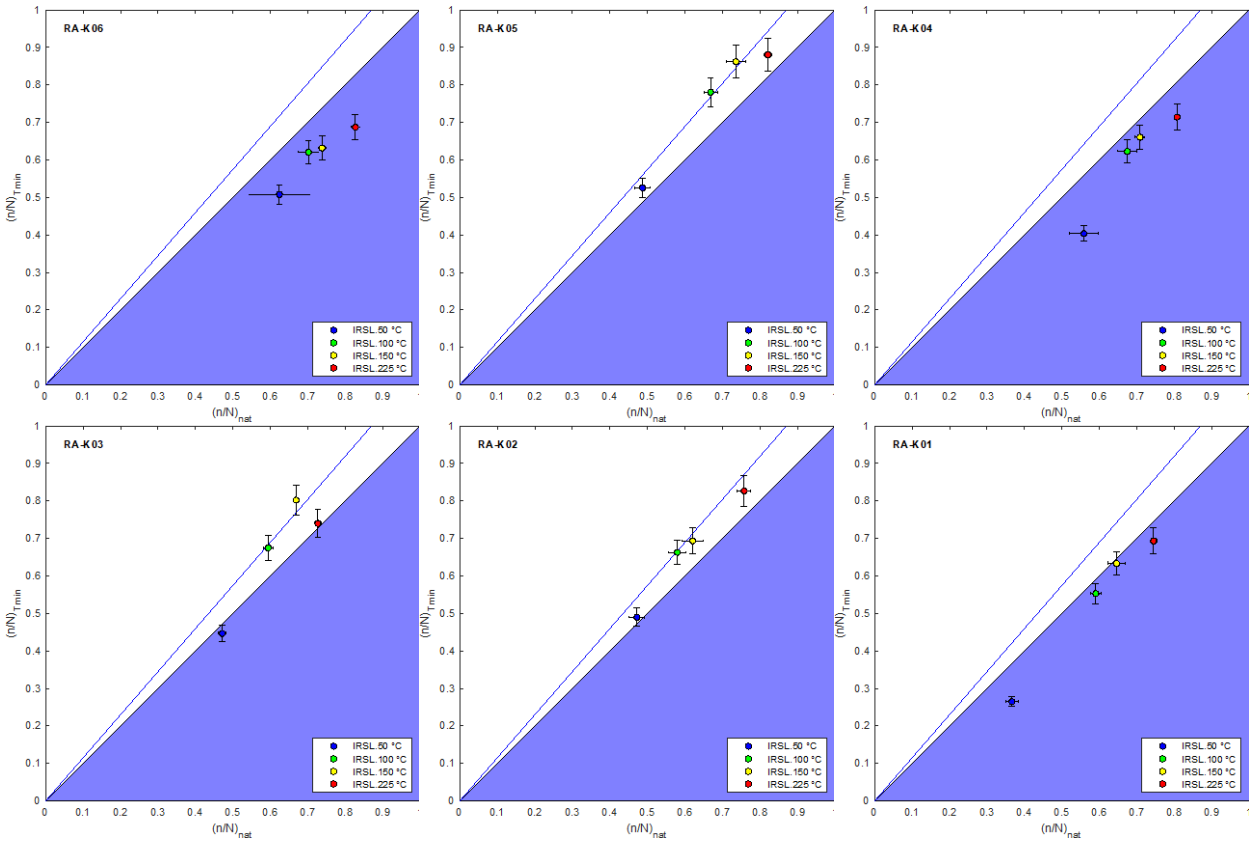

Fig. S5.4: *Surface temperature saturation plots for the RA-K transect, contrasting natural luminescence values, $\tilde{n}_{nat}$, with the luminescence values for a surface temperature of 20 °C, $\tilde{n}_{Tmin} = \tilde{n}_{20}$, predicted for each of the samples. The 1:1 line delimits saturated samples (blue area) to unsaturated samples (white area), with the saturation limit indicated by the blue line.*

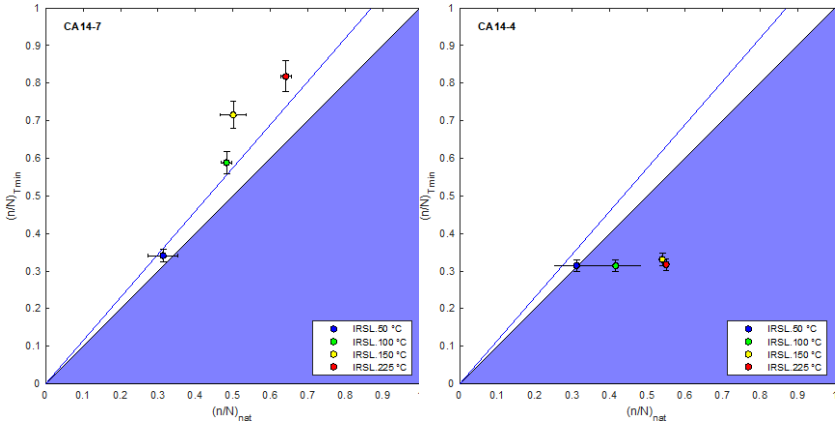

Fig. S5.5: *Surface temperature saturation plots for the CA14-4 and CA14-7 samples, contrasting natural luminescence values, $\tilde{n}_{nat}$, with the luminescence values for a surface temperature of 20 °C, $\tilde{n}_{Tmin} = \tilde{n}_{20}$, predicted for each of the samples. The 1:1 line delimits saturated samples (blue area) to unsaturated samples (white area), with the saturation limit indicated by the blue line.*

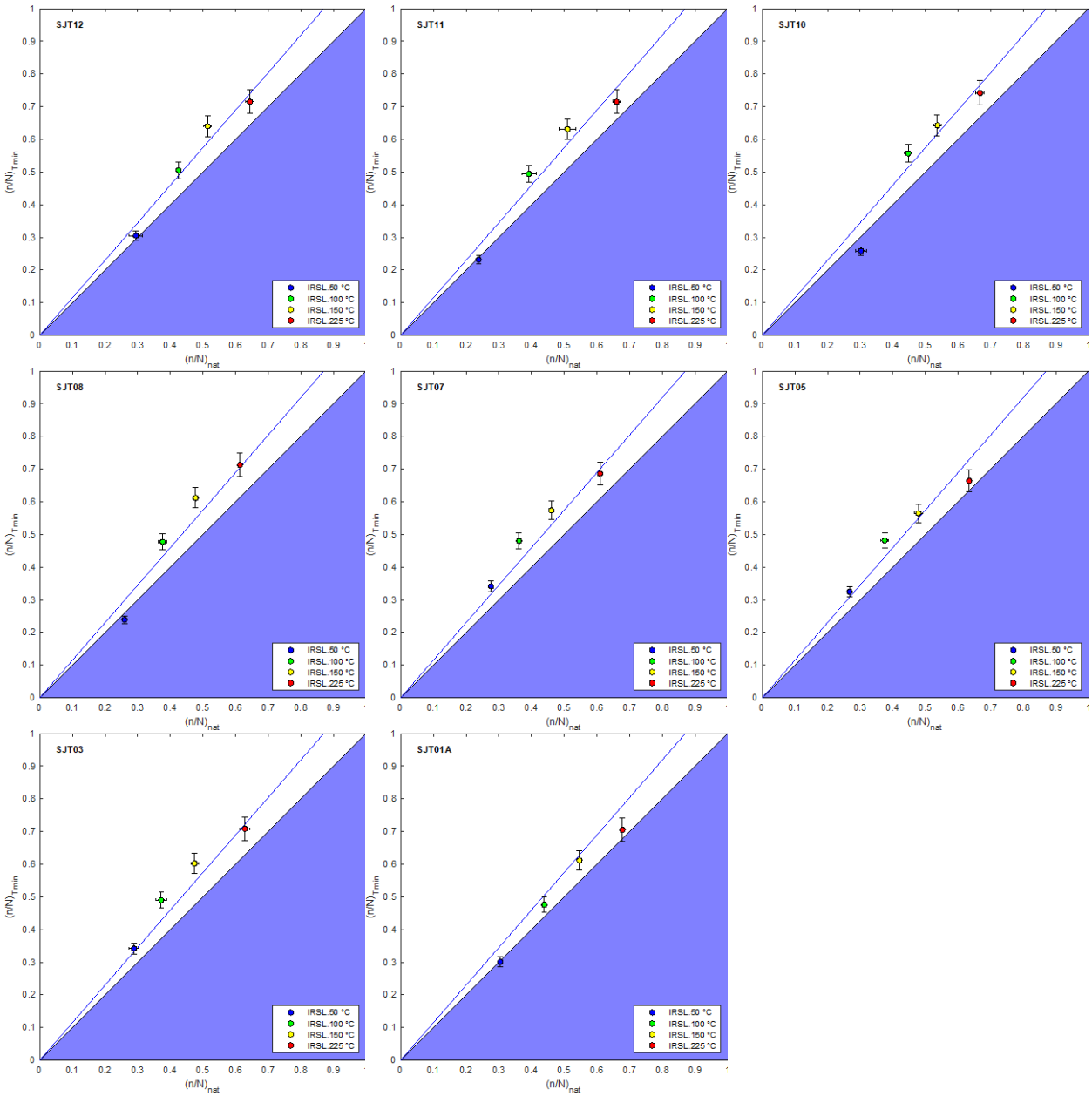

Fig. S5.6: *Surface temperature saturation plots for the SJT transect, contrasting natural luminescence values, $\tilde{n}_{nat}$, with the luminescence values for a surface temperature of 20 °C, $\tilde{n}_{Tmin} = \tilde{n}_{20}$, predicted for each of the samples. The 1:1 line delimits saturated samples (blue area) to unsaturated samples (white area), with the saturation limit indicated by the blue line.*